NAVAL POSTGRADUATE SCHOOL

MONTEREY, CALIFORNIA

THESIS

DYNAMIC MATERIAL PROPERTIES OF ORTHOTROPIC POLYMER AND MOLYBDENUM FOR USE IN NEXT GENERATION COMPOSITE ARMOR CONCEPT

by

Jonathan R. Garner

June 2011

Thesis Advisor:	Robert Hixson
Second Reader:	Jose Sinibaldi

Approved for public release; distribution is unlimited

THIS PAGE INTENTIONALLY LEFT BLANK

REPORT DOCUMENTATION PAGE		*Form Approved OMB No. 0704-0188*
Public reporting burden for this collection of information is estimated to average 1 hour per response, including the time for reviewing instruction, searching existing data sources, gathering and maintaining the data needed, and completing and reviewing the collection of information. Send comments regarding this burden estimate or any other aspect of this collection of information, including suggestions for reducing this burden, to Washington headquarters Services, Directorate for Information Operations and Reports, 1215 Jefferson Davis Highway, Suite 1204, Arlington, VA 22202-4302, and to the Office of Management and Budget, Paperwork Reduction Project (0704-0188) Washington DC 20503.		

1. AGENCY USE ONLY *(Leave blank)*	2. REPORT DATE June 2011	3. REPORT TYPE AND DATES COVERED Master's Thesis
4. TITLE AND SUBTITLE Dynamic Material Properties of Orthotropic Polymer and Molybdenum for Use in Next Generation Composite Armor Concept		**5. FUNDING NUMBERS**
6. AUTHOR(S) LT Jonathan R. Garner, USN		
7. PERFORMING ORGANIZATION NAME(S) AND ADDRESS(ES) Naval Postgraduate School Monterey, CA 93943-5000		**8. PERFORMING ORGANIZATION REPORT NUMBER**
9. SPONSORING /MONITORING AGENCY NAME(S) AND ADDRESS(ES) N/A		**10. SPONSORING/MONITORING AGENCY REPORT NUMBER**

11. SUPPLEMENTARY NOTES The views expressed in this thesis are those of the author and do not reflect the official policy or position of the Department of Defense or the U.S. Government. IRB Protocol number _____N/A_____.

12a. DISTRIBUTION / AVAILABILITY STATEMENT Approved for public release; distribution is unlimited	12b. DISTRIBUTION CODE

13. ABSTRACT (maximum 200 words)

Dyneema HB-25 is an orthotropic polyethylene fiber-epoxy matrix material that is being investigated for use in a next generation layered armor concept. Dyneema was chosen due to its high variation in sound speeds in the through direction and along the fiber direction, thereby making it a good candidate for a wave spreading layer in our proposed armored layer concept. The shock properties in the through fiber direction have been investigated using traditional window experiments and experiments using buffer materials at projectile velocities varying from 0.250 km/s to 1.800 km/s. The shock Hugoniot relationship was found to be non-linear in the low pressure regime that was investigated here and was found to be: $U_s = -1.673u_p^2 + 4.847u_p + 0.902$.

The shock properties of polycrystalline Molybdenum were also investigated; specifically the sound speed at shock state stress level. The relationship between sound speed and stress can be useful in predicting phase changes within materials. The low pressure regime of these properties was investigated in order to provide anchor data for previous work completed on Molybdenum.

14. SUBJECT TERMS Dyneema, Molybdenum, Hugoniot, shock physics			**15. NUMBER OF PAGES** 131
			16. PRICE CODE

17. SECURITY CLASSIFICATION OF REPORT Unclassified	**18. SECURITY CLASSIFICATION OF THIS PAGE** Unclassified	**19. SECURITY CLASSIFICATION OF ABSTRACT** Unclassified	**20. LIMITATION OF ABSTRACT** UU

THIS PAGE INTENTIONALLY LEFT BLANK

DYNAMIC MATERIAL PROPERTIES OF ORTHOTROPIC POLYMER AND MOLYBDENUM FOR USE IN NEXT GENERATION COMPOSITE ARMOR CONCEPT

Jonathan R. Garner
Lieutenant, United States Navy
B.S., University of New Mexico, 2004

Submitted in partial fulfillment of the
requirements for the degree of

MASTER OF SCIENCE IN APPLIED PHYSICS

from the

**NAVAL POSTGRADUATE SCHOOL
June 2011**

Author: Jonathan R. Garner

Approved by: Professor Robert Hixson
                 Thesis Advisor

                 Professor Jose Sinibaldi
                 Second Reader

                 Professor Andres Larraza
                 Chairman, Department of Physics

iii

THIS PAGE INTENTIONALLY LEFT BLANK

ABSTRACT

Dyneema HB-25 is an orthotropic polyethylene fiber-epoxy matrix material that is being investigated for use in a next generation layered armor concept. Dyneema was chosen due to its high variation in sound speeds in the through direction and along the fiber direction, thereby making it a good candidate for a wave spreading layer in our proposed armored layer concept. The shock properties in the through fiber direction have been investigated using traditional window experiments and experiments using buffer materials at projectile velocities varying from 0.250 km/s to 1.800 km/s. The shock Hugoniot relationship was found to be non-linear in the low pressure regime that was investigated here and was found to be: $U_s = -1.673u_p^2 + 4.847u_p + 0.902$.

The shock properties of polycrystalline Molybdenum were also investigated; specifically the sound speed at shock state stress level. The relationship between sound speed and stress can be useful in predicting phase changes within materials. The low pressure regime of these properties was investigated in order to provide anchor data for previous work completed on Molybdenum.

THIS PAGE INTENTIONALLY LEFT BLANK

TABLE OF CONTENTS

LIST OF FIGURES

x

THIS PAGE INTENTIONALLY LEFT BLANK

LIST OF TABLES

THIS PAGE INTENTIONALLY LEFT BLANK

LIST OF ACRONYMS AND ABBREVIATIONS

AL6061   Aluminum alloy 6061

ARL   Army Research Labs

Cu   Copper

EFP   Explosively formed projectiles

g/cc   gram per cubic centimeter

GPa   Gigapascals, one billion pascals of pressure or force per unit area

HEL   Hugoniot elastic limit

ISP   Institute For Shock Physics

mm   Millimeter, or one thousandth of a meter

mrad   Milliradians, or one thousandth of a radian angle measurement

ms   Milliseconds, or one thousandth of a second

NPS   Naval Postgraduate School

ns   nanosecond, one billionth of a second

PDV   photonic Doppler velocimetry

PSI   pounds per square inch

PZT   piezoelectric

RHA   Rolled Homogeneous Armor

SNL   Sandia National Lab

VISAR   Velocity interferometer system for any reflector

μm   Micrometer, one millionth of a meter

μs   Microsecond, one millionth of a second

WSU   Washington State University

THIS PAGE INTENTIONALLY LEFT BLANK

ACKNOWLEDGMENTS

First and foremost, I must express my utmost gratitude to my amazing bride and family. Without their support, I would not have been able to undertake and complete this endeavor.

Next, I would like to thank my thesis advisors, Professor Robert Hixson and Professor Jose Sinibaldi, for their support. Their expertise helped me to understand the various intricacies contained within this complicated field. Without their guidance, I would not have achieved the goal of completing this thesis.

The support of others was also instrumental in the successful completion of this research. Specifically, Dr. Gupta of the Institute for Shock Physics at Washington State University, who provided not only additional guidance and expertise that further provided for the success of this research, but the use of his facility to perform multiple experiments that could not be performed otherwise.

THIS PAGE INTENTIONALLY LEFT BLANK

I.   INTRODUCTION

A.   BACKGROUND

This thesis is a focused continuation of previous Naval Postgraduate School (NPS) research performed in 2009 and 2010 by Ong [1], Poh [2], and Denzel [3] to investigate the feasibility of using a composite layered structure for personnel body armor. Four components make up the structure of this notional composite armor, with each layer designed to perform a specific task: the first layer will plastically deform the projectile; the second layer disperses the energy laterally; the third absorbs a significant fraction of the remaining energy carried by the projectile; and the fourth provides structural support and prevents penetration through the composite armor.

The focus of this thesis will be on obtaining shock properties in the through direction of the wave spreading layer that could be used in the layered armor concept, specifically a polyurethane based fiber material known as Dyneema®. This material is known to be very anisotropic in such a way as to have very high wave velocities in the lateral direction. This causes shock waves to spread laterally at a higher rate than they move normally through the material. Once the desired fundamental dynamic properties are obtained, they will be used to update existing material models used in hydrocodes as formulated by Ong [1] and simulations will be performed in future research using these updated models to confirm the utility of this particular material in the layered armor concept.

In addition to studying the wave spreading material, this thesis will also investigate the shock properties of Molybdenum, specifically the sound speed at pressure due to dynamic loading. These sound speeds found will be used to help confirm the ultrahigh pressure phase change that was observed by Hixson [4], [5].

In order to better understand the dynamic mechanisms that occur in materials when impacted, fundamental shock physics experiments must be conducted. Using the results of these experiments, one can then obtain a better understanding of the

mechanisms occurring within materials that cause energy to be absorbed or dissipated. The energy absorption and momentum spreading in this armor concept will take place in four stages.

Stage1: Projectile defeat – A high strength material is used in this stage to plastically deform the incoming projectile using compressive forces thus decreasing the impulse and kinetic energy imparted to personnel. Projectile kinetic energy is converted to projectile internal energy through plastic deformation.

Stage 2: Wave Spreading – An orthotropic composite, in this research a material called Dyneema, which has a high lateral wave speed is used to spread the incoming shock wave in the lateral direction rather than the through direction thus further reducing the impulse delivered to personnel. Impact energy is spread out in this layer, changing a very localized region of high stress and energy into a larger area. This allows the next layer to better perform its function.

Stage 3: Energy Absorption – Using a porous material, much of the remaining kinetic energy of the projectile is converted to heat through the compressive interaction of the pores in the material (PV-work).

Stage 4: Penetration Prevention – A final layer of a hard rigid material is placed on the back surface of the layered concept to act as a final stopping layer to prevent penetration of a projectile should any kinetic energy remain and also acts as structural support layer for the porous layer. Figure 1 displays the layered armor concept.
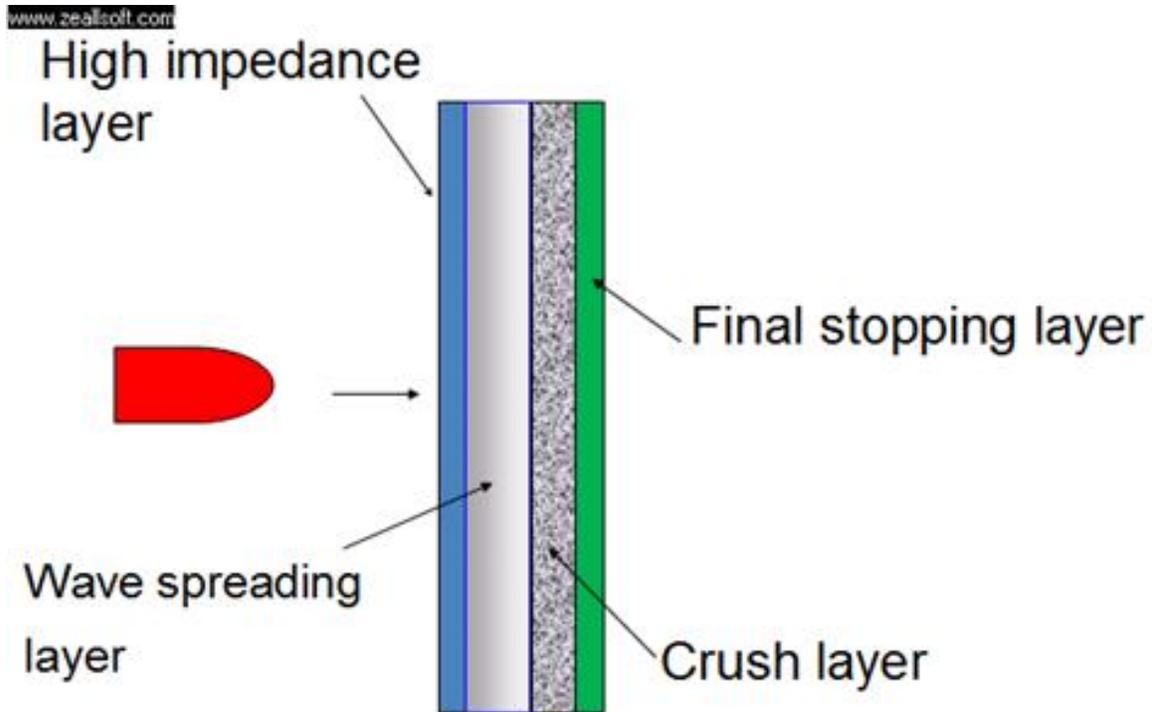
Figure 1.　Illustration of layered armor concept

B.　LITERATURE RESEARCH

1.　Ballistic Protection

Some of the current solutions to protecting personnel against projectile threats are essentially a continuation of medieval technologies. Early knights used chain mail or suits of metallic armor to protect against injury. As technology evolved, so did the ability to produce more lethal projectiles that were able to penetrate the armor being used. Many solutions involve using high strength materials (Y greater than 1 GPa; such as ceramics) to stop a threat, but these materials are still able to be defeated by even more advanced threats. However, technological advancements have been made such as combining high-strength ceramics with composite materials such as Kevlar Fiber Reinforces Polymers (KFRP), or Carbon Fiber Reinforced Polymers (CFRP). Yet, large issues continue with the use of these technologies, specifically, the high-density-required materials causing a

considerable weight to be carried by personnel on the battlefield, the lack of ability to provide protection from projectiles as they become more advanced, and poor multi-hit capability.

2. Projectile Threats

As noted above, projectile technology has outpaced protection technology. Current projectile threats have become more sophisticated, more deadly, and easier to produce. These advanced projectiles include EFPs (Explosively Formed Projectiles), shaped charge jets, as well as advanced traditional projectiles used in small and heavy arms. The intense heat and kinetic energy imparted by these newest classes of projectiles makes defeating them difficult. We are not yet tackling the many technological issues involved in stopping such advanced threats and have chosen our initial threat to be small arms fire with projectiles that travel at less than 1 km/s. As our concepts develop, we will look at possible defeat strategies for the more advanced threats, but that is outside the scope of this thesis.

3. Impetus for Ongoing Research

Current National security priorities have in recent years placed many personnel in harm's way where these new and inexpensive projectiles are being used on a regular basis. Many have been seriously injured or died from injuries due, in part, to their armor protection systems not being able to defeat the incoming projectiles. Some studies in the past, including Robbins et al. [6], have shown through numerical analysis that the concept of layered designed armor systems are feasible. Other studies have been completed on the feasibility of the individual layers that are proposed here, to be used in an armor system. Included in the list would be Gupta et al. [7] showing the ability of a wave spreading material to significantly dissipate the compressive forces of an incoming projectile, Wilkins et al. [8] showing that ceramics effectively provide sufficient plastic deformation to defeat incoming projectiles, and Herrman et al. [9] demonstrating the ability of porous materials to absorb energy due to shock compression.

Using approximations for materials proposed in this advanced armor concept, Ong [1] showed the feasibility for their use in a composite armor concept. As outlined

earlier, four layers were used in the armor concept. Figure 2 shows the success of the layered concept defeating a 15 mm length, 8 mm diameter tantalum projectile traveling at 1000m/s using a 16 mm thick composite plate. The same projectile completely penetrates a 16 mm thick plate of AISI 4340 armor grade steel.
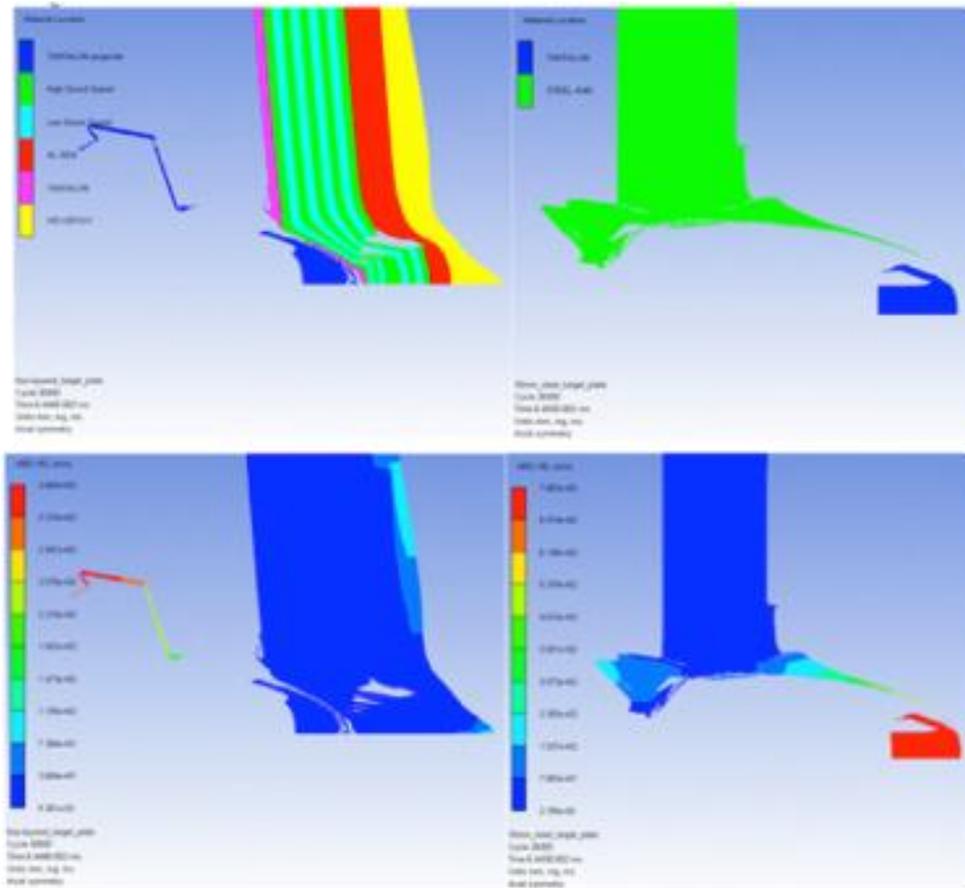
Figure 2.   Composite plate (left) shown by Poh defeating Tantalum projectile while armor grade steel (right) failed

This numerical model used for these simulations was developed using the Autodyn© hydrodynamic code. But the code is only as accurate as the models that were used for all of the materials involved, including the composite material. Many approximations were made in order to build the material models for the computer code that could not be verified experimentally. Denzel [3] provided experimental data for use in refining the material model for the ceramic used in the layered concept, while this research will provide some additional data to be used in the model of the wave spreading

layer and a potential substitute for the first layer, specifically approximating the material properties of Dyneema© and providing detailed measurements for Molybdenum respectively. Ong [1] developed a transverse orthotropic continuum model for Dyneema using simple approximations and educated guesses. This work consists, in part, of obtaining fundamental data that can help improve upon this approach.

Dyneema HB25 is a polyurethane fiber based material and is shown at the micron level in Figure 3. It is manufactured using strands of ultra high density polyurethane fiber that are lined up in a plane and then stacked in alternating directional layers and held together using a polyurethane binder. The exact material properties for this composite are not readily available in open literature due to the proprietary nature of the material and thus will be found using fundamental shock physics experiments. This research will focus on the through direction of Dyneema.
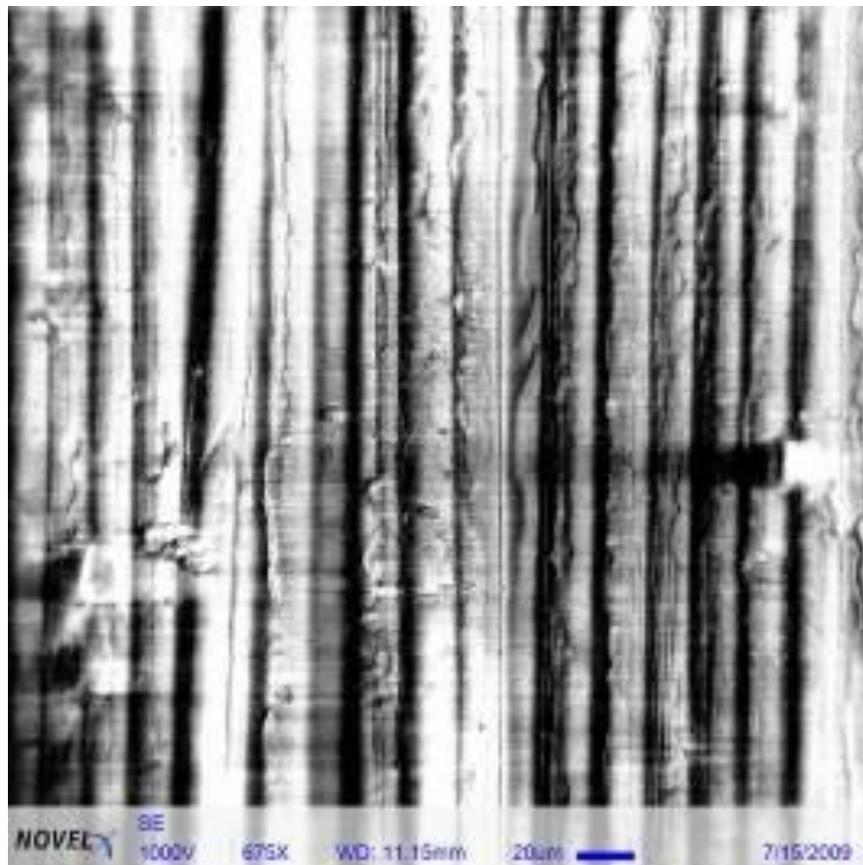
Figure 3.   Scanning electron microscope view of Dyneema at 675 times magnification [From 1]

Molybdenum is a group 6 element that naturally occurs in various stable compounds and then must undergo various materials processing to extract the pure element to form polycrystalline Molybdenum. The high melting temperature, corrosion resistance, and high strength allow for the possibility of use of Molybdenum or Molybdenum alloy as a final stopping layer in the layered armor concept [10]. This research will focus on providing evidence to support or refute possible solid-solid phase changes in Molybdenum in 200 GPa regime.

4.   Research Approach

Due to the challenges that this project presents, a careful and concise approach will be used to achieve the end goals and recommendations. This research begins with an overview of current shock theory based upon multiple years of previous development and uses fundamental shock compression techniques that have also been vetted through years of use. This research will focus primarily on obtaining the shock properties of Dyneema in the through thickness direction and obtaining sound speeds at low pressures in molybdenum. The molybdenum work was done to develop experimental tools and techniques on a simple metal that will ultimately be used on the complex material of interest, Dyneema. However, the data obtained on molybdenum will also be on interest in its own right in the high pressure community. In other words, we chose an interesting material to use to develop our shock compression techniques and expertise. Multiple single-stage gas gun experiments were performed both at the Naval Postgraduate School and at The Shock Physics Institute (ISP) at Washington State University (WSU) to acquire the required data to develop further material models used in the layered armor concept.

A brief overview of material models that have been previously developed will also be given. Using the relevant results from this research and previous work, the material models, equation of state, strength and failure models will be updated. The materials models that were updated are those for the ceramic, and Dyneema. Using these updated models, a numerical simulation using the hydro code AUTODYNE® was performed to further verify the validity of the layered armor concept.

THIS PAGE INTENTIONALLY LEFT BLANK

II. EXPERIMENTAL METHODS

A. INTRODUCTION TO SHOCK PHYSICS

1. Static Elastic-Plastic Theory

The goal of this research is to characterize the dynamic loading properties of two materials that are being characterized for armor applications. In order to dynamically characterize these materials, some theory about the dynamic response of materials in general must be understood. All materials respond dynamically to the impulsive loading imparted to them during a dynamic event, such as armor being impacted by small arms fire, in a way that is governed by their inherent properties. Dynamic deformations follow physical processes that are governed by the laws of physics and materials science. In order to better understand events such as this we will use a simple suite of dynamic experiments. But before studying the dynamic properties of materials, the static loading conditions must be understood.

When a material is loaded under a stress, it responds by contracting or expanding, depending on whether the stress applied puts the material in compression or in tension, respectively. Therefore, the material strain is proportional to the stress loading. This is graphically shown in Figure 4 for a material loaded under uniaxial stress conditions.
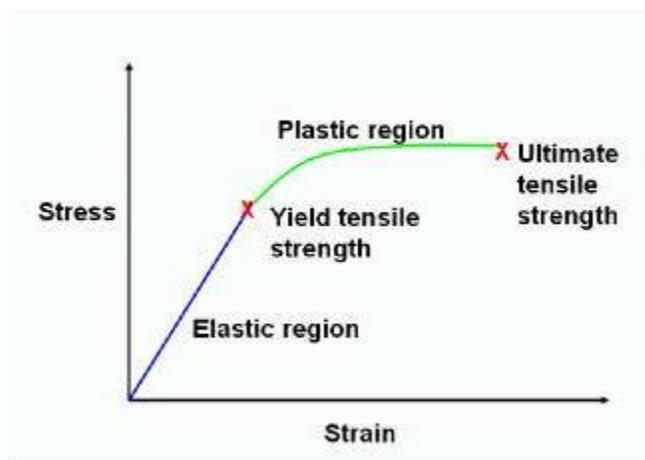
Figure 4. Typical stress strain curve for linear elastic materials

The relationship between stress and strain in the linear elastic region is characterized by a constant known as Young's modulus, E, and is given as the ratio of stress over strain:

$$E = \frac{\sigma_x}{\epsilon_x}$$

Young's modulus is a fundamental modulus for states of uniaxial stress; it is also referred to as the 'elastic modulus.' Once a material reaches the limit for linear response it begins to transition from elastic to plastic deformation. Strain that occurs as a result of plastic deformation is unrecoverable, and so by definition not elastic. The region of plastic deformation is an important region for the materials involved in this research. Since in armor applications materials are subjected to high velocity projectile impacts, where considerable plastic deformations are involved. However, the elastic deformation regime is also important for impact problems. In the elastic regime, the stresses and strains are related through the general constitutive relation:

$$
\begin{bmatrix} \sigma_{xx} \\ \sigma_{yy} \\ \sigma_{zz} \\ \sigma_{yz} \\ \sigma_{zx} \\ \sigma_{xy} \end{bmatrix}
=
\begin{bmatrix}
C_{11} & C_{12} & C_{13} & C_{14} & C_{15} & C_{16} \\
C_{21} & C_{22} & C_{23} & C_{24} & C_{25} & C_{26} \\
C_{31} & C_{32} & C_{33} & C_{34} & C_{35} & C_{36} \\
C_{41} & C_{42} & C_{43} & C_{44} & C_{45} & C_{46} \\
C_{51} & C_{52} & C_{53} & C_{54} & C_{55} & C_{56} \\
C_{61} & C_{62} & C_{63} & C_{64} & C_{65} & C_{66}
\end{bmatrix}
\begin{bmatrix} \varepsilon_{xx} \\ \varepsilon_{yy} \\ \varepsilon_{zz} \\ \varepsilon_{yz} \\ \varepsilon_{zx} \\ \varepsilon_{xy} \end{bmatrix}
$$

For isotropic materials this is simpler due to symmetries:

$$
\begin{bmatrix} \sigma_{xx} \\ \sigma_{yy} \\ \sigma_{zz} \\ \sigma_{yz} \\ \sigma_{zx} \\ \sigma_{xy} \end{bmatrix}
=
\begin{bmatrix}
\lambda + 2\mu & \lambda & \lambda & 0 & 0 & 0 \\
\lambda & \lambda + 2\mu & \lambda & 0 & 0 & 0 \\
\lambda & \lambda & \lambda + 2\mu & 0 & 0 & 0 \\
0 & 0 & 0 & \mu & 0 & 0 \\
0 & 0 & 0 & 0 & \mu & 0 \\
0 & 0 & 0 & 0 & 0 & \mu
\end{bmatrix}
\begin{bmatrix} \varepsilon_{xx} \\ \varepsilon_{yy} \\ \varepsilon_{zz} \\ \varepsilon_{yz} \\ \varepsilon_{zx} \\ \varepsilon_{xy} \end{bmatrix}
$$

Where μ and λ are the Lamé constants specific to that material and found using longitudinal and shear sounds speeds that will be discussed later. These constitutive relations become even simpler for special states of stress or strain. Using the Lamé

constants, additional information may be found to further classify a material, such as Young's (E), Shear (G), Bulk (K) and Longitudinal (F) moduli given respectively by:

$$E = \mu \, \frac{3\lambda + 2\mu}{\lambda + \mu}$$

$$G = \mu$$

$$K = \lambda + \frac{2}{3}\mu$$

$$F = \lambda + 2\mu$$

The Poisson's ratio of the material gives a relative "compressibility" of a material, and can also be found using the Lamé constants and is given by:

$$v = \frac{\lambda}{2} \, \frac{\lambda}{\lambda + \mu}$$

Similarly, a constitutive relation can be formulated for an orthotropic material. In the focus of this research, Dyneema will be characterized in all directions by the following relationships:

$$
\begin{bmatrix} \sigma_{xx} \\ \sigma_{yy} \\ \sigma_{zz} \\ \sigma_{yz} \\ \sigma_{zx} \\ \sigma_{xy} \end{bmatrix}
=
\begin{bmatrix}
\dfrac{1 - v_{yz}v_{zy}}{E_y E_z \Delta} & \dfrac{v_{yx} + v_{zx}v_{yz}}{E_y E_z \Delta} & \dfrac{v_{zx} + v_{yx}v_{zy}}{E_y E_z \Delta} & 0 & 0 & 0 \\
\dfrac{v_{xy} + v_{xz}v_{zy}}{E_x E_z \Delta} & \dfrac{1 - v_{zx}v_{xz}}{E_x E_z \Delta} & \dfrac{v_{zy} + v_{zx}v_{xy}}{E_x E_z \Delta} & 0 & 0 & 0 \\
\dfrac{v_{xz} + v_{xy}v_{yz}}{E_x E_y \Delta} & \dfrac{v_{yz} + v_{xz}v_{yx}}{E_x E_y \Delta} & \dfrac{1 - v_{xy}v_{yx}}{E_x E_y \Delta} & 0 & 0 & 0 \\
0 & 0 & 0 & 2G_{zy} & 0 & 0 \\
0 & 0 & 0 & 0 & 2G_{zx} & 0 \\
0 & 0 & 0 & 0 & 0 & 2G_{xy}
\end{bmatrix}
\begin{bmatrix} \varepsilon_{xx} \\ \varepsilon_{yy} \\ \varepsilon_{zz} \\ \varepsilon_{yz} \\ \varepsilon_{zx} \\ \varepsilon_{xy} \end{bmatrix}
$$

where,

$$\Delta = \frac{1 - v_{xy}v_{yx} - v_{yz}v_{zy} - v_{zx}v_{xz} - 2v_{xy}v_{yz}v_{zx}}{E_x E_y E_z}$$

And v is the Poisson ratio of the material in each of the principle directions of an orthotropic material as demonstrated by Ong [1].

11

If a sufficient number of these parameters are known, a material model can then be developed to accurately predict the response of materials under different loading conditions.

Once it is understood how a material will respond to a static load, the next logical step is to demonstrate the response of the material due to a dynamic load, specifically for shock wave loading conditions. If one sets up the experiment to be performed using planar impact geometry, the degrees of freedom of the problem become reduced. It can be assumed that all volume changes occur in a single direction and therefore the problem yields itself to a uniaxial strain loading analysis. The experiments in this thesis will be focused on this type of dynamic loading conditions.

2. Dynamic Elastic-Plastic Theory

The impact of one material by another creates two shockwaves, one in each material. These shocks travel in opposite directions. The shockwave in the impacted material carries useful information about the elastic and plastic response, and ultimately the failure mechanisms of the material being studied. In order to be able to obtain this information there must be an understanding of what causes these shock waves to form and the physics that occur during the dynamic event. Shock wave events can be characterized by the same basic conservation laws that govern the rest of the physical world; conservations of mass, momentum, and energy. If one looks at the shock as passing through a control volume and applies the conservation laws across the interface, 'jump' conditions that relate the initial pressure, density, and energy of the material to the material properties behind the shock front can be derived:

$$\frac{\rho_o}{\rho} = 1 - \frac{u_p}{U_s}$$

$$P - P_o = \rho_o U_s u_p$$

$$e - e_o = \frac{1}{2} \left(P + P_o \right) \left(\frac{1}{\rho_o} - \frac{1}{\rho} \right)$$

where,

12

$\rho_o \equiv$ Initial density of material

$\rho \equiv$ Density of material behind shock wave

$P_o \equiv$ Initial Pressure (stress) state in material

$P \equiv$ Pressure (stress) state in material behind shock wave

$e_o \equiv$ Initial specific energy in the material

$e \equiv$ Specific energy in material behind shock wave

$u_p \equiv$ Particle velocity behind shock wave

$U_s \equiv$ Shock speed of the shock wave propogating through the material

Note that these equations are derived with certain assumptions about the shock process, such as the existence of steady waves. By measuring certain key properties, and using these fundamental jump conditions for shock waves, one can develop an accurate equation of state (EOS) model for that material. The EOS contains fundamental thermodynamic information about the material that can be used to then predict how that material will respond to arbitrary shock compression. The EOS however, contains no information regarding the elastic-plastic response (dynamic strength) of the material. The shock Hugoniot of a material is a representation of its material properties under dynamic loading. Several coordinate systems can be used to represent the Hugoniot for a material, with two being very common. One useful representation of the Hugoniot is in shock velocity-particle velocity space. It was discovered in early shock experiments that when U_s and u_p values were measured and plotted, there was a linear relationship in most cases over some pressure range. That relationship is shown below, and can be represented in the equation form of:

$$U_s = C_o + S u_p$$

From previous years of research it has been shown that C_o can be taken to be approximately equal to the ambient bulk sound speed of the material and therefore gives an anchor point to the U_s-u_p relationship.
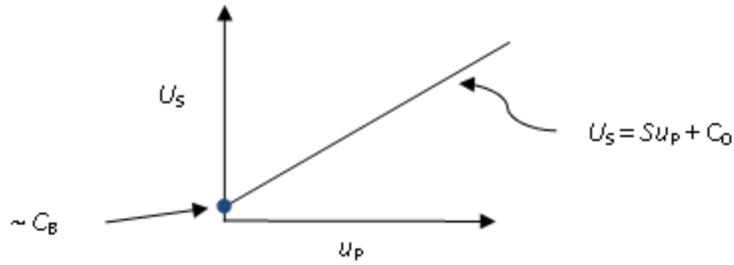
Figure 5.   Graphical representation of typical Hugoniot curve in U_s-u_p space

A very common second way in which to represent Hugoniot data is to plot the relationship between the pressure and the u_p behind the shock in the material. Since pressure is not a property easily measured in dynamic experiments, the jump conditions can be used to *calculate* pressure. If we substitute the above linear relationship between shock and particle velocity into the momentum shock jump condition, we obtain the following relationship:

$$P = \rho_o\ C_o + s\ u_p - u_o\quad u_p - u_o$$

and we see that pressure depends quadraticaly upon particle velocity. This gives us a functional relationship as shown below for the Hugoniot in this space. The graphical representation of the Hugoniot in P-u_p space is useful to be able to interpret the interactions that occur during an experiment with multiple shock interactions.   This will be discussed in more detail later.
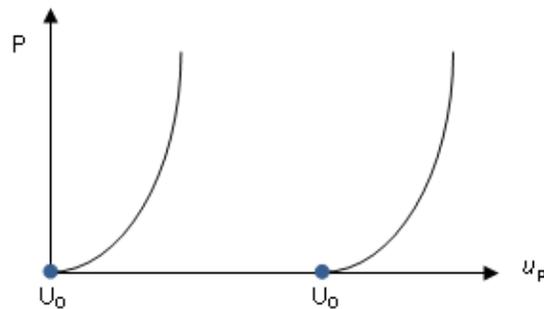
Figure 6.   Graphical representation of P-u_p curves for a typical material at different initial values dependent on initial shock conditions

Once the Hugoniot for a material is characterized, that information may then be used to develop an equation of state (EOS) for that material. Typically, the EOS of a material is defined as a relationship between pressure, temperature and specific volume (or a similar relationship between thermodynamic quantities) and shock data can be used to experimentally determine points to establish the relationship between relevant thermodynamic quantities. The $P-v$ relationship formed from the jump conditions is given by:

$$P - P_o = \frac{U_s^2}{v_o}\left(1 - \frac{v}{v_o}\right)$$

and is graphically represented in Figure 7.
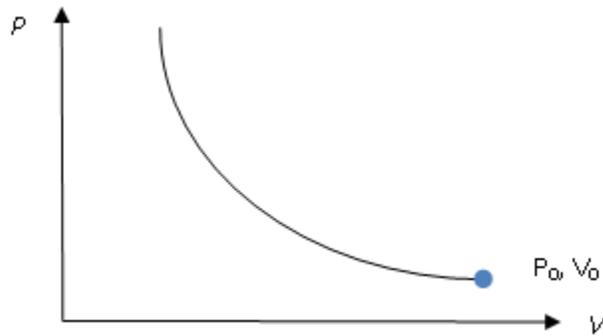
Figure 7.   Graphical representation of typical $P-v$ curve

It should be noted that the curve that is formed is a locus of points that are end states of the shock event, and not a continuous path of states that the material transitions through to reach the end state. Rather, the material travels from its initial state to the final state along what is known as a Rayleigh line that connects the initial to the final state. The slope of the Rayleigh line is given as:

$$slope = -\frac{U_s^2}{v_o^2}$$

and is depicted graphically as:

15
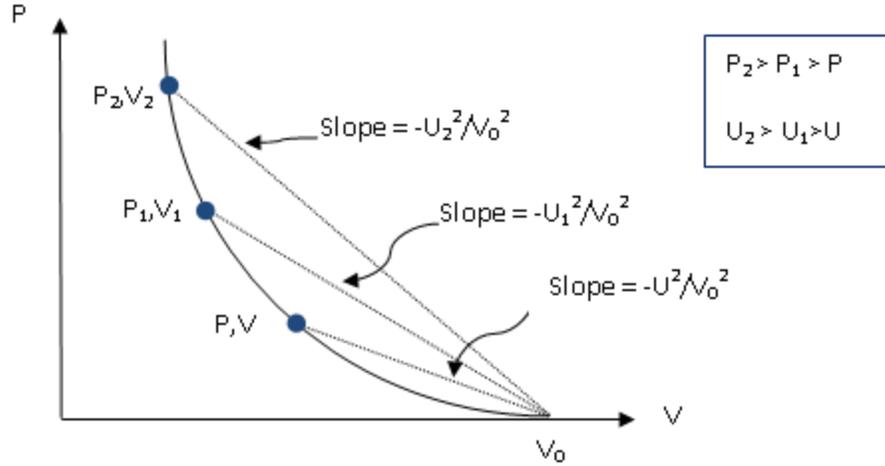
Figure 8.   Schematic view of initial and final points in $P-v$ states connected by different Rayleigh lines

The Hugoniot in $P-v$ space can be used to show graphically and analytically what occurs during the transition from elastic to plastic deformation. For this research, the experiments are setup such that the material tested is under uniaxial strain conditions. From this figure we clearly see that the shock speed depends upon the end state to which we are shocking. So as we shock to higher pressure the Rayleigh line becomes steeper, and shock velocity increases. This is all for a simple Hugoniot with only one branch. If there is an inflection point in the Hugoniot and we have two branches, then the shock response allows for more than just on stable shock wave.

Under these restrictive conditions and using the stress tensor for isotropic materials mentioned in the previous section, and assuming the direction of interest is the x-direction, the stress-strain relationship reduces to:

$$\sigma_x = \lambda + 2\mu \ \varepsilon_x$$

In dynamic yielding experiments the point at which this stress relationship exceeds the dynamic elastic limit is known as the Hugoniot Elastic Limit (HEL). Using young's modulus and rearranging the above equation, the HEL stress can be found in terms of Lame constants and simple yield strength as:

$$\sigma_{HEL} = Y\left(1 + \frac{\lambda}{2\mu}\right)$$

In terms of Poisson's ratio the HEL stress can be found using the following relationship.

$$\sigma_{HEL} = Y\left(\frac{1-v}{1-2v}\right)$$

Where, Y is the yield point determined from experiments done in a condition of uniaxial stress. This expression allows us to estimate the HEL from measured values of Y.

As mentioned above, if the Hugoniot in P-V space has an inflection point, we can have more than one shock. This is shown in the figure below. The inflection point causes a two wave structure to exist over some range of pressure. These waves consist of an elastic precursor wave that takes the material to the HEL state followed by a plastic wave that takes the material to the final state. Graphically this is represented in Figure 9.
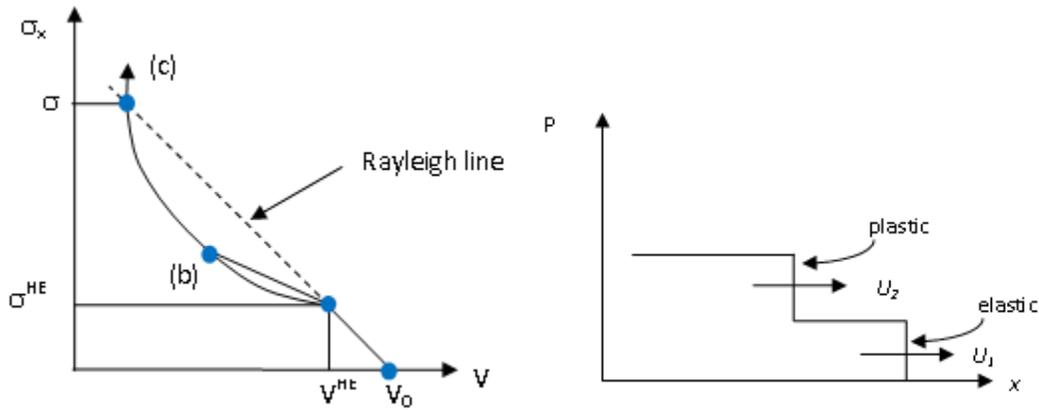
Figure 9.   Schematic of plastic and elastic waves traveling through a material in both $P-v$ and P-x space

The HEL can also be related to the particle speed and volume of the material behind the shock travelling through the material as well. The particle velocity for the HEL can be measured using fundamental shock experiments and then used to find the dynamic yield point. This relationship is given as:

17

$$\sigma_{HEL} = \left(\frac{u_p^{HEL}{}^2}{V_o - V_{HEL}} \right)$$

Note that once the materials have been adequately characterized under dynamic loading conditions, material response can then be predicted under other loading conditions.

B.   SAMPLE CHARACTERIZATION

In order to accurately predict the response of materials using the theory outlined in Chapter II, Section A, some fundamental measurements of the initial properties of the samples must be made. The most useful measurements that can be made are the initial density of the material and the shear and longitudinal sound speeds.

1.   Initial Density

Initial sample density is measured essentially by determining the sample mass and volume, and then dividing. Typically mass is very easy to measure on an accurate scale. Volume can be determined for regular objects by using dimensions and then volume formulae. But a better way is to do immersion and apply Archimedes principle. We do not have this capability currently in the dynamic testing laboratory at the NPS, so we rely on published densities, or send samples to other laboratories for immersion density testing. Initial density typically can be determined to a few tenths of a percent.

2.   Elastic Sound Speeds

In order to determine the elastic constants of the isotropic materials used in this research, the elastic sound speeds of those materials were measured. The method used to calculate sound speed is based on the simple relationship of velocity proportional to time of travel and distance traveled as given by:

$$c = \frac{x_{sample}}{t_{transit}}$$

In order to obtain the sound speeds, the basic method is to measure the thickness of the sample and send an ultrasonic pulse through the sample, using a high precision digitizer to measure the transit time through the material as indicated by echoes detected by the digitizer. A general pulse signal is shown:
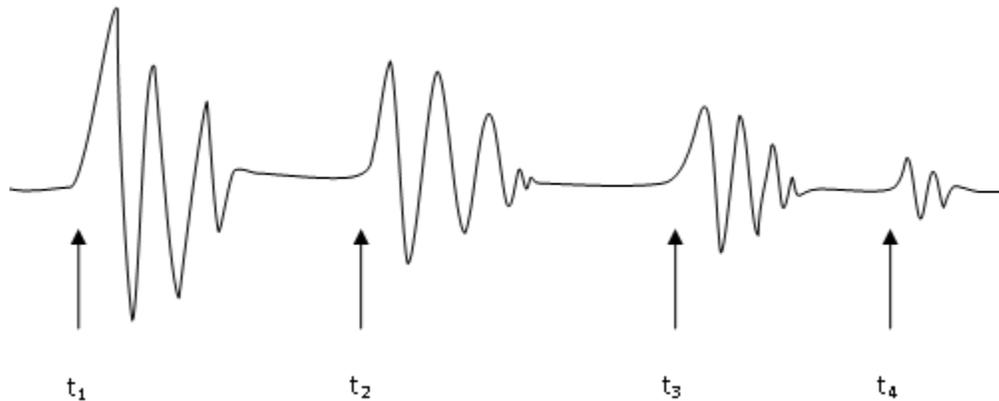
Figure 10.   Schematic representation of pulse traces from sound speed measurements

The time between each pulse record coincides to a complete round trip through the sample as shown in Figure 11. Therefore, the distance used in calculations is half this round trip time.
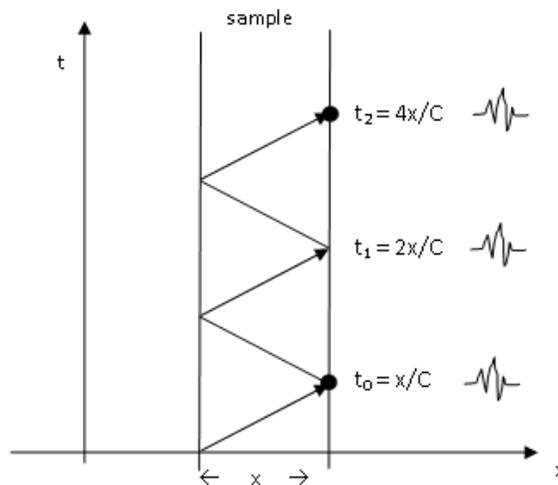
Figure 11.   Schematic relating time measurements to pulse waves in sound speed measurements

19

The times are used in a linear regression analysis to obtain a least squares fit to the data points. The slope of the best fit line coincides with the sound speed of the material as shown.

x	t
$2x_1$	t_1
$4x_2$	t_2
$6x_3$	t_3

$$slope = \frac{\Delta x}{\Delta t} = c$$
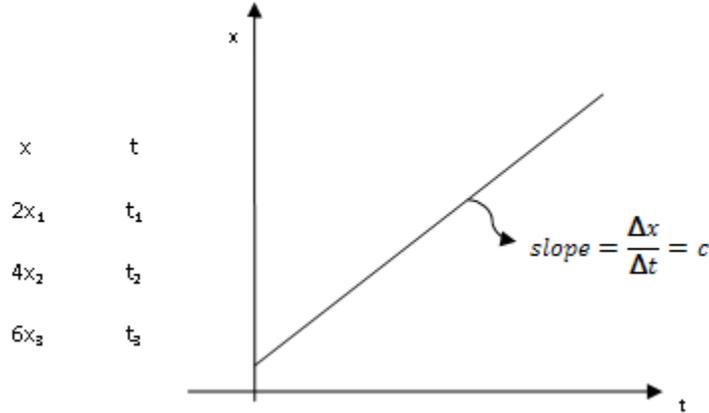
Figure 12.   Schematic representation regression analysis to obtain sound speeds

Once the sound speeds for a given material are measured, they can then be used to find the elastic constants of isotropic materials. These constants can be found using the following relationships between shear (C_S) and longitudinal (C_L) sound speeds and the elastic constants for isotropic materials:

$$C_L = \sqrt{\frac{\lambda + 2\mu}{\rho_o}}$$

$$C_S = \sqrt{\frac{\mu}{\rho_o}}$$

So, given a longitudinal and a shear velocity we can find values for the two Lame' constants λ and μ.

The longitudinal and shear sound speeds can also be used to find the bulk sound speed for the material using the following relation:

$$C_B = \sqrt{C_L^2 - \frac{4}{3}C_S^2}$$

This is a useful quantity in shock wave experiments and will be used in analysis later.

For this research, an ultrasonic pulse-echo transducer receiver system manufactured by Olympus was used in conjunction with a digital oscilloscope to measure elastic sound speeds of materials used. Both shear and longitudinal sound speed were measured. Figure 13 shows the physical set up of these sound speed measurements.
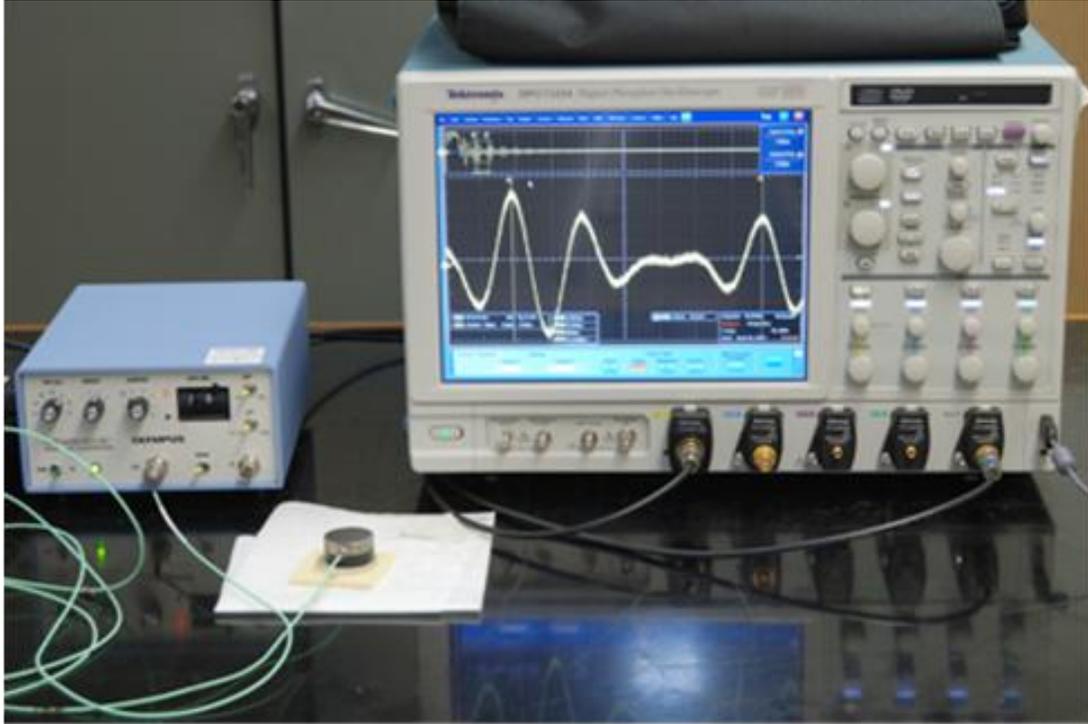
Figure 13.   Pulse echo setup for sound speed measurements

The results of these measurements are summarized in Table 1 and compared to previously published values of the same materials.

Table 1.   Summary of measured sound speeds compared to literature values

Material	Measured for this Research		Literature Value	
	C_L (mm/µs)	C_s (mm/µs)	C_L (mm/µs)	C_s (mm/µs)
Polycrystalline Molybdenum	6.48	3.48	6.44 [11]	3.48 [11]
OFHC Copper	4.74	2.26	4.76 [11]	2.33 [11]
Aluminum T-6061	6.31	3.10	6.40 [11]	3.15 [11]
Dyneema			2.12 [12]	0.99 [12]

As may be noted, there is not a result for a measurement of Dyneema in Table 1. This is due to the extreme dispersive effect of the material and a valid sound speed measurement was not obtainable with our equipment.

C.   HUGONIOT MEASUREMENT EXPERIMENTS

1.   Shock Compression Experimental Techniques

As was outlined above, a shock moving through a material can be characterized by the shock jump conditions:

$$\frac{\rho_o}{\rho} = 1 - \frac{u_p}{U_s}$$

$$P - P_o = \rho_o U_s u_p$$

$$e - e_o = \frac{1}{2}\left(P + P_o\right)\left(\frac{1}{\rho_o} - \frac{1}{\rho}\right)$$

But as one can see, there are five unknowns and only three equations; therefore, the jump conditions cannot be resolved analytically without additional information. Typically, two variables are measured experimentally and these are shock velocity and particle velocity. The measurement of particle velocity and shock velocity over a range of pressure is then used to build the Hugoniot EOS as discussed earlier. The outline of how to properly perform the shock compression experiments used in this research are outlined below including a short description of all parts and equipment used. A booking methodology was developed, along with a build sheet form to ensure that all pertinent pre-shot data were taken during the buildup of an experiment. The form used is presented in Appendix A.
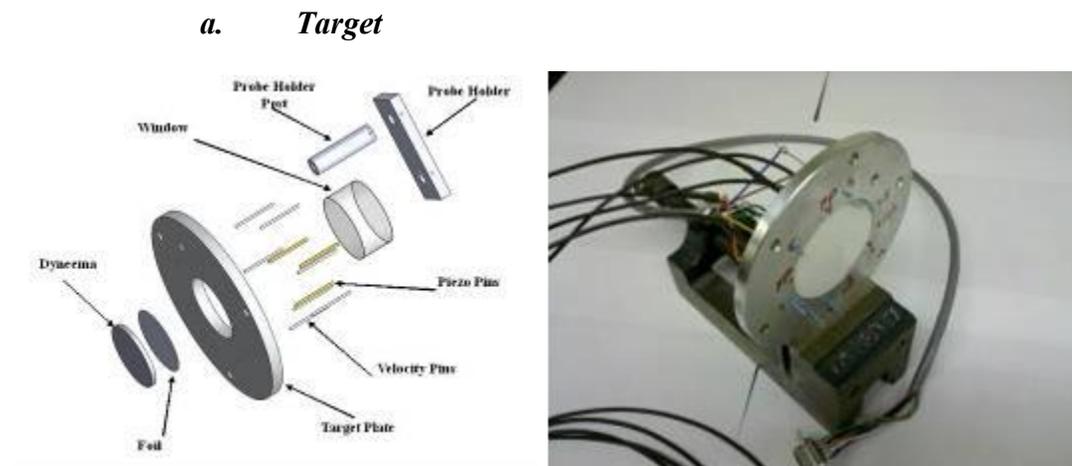
a. Target

Figure 14. Schematic and final view of entire target buildup used for a shock compression experiment

To perform a gas gun experiment both a target assembly and a projectile are required. A target assembly that was used for a Dyneema experiment is shown in Figure 14. The target consists of the basic subcomponents of: Target plate, VISAR probe, Velocity Pins, Piezoelectric Pins and the material sample.

(1) Target Plate. The first component used to build the target is the target plate. Figure 15 shows two simple target plate designs that can be used for shock compression techniques. The target plate is the building block on which all

23

other components must be attached to. The target plate used in this research was fabricated from 6061 Aluminum and modified for each individual experiment as required.
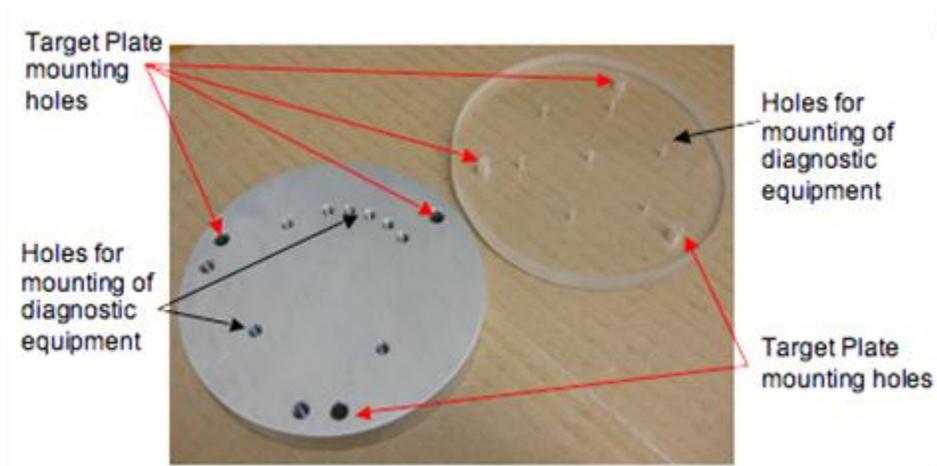
Figure 15.   Two different designs of target plates used

(2) VISAR.
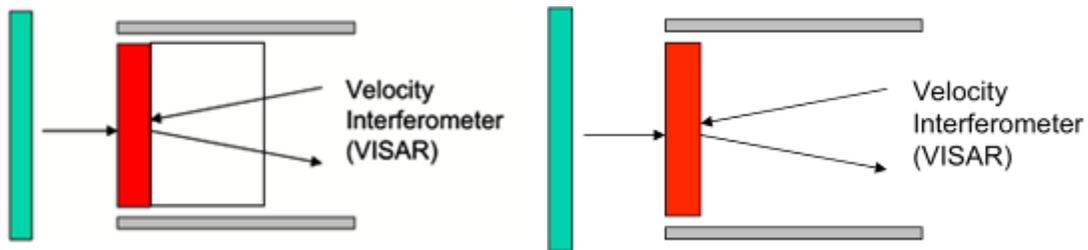
Figure 16.   Schematic representation of VISAR system use in shock compression experiments

In order to measure particle velocity on the rear surface of the materials being studied the diagnostic used was a Velocity Interferometer for Any Reflector (VISAR). VISAR is a velocity interferometer that has been widely used and developed for use in shock compression experiments. A general experimental setup used for a VISAR experiment is shown in Figure 16. The VISAR used for this research was manufactured by and procured from National Security Technologies (NSTEC). In depth analysis and operation of VISAR systems was explained by Hemsing [13] et al.

(2) Velocity Pins. In order to obtain an accurate measurement of the velocity at which the projectile impacts the target plate some sort of velocity measuring must be utilized. In this research that diagnostic tool was velocity pins. The velocity pins consist of electrically conductive metallic pins that short a charged capacitor in an RC circuit, and thereby cause a fast-rising pulse to be generated that is recorded on a digitizer. Six pins are arranged in a circular fashion around the material sample at an equidistant radius from the center of the target plate and at 60 degree intervals. Velocity pins are also "stepped" down, each pin is protruding from the front surface of the target plate at a stepped decreasing interval. The measured pulse times are then used to perform a least squares fit to find the times and therefore finding velocity from:

$$v_{projectile} = \frac{\Delta x_{pins}}{\Delta t_{pulse}}$$

Velocity of the projectile is then used later in the numerical analysis of the experiment. This regression fit is also used to determine the tilt of the projectile at impact.

(3) Piezoelectric Pins. Impact triggered piezoelectric (PZT) pins are use for multiple purposes in the experiment. These are small diameter, commercially procured lead-zirconium-titinate pins. First, two to four diametrically opposed PZT pin are mounted on in the target plate as flush as possible with the face of the target plate to obtain time fiducials that are used to obtain the impact time between the sample and impactor. Note that these times required corrections for the fact that they are slightly offset from the plane of the front of the target. Also note that these times will be different due to projectile tilt, and this must be taken into account when determining impact time from pin signals. Second, a single PZT trigger pin is set protruding from the face of the target plate. This PZT pin is used as a trigger mechanism for the high speed oscilloscopes used to record the data from all diagnostics..

(4) Sample. The final piece used in building the complete target is the material sample being studied. In this research target materials were Molybdenum and Dyneema. For simplicity all samples were fabricated into a circular shape with a predetermined thickness. For solid samples such as molybdenum, both sides

of the sample are lapped to within +/- 10μm of being flat and parallel. Dyneema being a flexible composite material means it cannot be lapped and is used as is, making sure to record accurate thickness variations.

Once the sample is properly prepared, a through hole consistent with the sample diameter is bored in the center of the target plate. The sample is then inserted into the target plate and edge glued into place with epoxy while ensuring that the sample face and target plate is as flush as possible. Deviations from flush are measured and recorded.

b.   *Projectile*
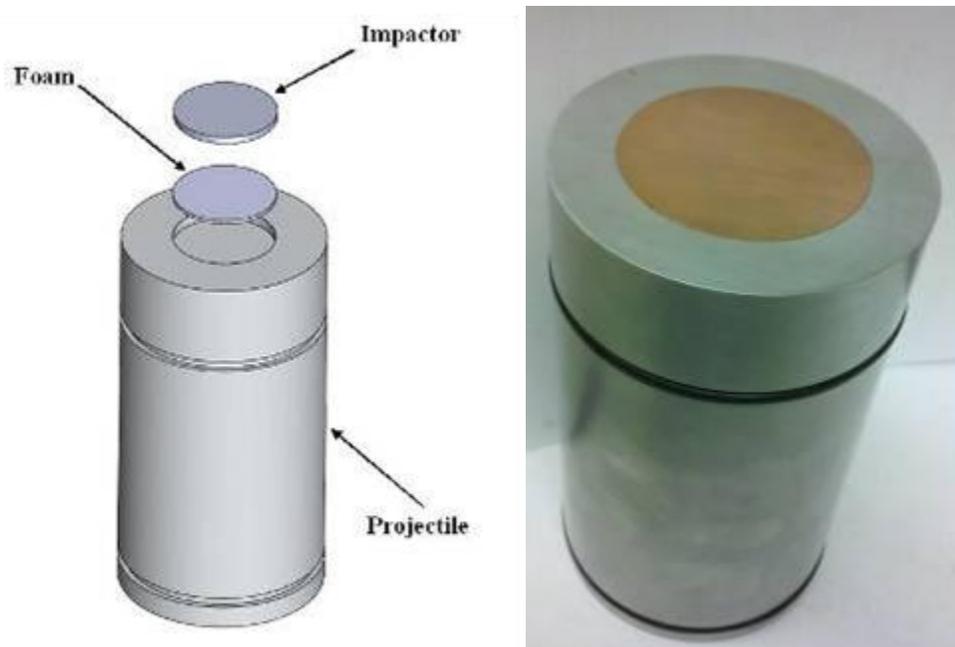
Figure 17.   Schematic and final product of projectile used in shock compression experiments

The second foundational piece required to perform fundamental shock compression experiments is the projectile. Shown in Figure 17 is a projectile used for both the Molybdenum and Dyneema experiments. The components used in the building of the projectile are the bullet and the impactor. Again, required measurements were recorded according to Appendix A.

(1) Impactor. The first component used in the assembly of the projectile is the impactor. A right circular cylinder of dimensions unique to the requirements of each experiment is fabricated from the material of choice for that experiment. For symmetric impact experiments the target sample and impactor are the same material. The impactor is then lapped to within +/- 10μm of flatness and inserted in the bullet.

(2) Bullet. The second component used in the fabrication of the projectile is the bullet. The bullet acts as the carrier of the impactor and is used to accelerate the impactor to the required experimental velocity. The bullets used in this research are fabricated using Aluminum 6061. After fabrication the face of the impact surface is lapped to within +/- 10μm of flatness. Once flat, a cavity that is of approximately the same dimensions of the impactor and any backing material is bored into the impact face of the bullet. The impactor and backing material, if necessary, are then inserted into the cavity and secured in place. The complete assembly is then lapped together to ensure co planarity and sound speeds are used to determine the final thickness of the impactor.
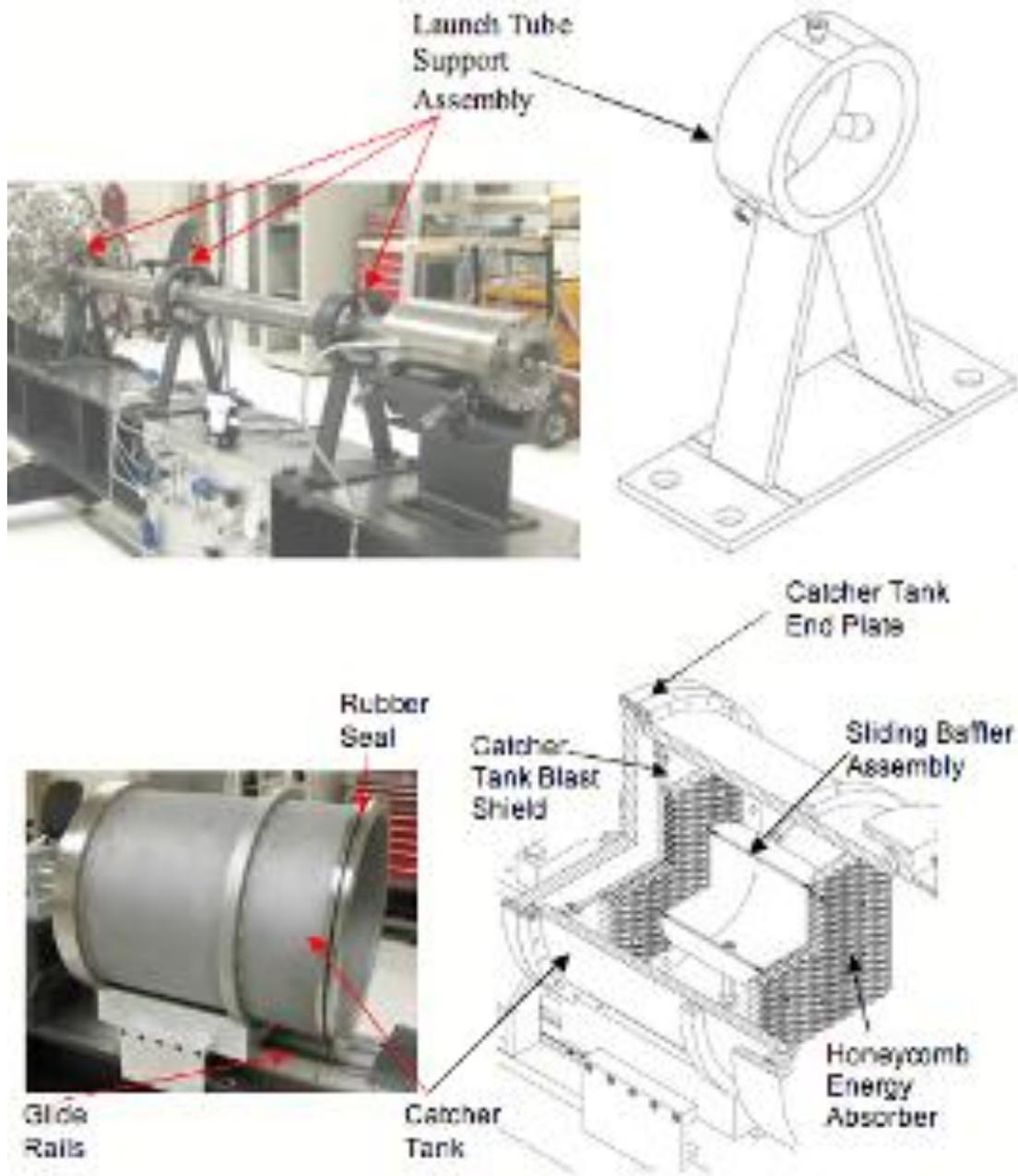
Figure 18.   Naval Postgraduate School low pressure gas gun at the Impact Physics Laboratory

The final piece of equipment required to perform fundamental shock compression experiments is a launcher, in which the projectile is accelerated to impact velocity. In this research the prime mover was the existing single stage light gas gun located at the Impact Physics Lab at the Naval Postgraduate School. The assembly, testing and operation are outlined by Ho [14] et al. and improvements performed by Denzel [3]. For the purposes of this research a new standard operating procedure was developed for standardized use of the gas gun and is contained in Appendix B.

2. Hugoniot Measurements

As discussed earlier, the fundamentals of shock physics used to develop accurate EOS models for materials are found in the shock jump conditions:

$$\frac{\rho_o}{\rho} = 1 - \frac{u_p}{U_s}$$

$$P - P_o = \rho_o U_s u_p$$

$$e - e_o = \frac{1}{2}\left(P + P_o\right)\left(\frac{1}{\rho_o} - \frac{1}{\rho}\right)$$

The parameters to be measured in order to resolve the jump conditions are the shock speed and particle speed behind the shock wave at different driver velocities. The first parameter to be measured is that of shock speed which is calculated using the transit time that the shock takes to travel through the sample as shown in Figure 19.
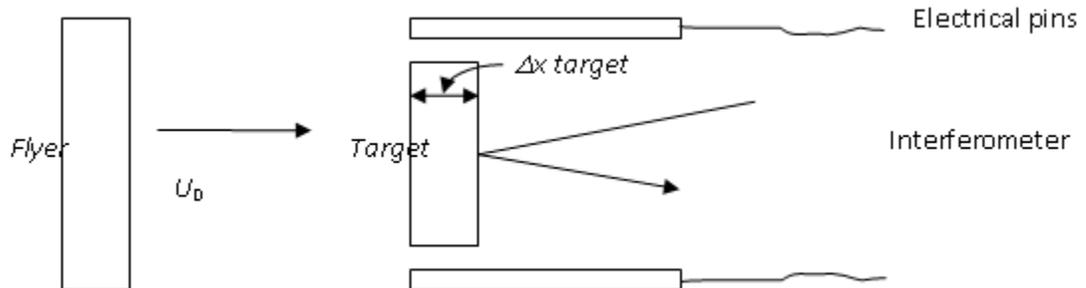
Figure 19.   Schematic representation typical shock experiment

For this research, shock transit times are calculated using timing fiducials obtained from the PZT pins that are flush with the target plate and sample, and shock

arrival time at the back of the sample from the time-resolved back surface velocity profile measured with the VISAR diagnostics system.   One complication is that there are different system delay times in the VISAR and pin units.   This is compensated for by measuring delays and applying an appropriate correction factor. Once the transit time is calculated it is a matter of a simple velocity relationship to determine the shock velocity through the sample.

The second parameter that must be measured in order to characterize a material is the particle velocity behind the shock wave moving through the material. For symmetric impacts the measurement of particle velocity can be shown to be half of the flyer velocity. This can be seen graphically by superimposing a generic $P - u_p$ Hugoniot for the flyer and target on the same plot. Where the two Hugoniots intersect will be the common shared state between the target and flyer given by the jump conditions. This is shown graphically in Figure 20.
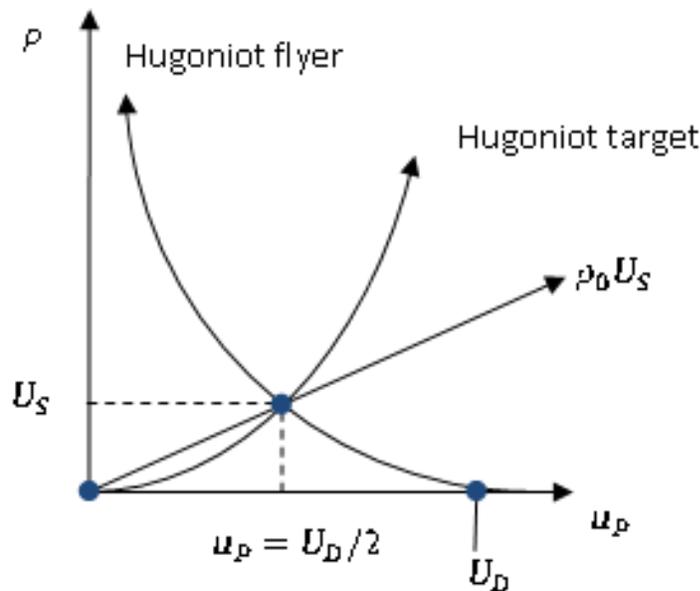
Figure 20.   Schematic representation of interactions between a flyer and target

This same graphical approach can be used for un-symmetric impacts using impactor materials for which the Hugoniot is already known.   The experimental method

that is used to measure particle velocity is somewhat more complicated. Typically when performing an experiment to measure the target particle velocity for a given flyer velocity a window is used on the rear of the sample to prevent the free surface release on the rear of the sample. The resultant particle velocity measured by the VISAR diagnostics is not the actual particle velocity behind the shock wave in the target material, but rather the particle velocity at the interface of the two materials as shown below in x-t space.
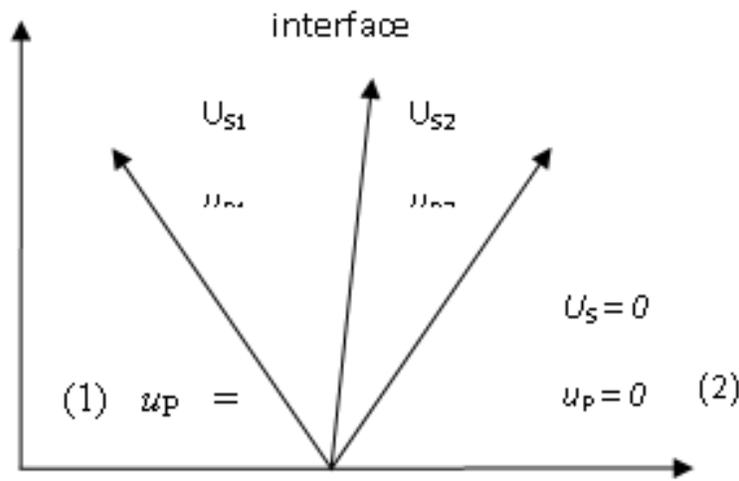
Figure 21.   Schematic representation of the state of two materials in contact during a shock event

The wave interactions at the surface of the rear of the sample and the window occur according to the shock impedance of each of the materials. Shock impedance is defined as:

$$Z_{shock} = U_s \rho_o$$

For an initially right going wave in the target material, which is labeled material A, and the window is labeled material B, the interactions at the surface between these materials follow the subsequent rules; (1) if $Z_A > Z_B$ a release wave will be reflected back into material A and the resulting pressure in both A and B will be less than the initial pressure

31

in A, and (2) if $Z_A < Z_B$ a re-shock and the resulting pressure in both A and B will be greater than the initial pressure A. This is shown graphically in $P-u_p$ space in Figure 22 for the $Z_A > Z_B$ case.
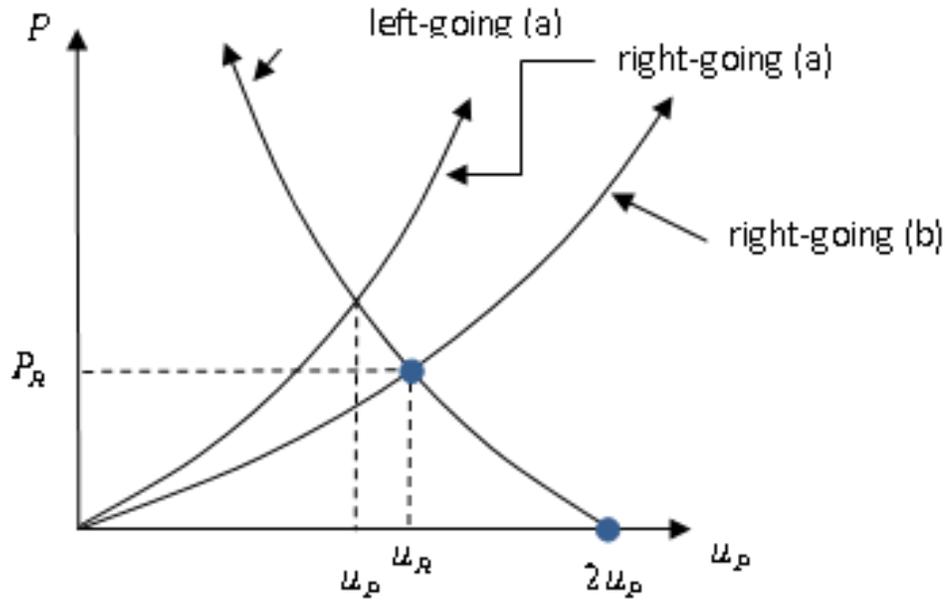
Figure 22.   Schematic representation of wave interactions used for impedance matching technique in P-u$_p$ space

The Initial and final states in the target material are then connected linearly by:

$$P_a - P_b = -Z_a \, u_a - u_b \quad .$$

Using the relation from the jump conditions:

$$P = Zu_p$$

The final particle velocity in the target can be found to be in both case (1) and case (2):

$$u_a = \left(\frac{\rho_{o_b}}{\rho_{o_a}}\right)\left(\frac{U_{s_b}}{U_{s_a}}\right)u_b\left(\frac{Z_b + Z_a}{2Z_b}\right)$$

This is the particle velocity in the target material in relation to the measured interface particle velocity from the VISAR data. This is a key point, as this relation allows us to calculate the particle velocity that was behind the incident shock in material A from the measured interface velocity. It is the particle velocity behind the incident shock in A that we need to determine a Hugoniot point in material A.

The preferred way of obtaining the particle velocity in the target material is to use impedance matching across the interface of the impactor and the target sample. In this method the Hugoniot of the impactor must be known and the Hugoniot of the target, though not characterized will also be given in the form:

$$U_s = c + Su_p$$

We must also measure the shock velocity in the target material. It is known that the pressure at the interface is equal on both sides of the interface, and that the particle velocity in the target is equal to the driver velocity minus the particle velocity in the impactor from the conservation of momentum. Therefore, using the assumed form of the Hugoniot for both the impactor and target, and inserting that Hugoniot into the pressure jump condition and setting the pressure in the impactor and the target equal, the following equation can be obtained:

$$\rho_{o_f} s_f\ u_{p_t}^2 - 2\rho_{o_f} s_f U_D + \rho_{o_f} c_f + \rho_{o_t} U_{s_t}\ u_{p_t} + \rho_{o_f}\ s_1 U_D^2 + c_f U_D\ = 0$$

where the parameters are defined as:

$\rho_o \equiv$ Initial density
$s \equiv$ Slope of known Hugoniot data
$U_D \equiv$ Projectile velocity
$c \equiv$ Intercept value of known Hugoniot data
$u_p \equiv$ Particle velocity

This equation can then be solved using the quadratic equation and will yield two roots, only one of which will be of any physical sense. This methodology of calculating the particle velocity of the target is used when the wave profile obtained from a window shot is shown to be more complex than a classical flattop trace.

3. Edge Releases

Another issue that must be taken into account when performing a shock compression experiment is the edge releases that occurs in the target material. Edge releases occur due to the shockwave interacting with the edge interface of the target and causing a release to travel sideways into the target material that then interacts with the shockwave traveling normally through the material. For isotropic materials, such as Molybdenum, the time at which this edge release reaches the back of the target sample can be estimated assuming that the release wave travels at a forty five degree angle from the edge of the sample. This estimation uses the longitudinal sound speeds of the impactor and target material as measured using the techniques prior to the shock compression experiment as outlined earlier. Letting l be the thickness, or length that the lateral shock wave must travel through, of the target material, and r be the radius of the target sample, the time that the edge wave reaches the rear surface of the target material for cases in which $C_i > C_t$ can be approximated by:

$$t \approx \frac{r}{C_i} + \frac{l}{C_i}\sqrt{\frac{C_l^2}{C_t^2} - 1}$$

where C_i and C_t are the ambient longitudinal sound speeds of the impactor and target respectively. For cases in which $C_i \leq C_t$ the time of edge release arrival at the rear of the target sample can be approximated by:

$$t \approx \frac{\sqrt{r^2 + l^2}}{C_t}$$

For orthotropic materials, such as Dyneema, this approximation does not hold. In the case of Dyneema it is assumed that the sound speeds in the fiber direction are

34

approximately 3-4 times faster than the sound speed in the through direction as shown in Chapman [11]. Since the through-thickness sound speed is much less than the axial fiber sound speed it is assumed that the edge release wave travels at the sound speed of the fiber at a near perpendicular direction relative to the through-thickness wave. Therefore, the time that the edge release wave reaches the rear of the target can be approximated by:

$$t \approx \frac{r}{C_{fiber}}$$

Using these approximations allows the experimentalist to ensure that the target is thin enough and has a large enough radius such that the edge release wave does not overtake the shockwave prior to reaching the rear surface of the target. This was a very important consideration for the Dyneema experiments.

D.   SPALL MEASUREMENTS

Another goal of this research was to measure the spall strength of pure Molybdenum metal to be able to do accurate computer simulations of systems that include this metal. Spall is defined as the dynamic strength of a material while under a dynamic tensile stress rather than a compressive stress. A spall event in a shock compression experiment is achieved by using a free surface on the rear of the target material, so that a release wave will be reflected there. This allows for the release waves that are reflected off of the rear of the target material to interact with the release waves that originate from the rear of the impactor material. These wave interactions form a region of negative (tensile) stress within the target. This is shown graphically in x-t space.
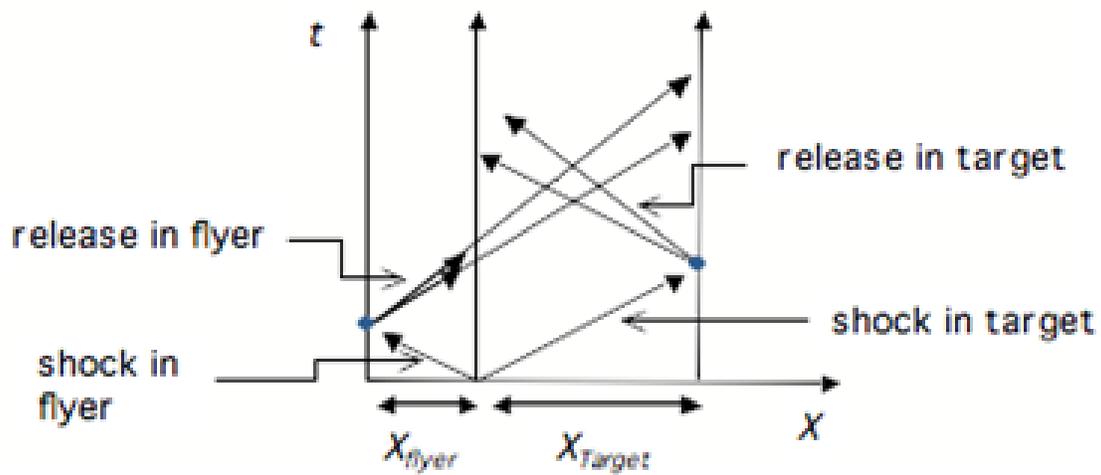
Figure 23.   Schematic x-t diagram of a generic spall experiment

If the tensile stress in this region is greater than the spall strength of the material, the material will fail. When this occurs the VISAR record will appear generically as:
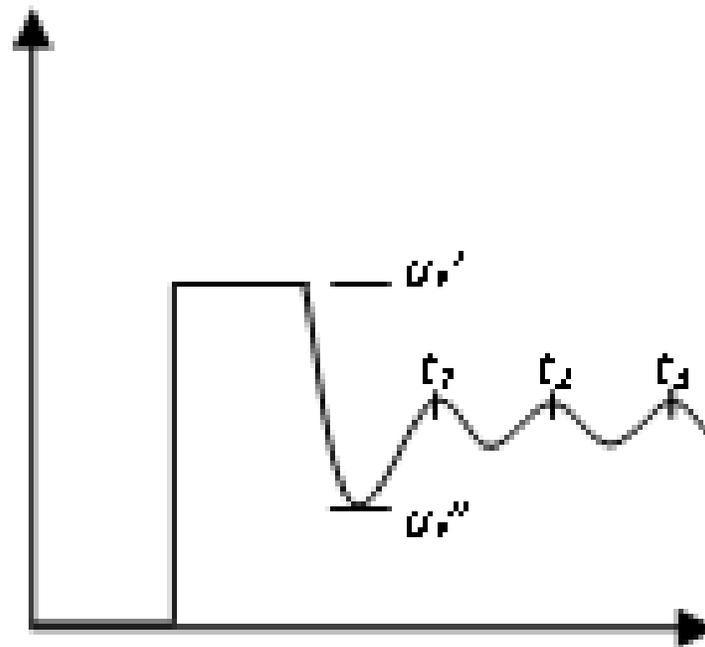
Figure 24.   Schematic representation of required measurements to be taken from a VISAR trace for spall calculations

Note that the 'dip' that is behind the flat top of this wave profile is what contains information about the spall process. We will not go into the details of the spall process here, but note that what we wish to measure is the difference in particle velocity between the flat top value and the value at the bottom of the 'dip' which is given by Δu_p where it is understood the u_p here is actually a free surface velocity.

To first order approximation the spall strength can be calculated by using the momentum jump condition:

$$\sigma_{spall} = \frac{1}{2} \rho_o C_b \Delta u_p$$

where C_b is the bulk sound speed as discussed earlier. But Use of the bulk sound speed here is not rigorously correct, but allows for an estimation of the real spall strength. To achieve a more accurate measurement a correction to the spall measurement must be made to account for the overtaking of the elastic wave in the material. This correction is known as a Romanchenko correction. The comparison of the measured to actual particle velocities during the spall signature is shown graphically.
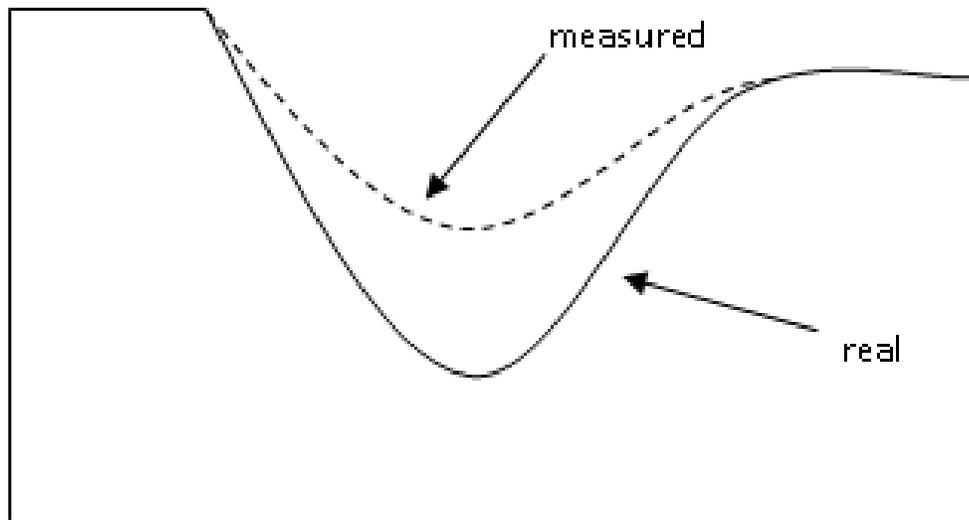
Figure 25.   Schematic representation of real versus measured spall traces

37

This correction is achieved by using:

$$\sigma_{spall} = \frac{1}{2}\rho_o C_b \ \Delta u_{fs} + \delta$$

where δ is defined as

$$\delta = h\left(\frac{1}{C_b} - \frac{1}{C_L}\right)\frac{\dot{u}_1 \dot{u}_2}{\dot{u}_1 + \dot{u}_2}$$

With h is defined as the spall thickness and found using:

$$h = \ t_3 - t_1 \ \frac{C_b C_L}{C_b + C_L}$$

where C_L is the longitudinal sound speed of the target material, t_1, t_3, $\dot{u}_1$, and $\dot{u}_2$ are measured from a generic VISAR record as shown below in Figure().
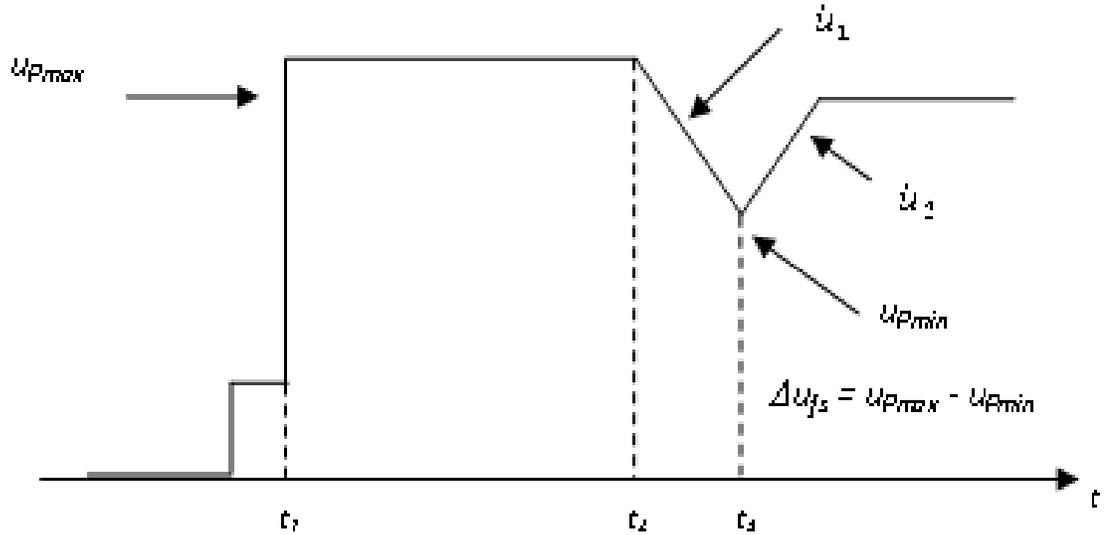
Figure 26.   Schematic view of measurements to be taken from a VISAR trace for use in spall correction calculation

E.   SOUND SPEED AT PRESSURE MEASUREMENTS

A separate goal of this research was to measure the sound speed in Molybdenum at high pressure. This means that the sound speed at the pressure achieved by the shock

event was measured. Sound speed at pressure can be a useful tool to predict phase changes in a material under dynamic loading, and is a key parameter for constraining EOS's. Using a simple velocity relationship corresponding to the times measured from the VISAR record, and the thickness of the target and flyer, as shown in Figures 27 and 28, the sound speed at the pressure of the shock can be calculated.
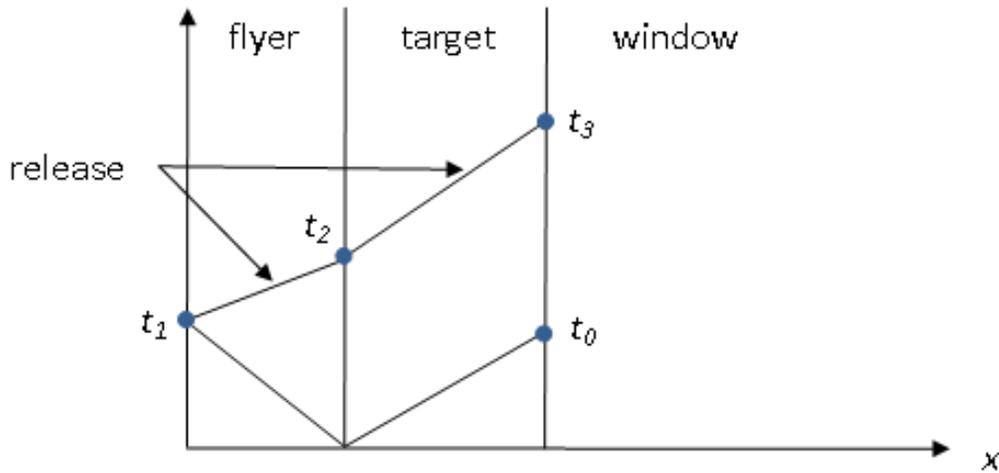
Figure 27.   Schematic x-t diagram of typical sound speed at pressure measurement
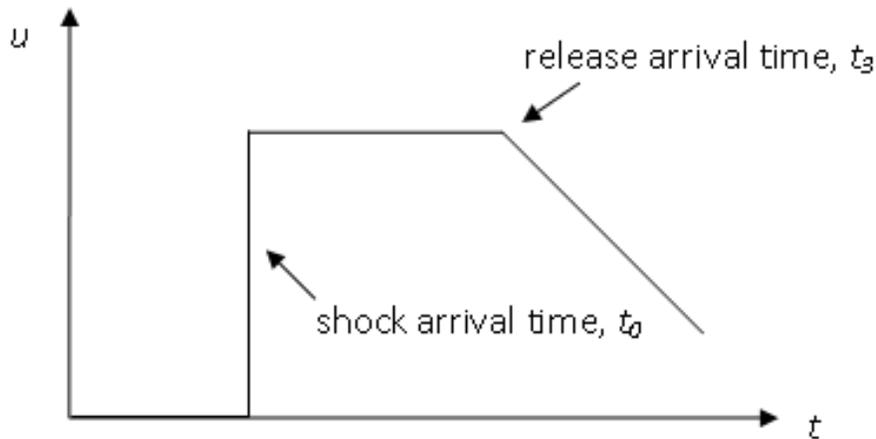
Figure 28.   Schematic particle velocity versus time trace showing were measurements are taken for sound speed at pressure calculations

Sound speeds at various pressures in Molybdenum were originally measured by Hixson [4] et al., where a solid to solid phase transition was theorized to be occurring in

the low pressure region. Using symmetric impact shock compression experiments at various low flyer velocities, this research will insert new data points to further corroborate or contradict existing theoretical EOS models for Molybdenum.

F.   UNCERTAINTY ANALYSIS

The final step in completely understanding the dynamic events that occur during a shock compression experiment is to understand the error involved in the measurements being taken during the experiment and the values that are calculated from those measurements. For a general equation of K:

$$K = F(A, B)$$

the uncertainty of Z is dependent on the uncertainty of the parameters A and B and given by:

$$\Delta K = \left(\left(\frac{\partial F}{\partial A} \right)^2 \Delta A^2 + \left(\frac{\partial F}{\partial B} \right)^2 \Delta B^2 \right)^{1/2}$$

This general expression for uncertainty can then be applied to the specific parameters measured and calculated in this research. Parameters that are focused on in this research are the sound speed at pressure, shock impedance, shock speed, stress state and the associated particle velocities achieved for each experiment.

Shock speed for an experiment in this research is dependent on two factors; distance and time, therefore the error in the calculated shock speed can be shown to be:

$$\Delta U_s = \left(\left(\frac{\Delta x}{t} \right)^2 + \left(\frac{x \Delta t}{t^2} \right)^2 \right)^{1/2}$$

and the fractional uncertainty in calculated shock speed is:

$$\frac{\Delta U_s}{U_s} = \left(\left(\frac{\Delta x}{x} \right)^2 + \left(\frac{\Delta t}{t} \right)^2 \right)^{1/2}$$

Similarly, the stress state that is achieved during the shock event is dependent on initial density, shock speed and particle speed as shown in the jump conditions earlier. The error in the stress can be shown to be:

$$\Delta P = \left[\left(U_s u_p \Delta \rho_o \right)^2 + \left(U_s \rho_o \Delta u_p \right)^2 + \left(\rho_o u_p \Delta U_s \right)^2 \right]^{\frac{1}{2}}$$

with the fractional uncertainty given as:

$$\frac{\Delta P}{P} = \left[\left(\frac{\Delta \rho_o}{\rho_o} \right)^2 + \left(\frac{\Delta U_s}{U_s} \right)^2 + \left(\frac{\Delta u_p}{u_p} \right)^2 \right]^{\frac{1}{2}}$$

Shock impedance can also be determined along the same logical path as the previous examples. The error in the shock impedance can then be shown to be:

$$\Delta Z = \left[\left(U_s \Delta \rho_o \right)^2 + \left(\rho_o \Delta U_s \right)^2 \right]^{\frac{1}{2}}$$

Determining the uncertainty in the particle velocity can be somewhat more challenging. For shots that use a window interface when measuring particle velocities, a second calculation using impedance matching must be performed in order to obtain the particle velocity behind the shock front within the target. The relationship to determine the target pressure behind the shock wave was given previously as:

$$P_a = P_b \left(\frac{Z_a + Z_b}{2Z_b} \right)$$

where a denotes the first material and b denotes the second material respectively. Error in the second material pressure is then given as:

$$\Delta P_a = \left[\left(\frac{\partial P_a}{\partial P_b} \right)^2 \Delta P_b^2 + \left(\frac{\partial P_b}{\partial Z_a} \right)^2 \Delta Z_a^2 + \left(\frac{\partial P_b}{\partial Z_a} \right)^2 \Delta Z_b^2 \right]^{\frac{1}{2}}$$

After taking the partial derivatives and dividing both sides of the equation by P_T, the fractional uncertainty is given by:

$$\frac{\Delta P_a}{P_a} = \left(\left(\frac{\Delta P_b}{P_b} \right)^2 + \left(\frac{\Delta Z_a}{Z_a + Z_b} \right)^2 + \left(\frac{Z_a}{Z_a + Z_b} \right)^2 \left(\frac{\Delta Z_b}{Z_b} \right)^2 \right)^{1/2}$$

where, $\Delta P_b / P_b$ is found using an earlier calculation. Once $\Delta P_a / P_a$ is found, then it can be plugged back into the generic form of the fractional uncertainty in pressure and rearranged to solve for the fractional uncertainty in the particle velocity behind the shock wave in the target and yields:

$$\frac{\Delta u_p}{u_p} = \left(\left(\frac{\Delta P}{P} \right)^2 - \left(\frac{\Delta \rho_o}{\rho_o} \right)^2 - \left(\frac{\Delta U_s}{U_s} \right)^2 \right)^{1/2}$$

In the analysis of the error of sound speed at pressure measurements for Molybdenum, the error in the shock density is given by:

$$\Delta \rho = \left(\left(\frac{\rho_o u_p}{U_s - u_p{}^2} \right)^2 \Delta U_s^2 + \left(\frac{\rho_o U_s}{U_s - u_p{}^2} \right)^2 \Delta u_p^2 \right)^{1/2}$$

With the fractional uncertainty in the shock density found to be:

$$\frac{\Delta \rho}{\rho} = \left(\left(\frac{u_p}{U_s - u_p} \right)^2 \left(\frac{\Delta U_s}{U_s} \right)^2 + \left(\frac{\Delta u_p}{U_s - u_p} \right)^2 \right)^{1/2}$$

The sound speed at pressure measurement is analogous to the measurement of shock speed and therefore the error in the in the sound speed is found to be:

$$\Delta c = \left(\left(\frac{\Delta x}{t} \right)^2 + \left(\frac{x \Delta t}{t^2} \right)^2 \right)^{1/2}$$

And the fractional uncertainty in the sound speed measurement is:

$$\frac{\Delta c}{c} = \left(\left(\frac{\Delta x}{x} \right)^2 + \left(\frac{\Delta t}{t} \right)^2 \right)^{1/2}$$

Finding the uncertainty in the particle velocity of a target using the impedance matching techniques across the impactor-target interface become much more complicated very quickly. The final quadratic relationship to find the particle velocity in the target was found to be:

$$\rho_{o_f} s_f \ u_{p_t}^2 - \ 2\rho_{o_f} s_f U_D + \rho_{o_f} c_f + \rho_{o_t} U_{s_t} \ u_{p_t} + \rho_{o_f} \ s_f U_D^2 + c_f U_D \ = 0$$

The particle velocity is found using the quadratic equation:

$$u_p = \frac{-b \pm \sqrt{b^2 - 4ac}}{2a}$$

Where:

$$a = \rho_{o_f} s_f$$

$$b = - \ 2\rho_{o_f} s_f U_D + \rho_{o_f} c_f + \rho_{o_t} U_{s_t}$$

$$c = \rho_{o_f} \ s_1 U_D^2 + c_f U_D$$

Therefore, the uncertainty in the particle velocity is then:

$$\Delta u_p = \left[\left(\frac{\partial u_p}{\partial a} \right)^2 \Delta a^2 + \left(\frac{\partial u_p}{\partial b} \right)^2 \Delta b^2 + \left(\frac{\partial u_p}{\partial c} \right)^2 \Delta c^2 \right]^{\frac{1}{2}}$$

The uncertainty in a is ignored since the Hugoniot of the flyer is well characterized and the density of the flyer is known to be within a negligible error. That leaves the b and c terms. The terms used to plug into the overall above equations were found to be:

$$\frac{\partial u_p}{\partial b} = \left(\frac{1}{2a}\right)\left(-1 \pm \frac{2b}{\sqrt{b^2 - 4ac}}\right)$$

$$\frac{\partial u_p}{\partial c} = \pm\left(\frac{1}{2a}\right)\left(\frac{-4a}{\sqrt{b^2 - 4ac}}\right)$$

$$\Delta b = \left[\left(2\rho_{o_f} s_f\right)^2 \Delta U_D^2 + \left(\rho_{o_t}\right)^2 \Delta U_{s_t}^2 + \left(U_{s_t}\right)^2 \Delta \rho_{o_t}^2\right]^{\frac{1}{2}}$$

$$\Delta c = \left[\left(\rho_{o_f}\right)\left(2 s_f U_D + c_f\right)^2 \Delta U_D^2\right]^{\frac{1}{2}}$$

These preceding equations and analysis will be used to compute the uncertainty of the measured and calculated parameters of interest within contained within this research.

III. EXPERIMENTAL SETUP AND RESULTS

A. MOLYBDENUM

1. Molybdenum Sound Speed at Pressure Measurements

a. NPS Experiments
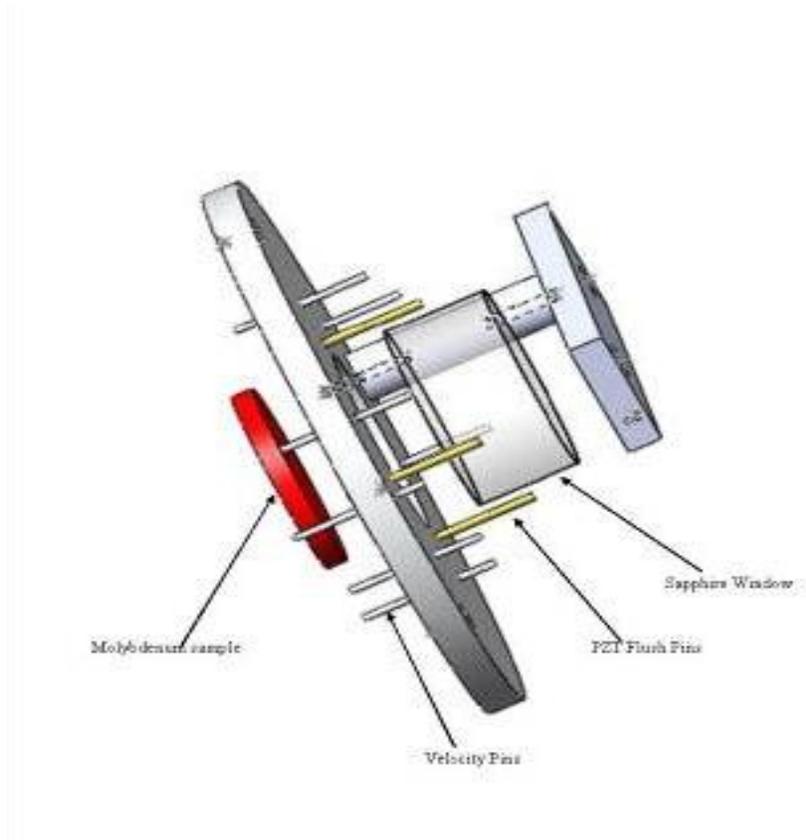
Figure 29.   Schematic view of Molybdenum Target

Figure 29 shows a schematic representation of the target setup for the sound speed at pressure measurements performed in this research. As can be seen, the sample is backed by a viewing window, in this case sapphire, that ensure a full free surface release back into the target does not occur. Diagnostics used in these experiments were single point VISAR, two diametrically opposing flush PZT pins for measuring a reference impact time at the front of the target sample and six velocity pins at a fixed

45

radius at sixty degree intervals around the target sample at stepped protrusion lengths for projectile tilt and projectile velocity measurement. A total of two successful Molybdenum shots were completed at the Impact Physics Laboratory at NPS and are discussed below.

(1)   NPS Shot # 10_8

(a)   *Shot Design*. This shot was the first attempt to extract a sound speed at an induced specific stress state in Molybdenum. In order to anticipate the results of the experiment a rough hand calculation was performed using assumptions to predict the expected results. For simplicity a symmetric impact experiment was chosen using a target thickness of 4mm, an impactor thickness of 3mm and a 19mm z-cut sapphire window behind the sample for this experiment. Using known Hugoniot data as found in Marsh [11] et al., a desired projectile velocity of 0.3 km/s, and approximating the sound speed at pressure as 20% higher than ambient sound speed, an approximate x-t diagram was constructed to represent anticipated results as shown in Figure 30.
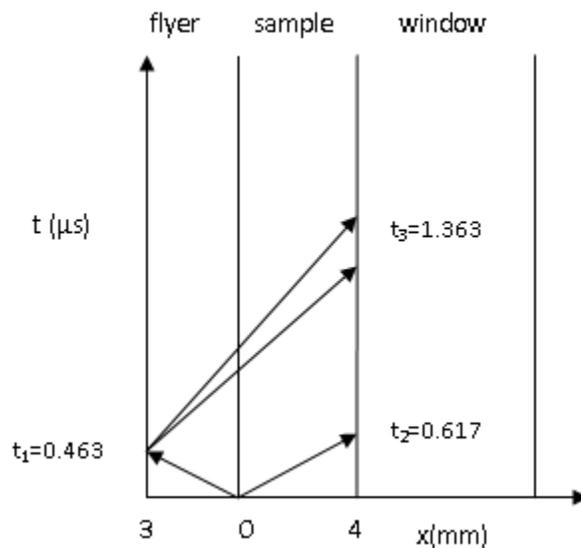
Figure 30.   Preliminary x-t diagram of symmetric Molybdenum shot

The anticipated arrival time of the shock wave at the target-window interface was 0.617μs after impact and the release wave was expected to arrive

at the same interface 0.746μs later. Using the designed diameter for the target sample the edge releases were expected to pinch off the through wave at 3.22μs after impact, which was well after the desired event of interest is completed.

(b) Shot summary. To achieve the desired projectile velocity of 0.3 km/s, using a projectile mass of 489.8 grams, the breech pressure that was required was $880 \, {}^{lbf}/_{in^2}$. The final dimensions of the Molybdenum impactor and target was 1.5 inch diameter for both target and impactor; and 2.915 mm and 3.877 mm thickness for impactor and target respectively. The shot was successful. All flush pins and velocity pins triggered as expected giving good signal for projectile velocity, projectile tilt, and a time fiducial marking the time of impact. Good VISAR data were obtained from the diagnostics with a flattop lasting approximately 0.9μs at an interface velocity of 0.161 km/s. The VISAR record is shown in Figure 31. Markers indicate were times were taken to be used in data analysis.
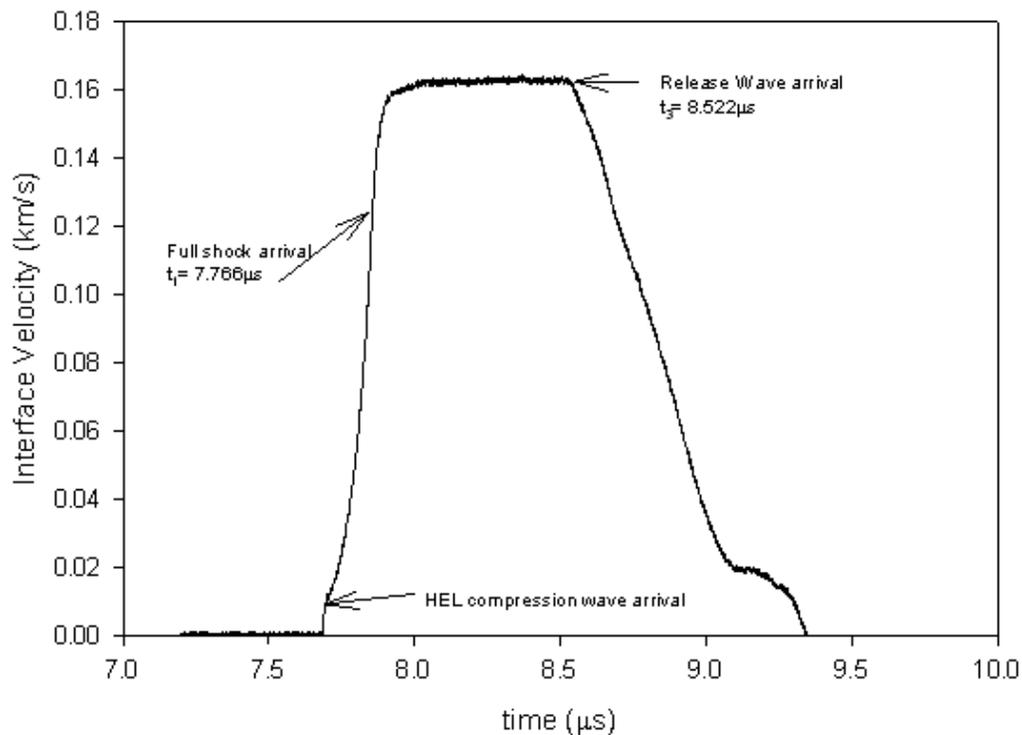
Figure 31.   VISAR record of Molybdenum symmetric impact of NPS shot 10_8

47

(2) NPS Shot #11_4

(c)   Shot design. Shot 11_4 was a second attempt to measure the sound speed at stress state in the very low pressure regime for polycrystalline Molybdenum. In order to minimize the error associated with the two wave structure in the target, the design of this shot was slightly different than that of earlier sound speed shots. The variable that was changed to minimize errors was that of the thickness of the impactor and the target. Lowering the thickness of the impactor decreases the amount of material that has not been shocked to the final plastic state that the reflected initial wave from the rear of the impactor must travel through before interacting with the second wave that is still traveling to the left.

It was chosen to perform this shot at a slightly higher projectile velocity than that of shot 10_8 in order to establish the beggings of a trend in the low pressure regime. The anticipated x-t diagram for the initial approximations is shown in Figure 32.
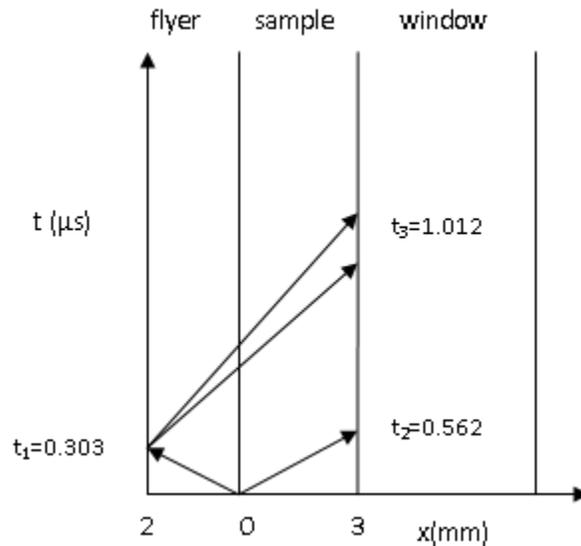
Figure 32.   Preliminary x-t diagram of NPS shot #11_4

(d) Shot Summary

48

Figure 33.   Final construction of NPS shot # 11_4

The final dimensions that were used for NPS shot #11_4 are summarized in Table 2, including actual projectile velocity achieved and Figure 33 shows the final construction of the target and projectile used.

Table 2.   Final experimental parameters for NPS shot# 11_4

Shot Number	Target Material	Expected Projectile Velocity (km/s)	Target Density (g/cc)	Target Thickness (mm)	Impactor Material	Impactor Density (g/cc)	Impactor Thickness (mm)
11_4	Molybdenum	0.350	10.200	2.946	Molybdenum	10.200	2.164

The diagnostics used in this shot were velocity pins, flush pins to provide a reference time of impact, and single channel VISAR. All velocity pins triggered as

49

expected, and both flush pins triggered giving a good reference time of impact. The VISAR system triggered as expected and a strong signal was received that yielded a traditional flattop and indications of both an elastic and plastic wave arrival as well as the expected release point from the reflected wave from the rear of the impactor. The VISAR record is shown in Figure 34.

NPS shot #11_4 VISAR trace
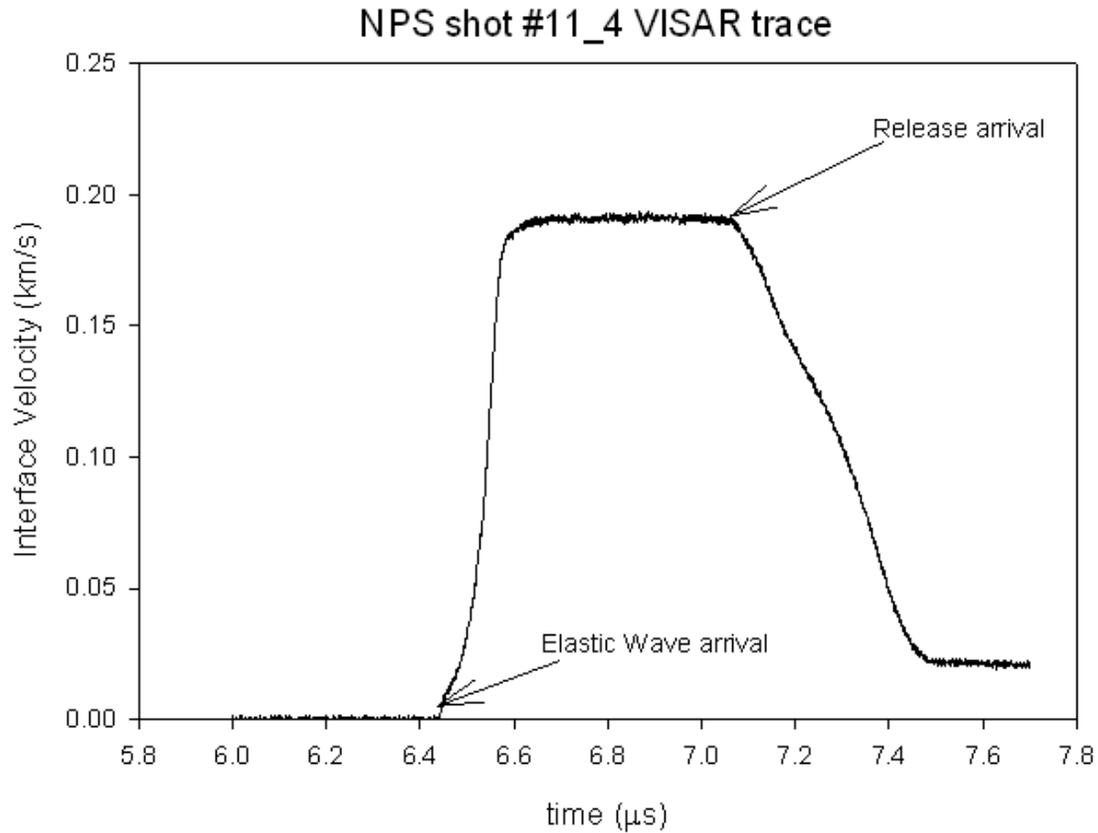
Figure 34.   VISAR record for NPS shot #11_4

b.   *Washington State University Experiment*

(1) Shot Design. The purpose of the experiment that was performed at the Institute for Shock Physics (ISP) at Washington State University (WSU) was to obtain a sound speed at pressure measurement in the midrange regime between the high pressure research performed by Hixson [4] and the low pressure research performed in this research.

50

In order to achieve a pressure state in the desired regime, it was decided to perform this experiment on the 30mm bore powder gun at WSU. Due to the higher stress state desired for this experiment, the initial symmetric design used at NPS needed to be abandoned. The reason was that the sapphire window on the rear of the target sample is known to become opaque in the 15-16 GPa range as shown by Barker [15]. Therefore, it was decided to perform what is referred to as a reverse ballistic experiment. The impactor would remain Molybdenum, but the target material would now be a Lithium Fluoride (LiF) window vapor plated with a reflective material at the impact surface. This kind of experiment is often referred to as 'reverse ballistic' in the shock compression community. Since the shock Hugoniot of Molybdenum is well characterized, the necessity for performing a shock speed measurement is no longer present. Figure 35 shows a cartoon view of the initial geometry expected for this experiment.
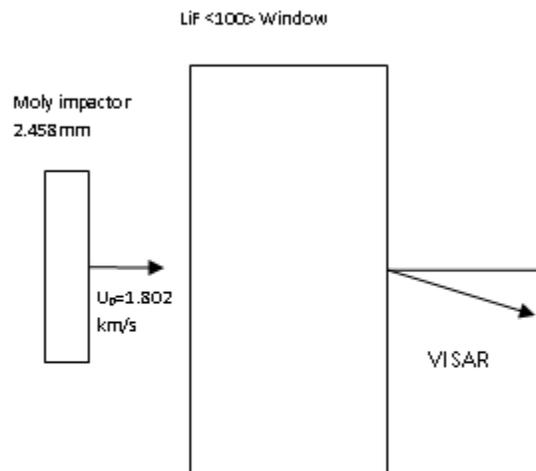
Figure 35.   Initial geometry for WSU reverse ballistic experiment

A simplification that arises due to the shot geometry is that there is no longer a need to adjust the shock arrival at the viewing interface to a reference time based on a known shock Hugoniot of the target. Now the viewing surface for the VISAR is directly focused on the impact surface therefore the impact reference time is directly measured with a high degree of accuracy. The shot was designed for the impactor to be

51

2.5mm tick and a diameter of 27mm impacting a 38mm diameter, and 12.8mm thick LiF window target at 1.8 km/sec. From known Hugoniot of LiF and Molybdenum from Marsh [13], an initial t-x diagram of the expected results was constructed and is shown in Figure 36.
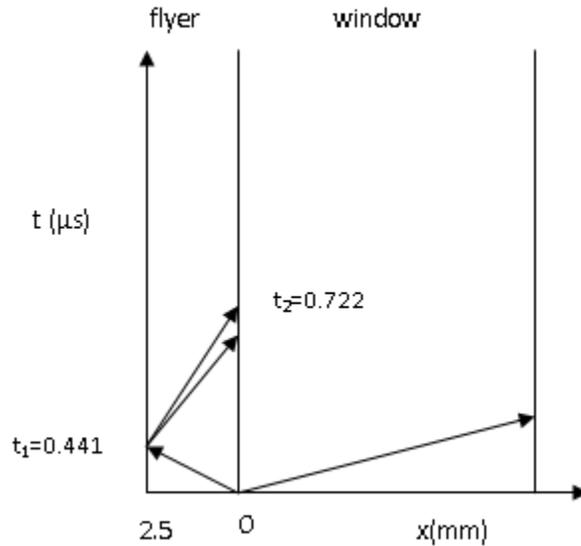
Figure 36.   Preliminary x-t diagram for WSU Molybdenum sound speed at pressure experiment

At this higher impact speed and due to the difference in size of the target and impactor, the effect of edge releases needed to be closely analyzed and taken into account of the shot design. Using the edge release calculation as discussed earlier and assuming that the edge releases would be limited by the smaller impactor diameter rather than the diameter of the target, it was found that the edge release wave in the target would pinch off the lateral shock wave in ~1.6µs, which is well after the expected release arrival time as predicted by the initial x-t diagram.

Diagnostics that were used in this experiment included single point VISAR to measure the shock wave at the impact plane, and three more channels of VISAR diametrically positioned around the center VISAR for projectile tilt calculations. The final material measurements for the impactor and target are summarized in Table 3.

Table 3.   Initial shot characteristics of WSU reverse ballistic experiment

Shot Number	Target Material	Expected Projectile Velocity (km/s)	Target Density (g/cc)	Target Thickness (mm)	Impactor Material	Impactor Density (g/cc)	Impactor Thickness (mm)
WSU Mo	LiF	1.800	2.640	12.760	Molybdenum	10.200	2.458

(2) Shot Summary. Figure 37 shows two views of the final target setup that was used for the reverse ballistic experiment.

Figure 37.   Front and rear surface views of LiF target after final assembly

The Molybdenum-LiF reverse ballistic shot at WSU was performed without incident. The measured impact speed was 1.802 km/sec. Good VISAR traces were obtained from all channels. As expected a sharp rise was observed at the time of impact on the Viewing surface and a stable flattop was measured lasting approximately 0.7μs in length. The measured interface particle velocity was 1.376km/sec, which is good agreement with the expected interface velocity predicted from known Hugoniot data. The VISAR record is shown in Figure 38 with the required times for calculating sound speed at stress annotated.

WSU Molybdenum-LiF VISAR trace

Release arrival
$t_2 = 6.043$

Impact
$t_0 = 5.344\mu s$
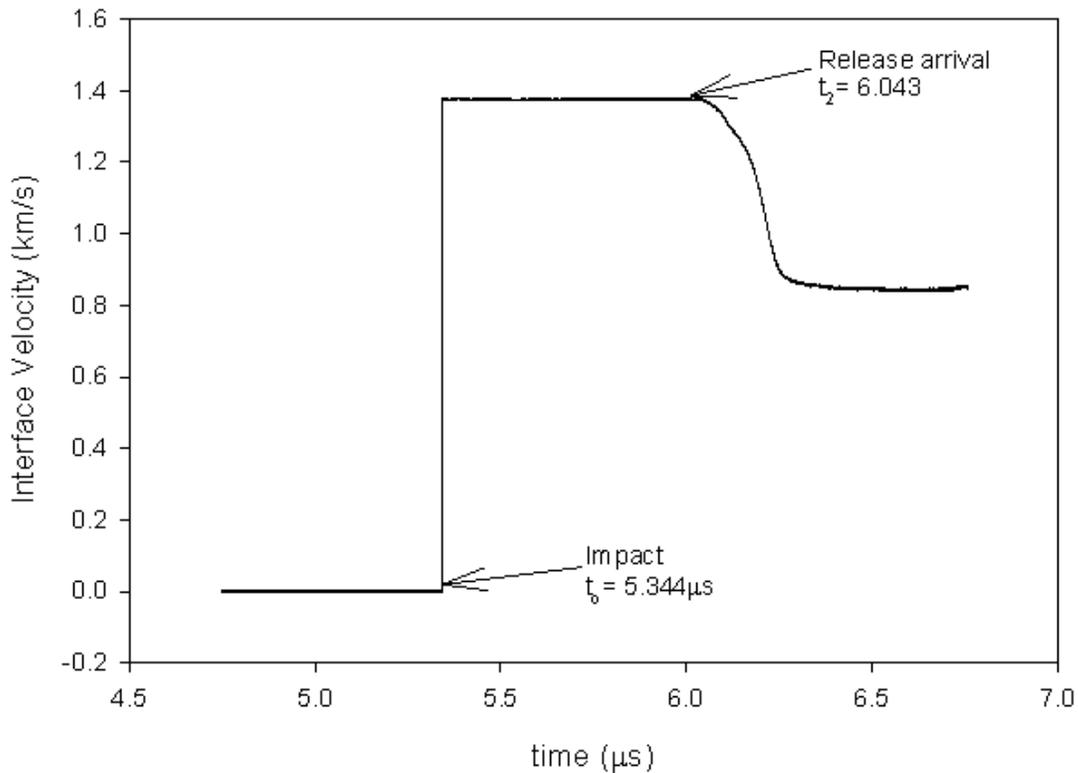
Figure 38.   VISAR record for WSU molybdenum sound speed at pressure shot

c.   *Sound Speed at Pressure Data Analysis*

The basic analysis techniques outlined in Chapter II of this research can be used to determine relevant parameters that can be calculated from the data collected during the performance of these experiments with a fair amount of accuracy, but complications due to material strength must be taken into account.

Since the Hugoniot of Molybdenum is well established and tabulated by Marsh [4], all shock speeds used for analysis will draw from the known Hugoniot of Molybdenum. Additionally, due to the relatively low stresses achieved within the Molybdenum samples during these experiments, it cannot be assumed that the plastic wave has overdriven the elastic precursor wave and therefore this two wave structure within the material must be accounted for.

54

The HEL for Molybdenum was shown to be relatively constant at ~2.3-2.8 GPa independent of final stress state by Furnish [16]. However, the HEL measured for this research was from the free surface velocity of the spall measurement in Chapter III.2 was consistent with a much lower value. This is likely due to the differences in initial materials processing performed on the samples prior to delivery. Therefore, it can be assumed that the elastic compression wave that travels through the Molybdenum will travel at the same speed regardless of final stress state in the sample. For this research, it will be assumed that the elastic wave will travel ambient longitudinal sound speed as measured earlier. The plastic wave that is traveling in the impactor will travel at the known shock speed under the given experimental conditions. The final x-t diagram for all Molybdenum sound speed at stress experiments are given in Figure 39, Figure 40, and Figure 41.
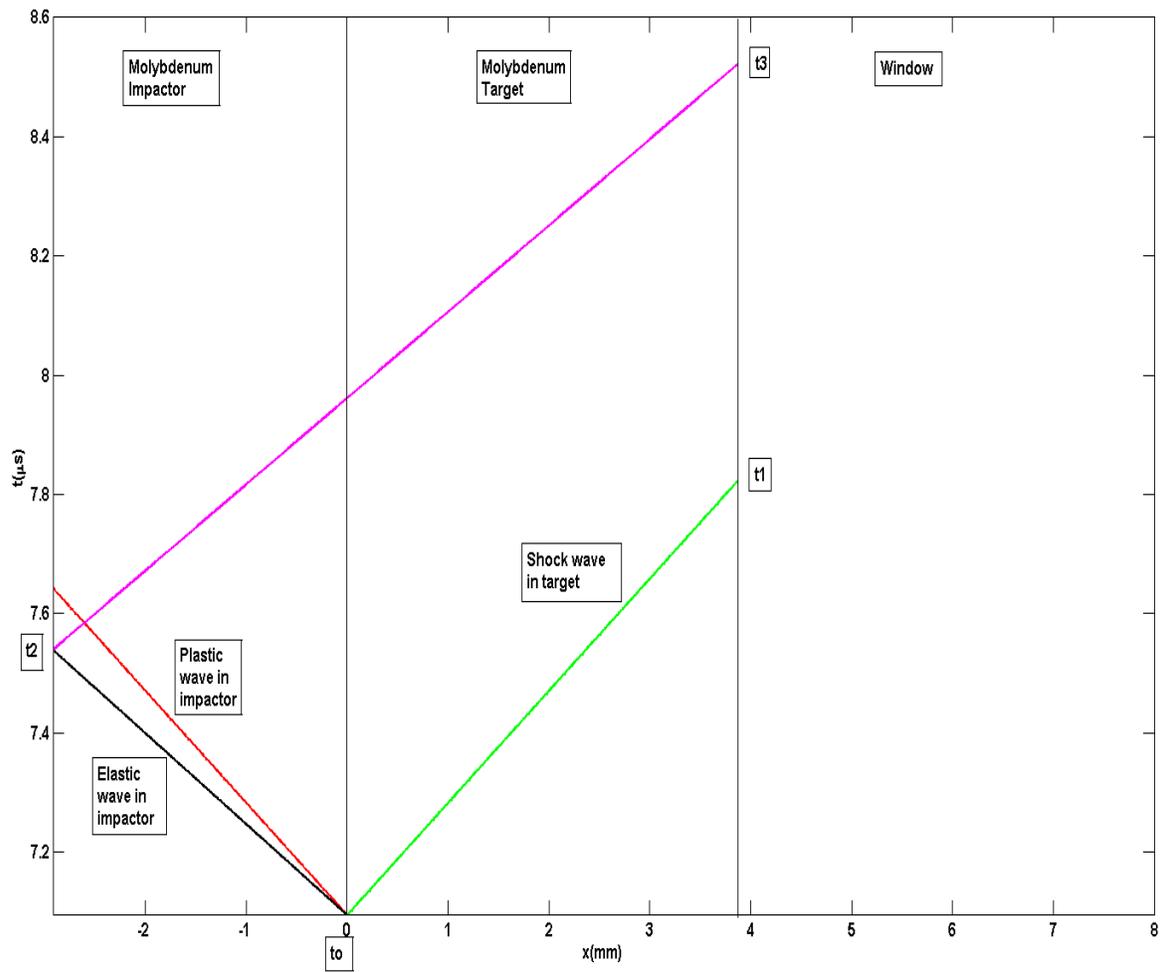
Figure 39.　　Final x-t diagram of NPS shot 10_8
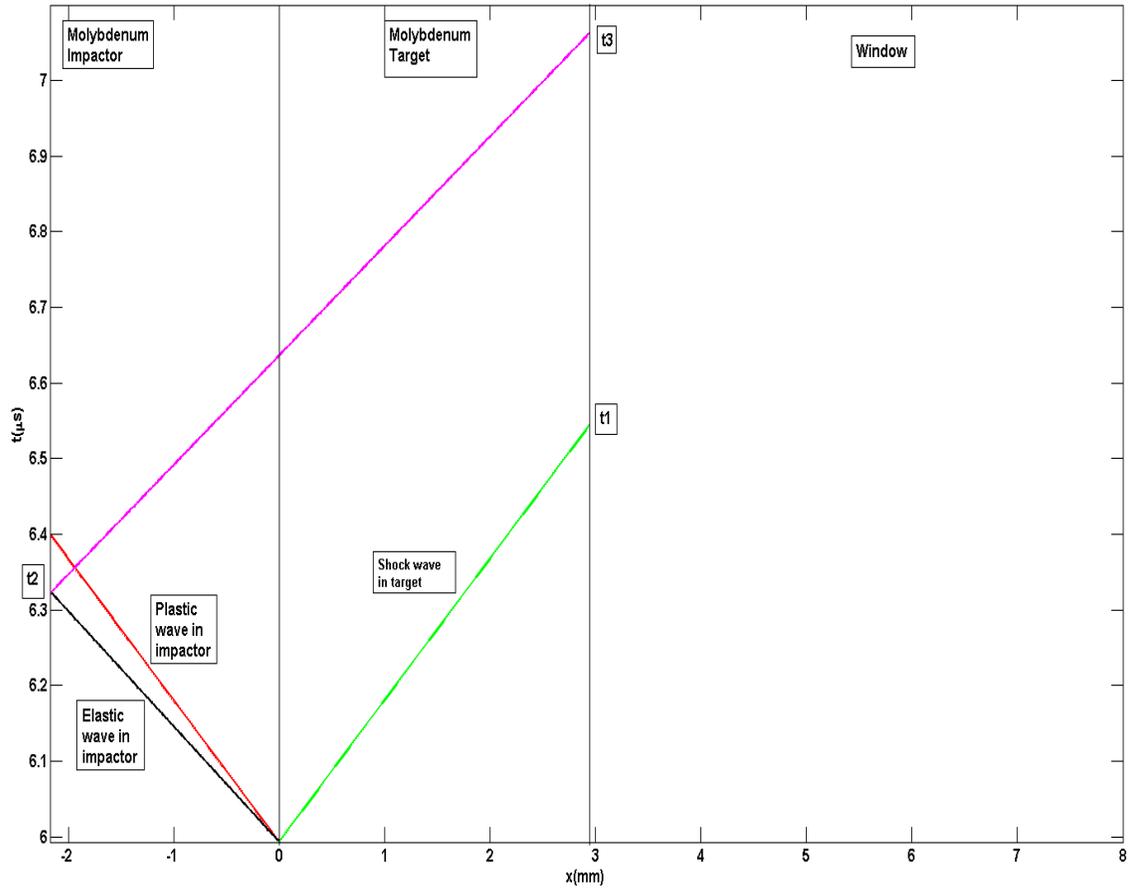
Figure 40.   Final x-t diagram of NPS shot #11_4
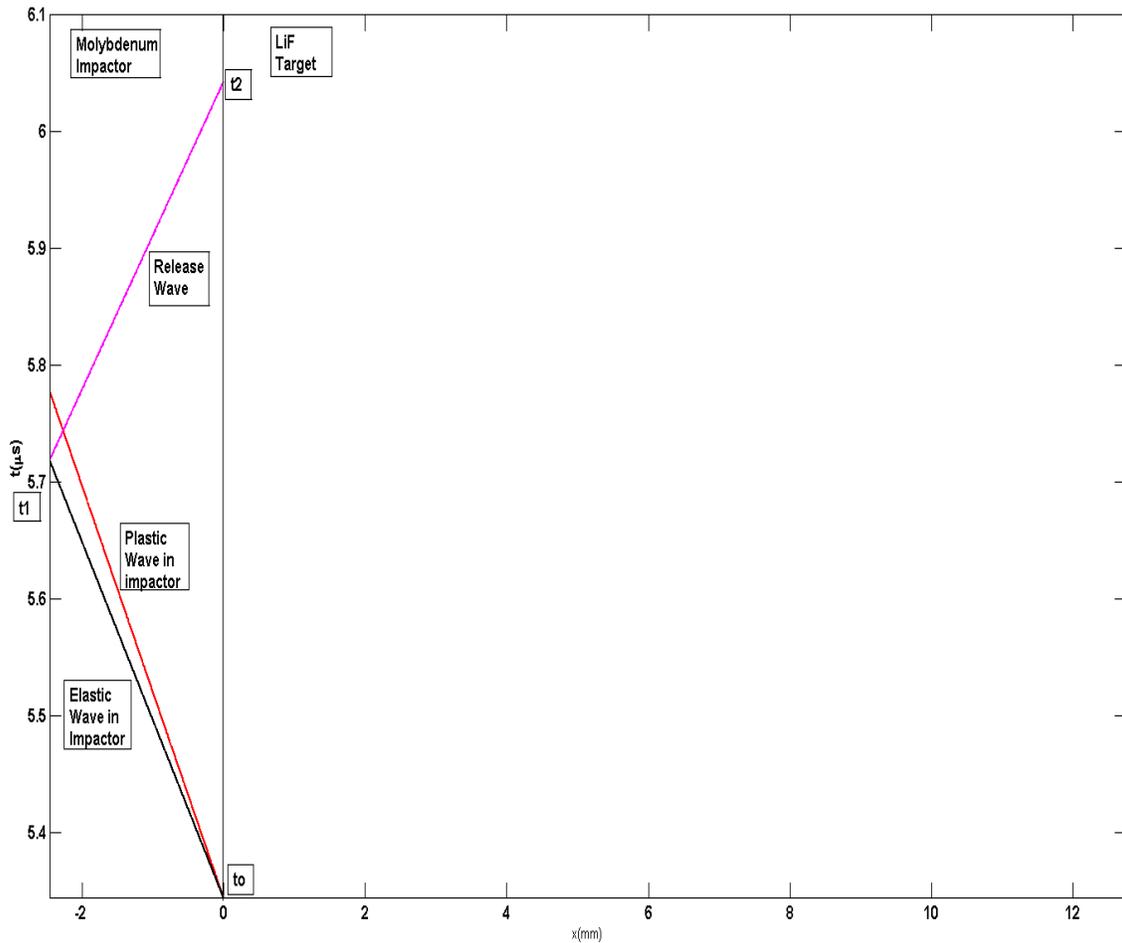
Figure 41.   Final x-t diagram of WSU Molybdenum reverse ballistic experiment

As can be seen from these x-t diagrams, the reflected elastic release wave from the back of the impactor will travel through a portion of material that is not yet at the final plastic state since the plastic wave has not yet reached that region. Therefore, the initial speed of this release wave is not yet at the full sound speed at the induced pressure state. The reflected elastic wave then interacts with the left going plastic wave that causes a small change in observed sound speed. For this research, the distance that the release wave travels prior to interacting with the plastic wave is small compared to the overall distance traveled by the release wave; therefore, it will be assumed that the right going release wave to the viewing interface as traveling at the full sound speed at stress state,

58

and an appropriate error will be attached to the calculation of the final sound speed at stress value. Through careful analysis, it was determined that the measured sound speed at pressure for these experiments was measured as systematically lower that actual values due to these complex wave interactions, and that approximately an additional uncertainty of 1% in the sound speed measurement was required to account for these wave interactions.

The final values calculated relevant to the sound speed at stress experiments are found in Table 4.

Table 4.   Calculated values from Molybdenum Sound Speed at stress experiments

Shot Number	Target Material	Measured Projectile Velocity (km/s)	Tilt (mrad)	Shock Speed in Mo (km/s)	Particle Speed in Mo (km/s)	Stress (GPa)	Measured Sound Speed at Stress in Mo (km/s)	Calculated Shock Density in Mo (g/cc)
10_8	Molybdenum	0.311 ± 0.004	6.978	5.316	0.156	8.470	6.902	10.507
WSU	LiF	1.802 ± 0.0014	2.3	5.664	0.430	25.176	7.657	11.037
11_4	Molybdenum	0.351 ± 0.005	3.07	5.340	0.176	9.574	6.859	10.547

d.   *Molybdenum Sound Speed at Pressure Uncertainty Analysis*

The largest sources of error associated with the measurement of the sound speed at pressure for Molybdenum can be attributed to three factors; one, the inability to measure thickness of samples at the NPS facility accurately to a micron level, two, the variance in where to pick a time from the VISAR trace as a marker for when the release wave reaches the sample-window interface, and three, the perturbation of the release wave as it travels back through the impactor after reflection and interacts with the trailing

plastic wave that has not yet reached the rear of the impactor. The first two factors can be accounted for using the analysis outlined in Chapter II of this research, but the third requires a bit more thought and is accounted for as discussed in Chapter III.1.c.

Using the analysis outlined in Chapter II, the percent error in the shock state density and the sound speed at pressure were calculated from reasonable error assumptions in measured values of shock speed, particle speed, thickness of impactor and target and times of release taken from the VISAR trace. Table 5 summarizes the calculated percent error for the sound speed at pressure measurements performed for this research.

Table 5.   Summary of calculated percent error for Molybdenum Sound Speed at pressure measurements

Shot Number	Sound Speed at Pressure Percent Error	Density at Shock State Percent Error
10_8	4.0%	3.0%
WSU	5.1%	0.9%
11_4	4.7%	3.4%

2. Molybdenum Spall Measurement 2 (NPS Shot # 10_12)

a. Shot Design
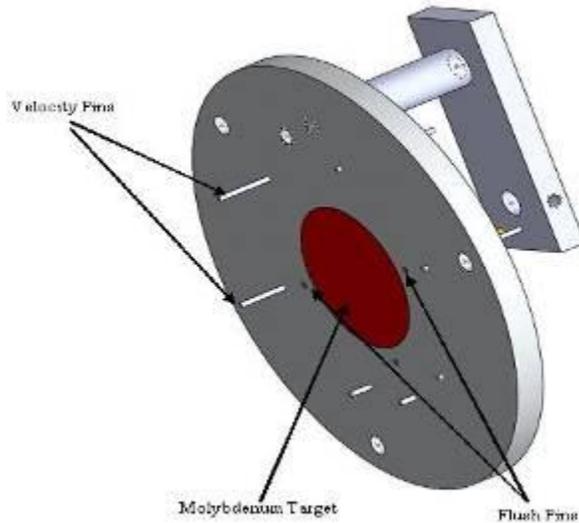
Figure 42.   Schematic setup of Molybdenum spall target.

NPS shot #10_12 was designed to measure the spall strength of Molybdenum under defined shock conditions. As shown in Figure 42 diagnostics used for this shot were PZT flush pins and trigger pin, velocity pins and single channel VISAR. For this experiment it was chosen to perform an unsymmetric impact experiment due to the short supply of Molybdenum samples on hand, therefore an OFHC Copper impactor was used. In order to ensure that spall occurred in the Molybdenum sample, a hand calculation of expected shock conditions was performed. Using a target thickness of 6mm and an impactor thickness of 2.75mm at a flyer velocity of 0.3km/s, an x-t diagram for the event was constructed and is shown in Figure 43. It was expected that for these experimental conditions spall would occur within the Molybdenum sample and would produce a spall scab of approximately 1.8mm thick.
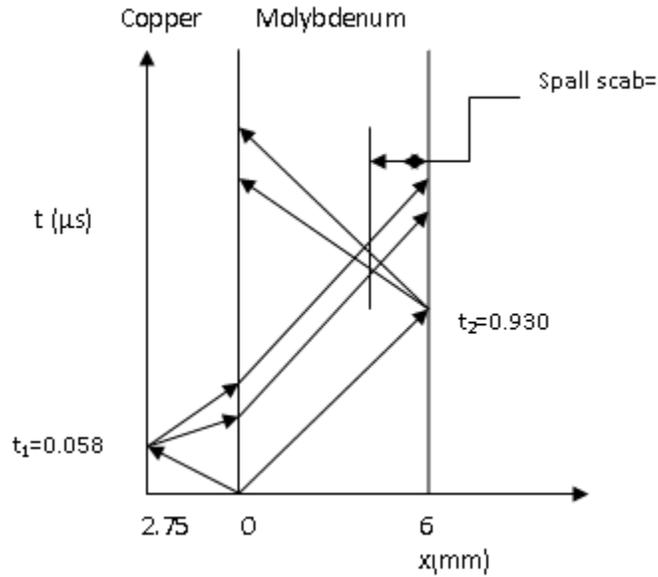
Figure 43.   Preliminary x-t diagram of Molybdenum spall experiment

The final mass of the projectile used was 483.7g which required a breech pressure of 880psi to achieve a desired driver speed of 0.300 km/sec. Initial shot parameters are summarized in Table 6.

Table 6.   Summary of initial parameters for Molybdenum spall shot

Shot Number	Target Material	Expected Projectile Velocity (km/s)	Target Density (g/cc)	Target Thickness (mm)	Impactor Material	Impactor Density (g/cc)	Impactor Thickness (mm)
10_12	Molybdenum	0.300	10.22	5.649	OFHC Cu	8.93	2.602

b.   *Shot Summary and Data Analysis*
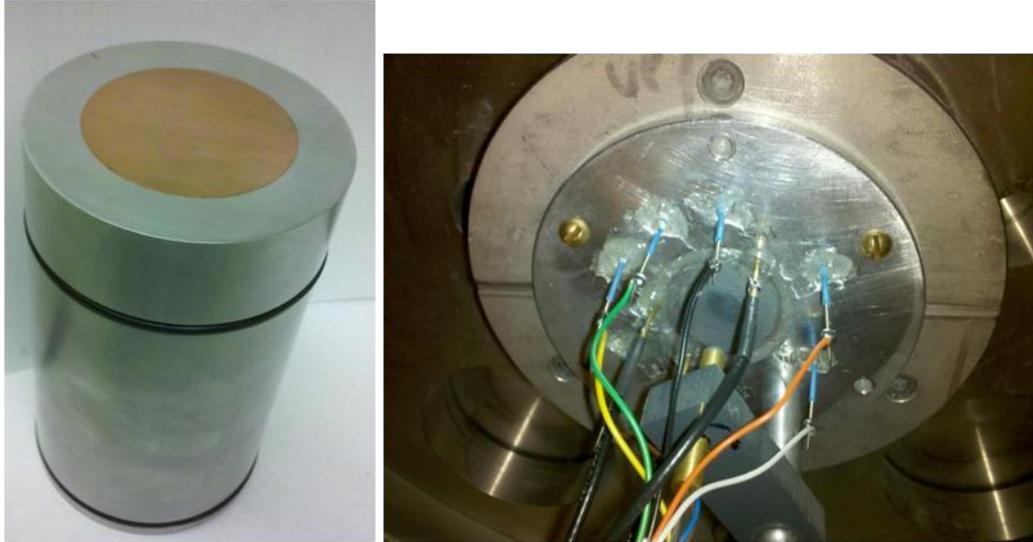
Figure 44.   Final projectile and target buildup of Molybdenum spall experiment

The final setup of shot 10_12 is shown in Figure 44 with a fully constructed target and bullet with impactor mounted. As can be seen there is not a widow present on the rear surface of the Molybdenum sample and this allows the free surface reflections that are needed to occur for the spall event to happen.

Both PZT flush pins triggered as expected to give a reference time fiducial of the impact. All velocity pins triggered as expected to give a data set to calculate the actual driver velocity at time of impact and a value of projectile tilt at impact. A high-quality VISAR trace was recorded showing a fairly uniform flat top upon full shock arrival, a release   as the reflections from the spall scab reach the rear surface and oscillations on the tail of the trace as expected as more reflections from the spall scab reached rear surface. The VISAR trace is shown in Figure 45.

Molybdenum Spall VISAR Record
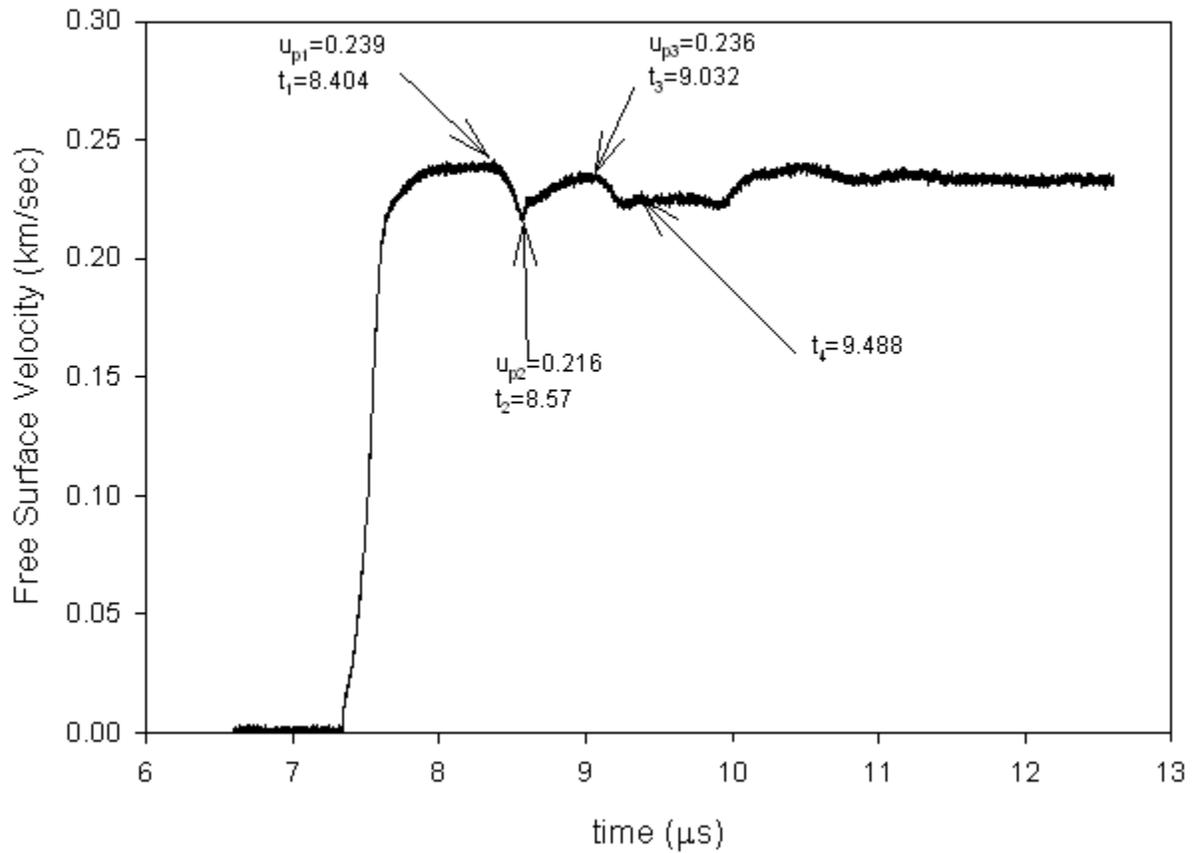
Figure 45.   Molybdenum Spall experiment VISAR results with times annotated that
were used for calculations

Using the techniques developed in Chapter II of this research multiple
parameters were calculated from the VISAR record. These include; shock speed in the
sample, particle speed in the sample, pressure achieved in the sample, spall strength of
the sample, and spall scab thickness of the sample. We also observe an elastic wave in
this experiment that allows us to calculate the Hugoniot Elastic Limit (HEL) for this Mo
sample.   The results of this analysis are summarized in Table 7.

Table 7.   Summary of Calculated values for Molybdenum spall shot

Shot Number	Target Material	Measured Projectile Velocity (km/s)	Tilt (mrad)	Shock Speed (km/s)	Particle Speed (km/s)	Stress (GPa)	Spall Strength (GPa)	Spall Scab Thickness (mm)	HEL (GPa)
10_12	Molybdenum	0.302 ± 0.0001	1.948	5.053	0.120	6.11	0.644	1.299	0.572

Taking into account the differences in the final and initial sample and target thickness differences, the estimated spall scab shows good agreement with what thickness actually was calculated. This leads to the conclusion that the rest of the parameters calculated for this shot are within reasonable values and exact uncertainty will be discussed below.

B.   DYNEEMA HUGONIOT SHOTS

1.   NPS Experiments
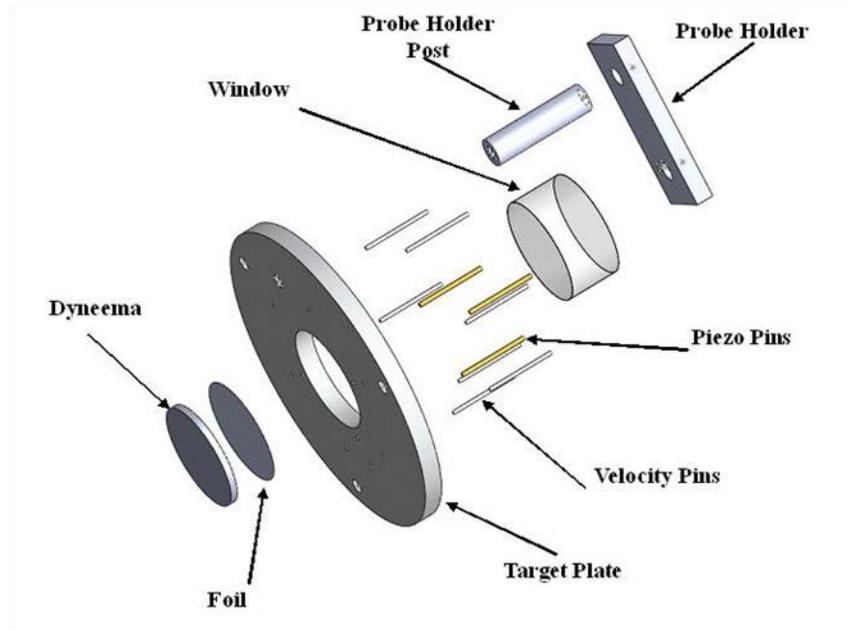
Figure 46.   Schematic representation of first generation NPS Dyneema Target

The first series of Dyneema experiments that were performed at NPS were designed classical Hugoniot experiments to measure the shock Hugoniot for this complex material. This target design consisted of a circular Dyneema sample mounted within an aluminum target plate. A thin foil was glued to the Dyneema to provide a reflective surface for use with the VISAR system due to the Dyneema's lack of reflectivity. The foil was then backed by a PMMA window for diagnostic viewing. This foil was made of aluminum, chosen because of its relatively low shock impedance. Diagnostics used for the experiments were; two or four diametrically opposing PZT flush pins for obtaining an impact reference time, single point VISAR, a PZT trigger pin, and velocity pins for obtaining projectile speed and tilt measurements. The first three shots in the series were successful but yielded complex data. We will discuss below a redesign of the target setup, done to yield data that is more amenable to a clear interpretation.

a. *NPS Shot #s 10_11 and 10_15*

(1) Shot Design. For Dyneema, not much data is available on its shock properties. Therefore, many assumptions were required to be made during the design phase. Chapman [12] et al. had measured the shock speed in the through-thickness direction of Dyneema but using a different experimental method. For initial estimates, it was decided to model the Dyneema as a polyurethane sample and use known Hugoniot data from Marsh [11] as a guide in design. Another assumption that was required was for sound speeds in the through-thickness and lateral directions. This is needed because Dyneema is anisotropic in its mechanical properties. The perpendicular sound speed was taken to be approximately six times greater than that of the through sound speed which was approximated as 2km/s. The assumptions are necessary because we found no literature values for these sound speeds for this particular kind of Dyneema composite, and were unable to measure sound speeds because of very high acoustic attenuation. This through thickness sound speed was used to approximate a preliminary x-t diagram to model the expected experiment as shown in Figure 47.

66
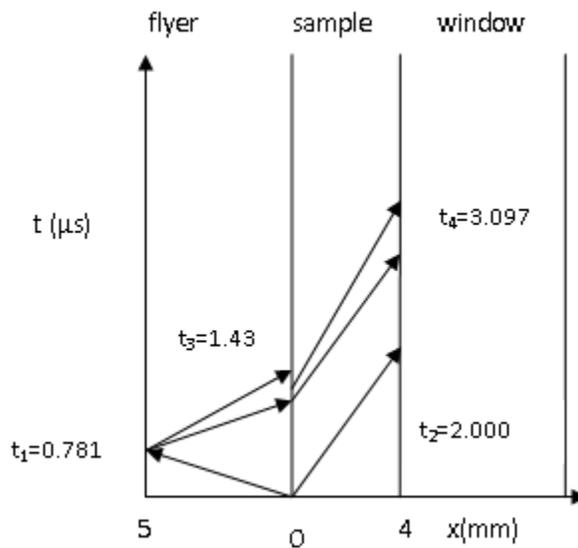
Figure 47.   Estimated t-x diagram of T6061 Al impacting Dyneema using polyurethane approximations

The largest effect of the difference in thorough-thickness and lateral sound speeds was on whether or not the edge releases would pinch of the shock front prior to the VISAR system recording applicable useful data. Using the techniques outlined in Chapter II it was found that the expected edge releases would pinch off the through shock wave approximately 2.2-2.3μs after impact occurred. This time is well after the shock arrival at the target/window interface. This shows that a Dyneema sample 4mm thick and 55mm in diameter would be sufficient to obtain useable Hugoniot data.

In order to simplify data analysis after completion of the experiments, a well characterized material needed to be chosen as an impactor. For this series, 6061-T6 Aluminum was chosen, for its abundance of shock property data, and ease of fabrication

In order to prove reproducibility, shot #10_15 was designed to be as close as possible in design to shot #10_11 to check for reproducibility. Table 8 shows the actual initial shot parameters for shots 10_11 and 10_15,

Table 8.   Initial Shot parameters for the first two Dyneema series Hugoniot
experiments

Shot Number	Target Material	Expected Projectile Velocity (km/s)	Target Density (g/cc)	Target Thickness (mm)	Impactor Material	Impactor Density (g/cc)	Impactor Thickness (mm)
10_11	Dyneema	0.400	0.95	4.21	6061 Al	2.703	4.634
10_15	Dyneema	0.400	0.95	4.15	6061 Al	2.703	4.403

(2) Shot Summary and Data Analysis
        (a) Shot #10_11. Shot #10_11 used four diametrically opposed PZT flush pins, all of which triggered and gave a good signal trace for calculating an impact time fiducial. All velocity pins triggered allowing a good calculation of projectile velocity and tilt. VISAR data was successfully recorded from the rear surface of the Dyneema sample, but did not show a traditional flattop as seen for more simple materials. This is likely due to reflection and wave interactions at the interface of each fiber/epoxy layer within the Dyneema. Analysis was further complicated by a lost fringe within the VISAR system during data collection. The final VISAR trace is shown in Figure 48.

Dyneema shot 10_11 VISAR record
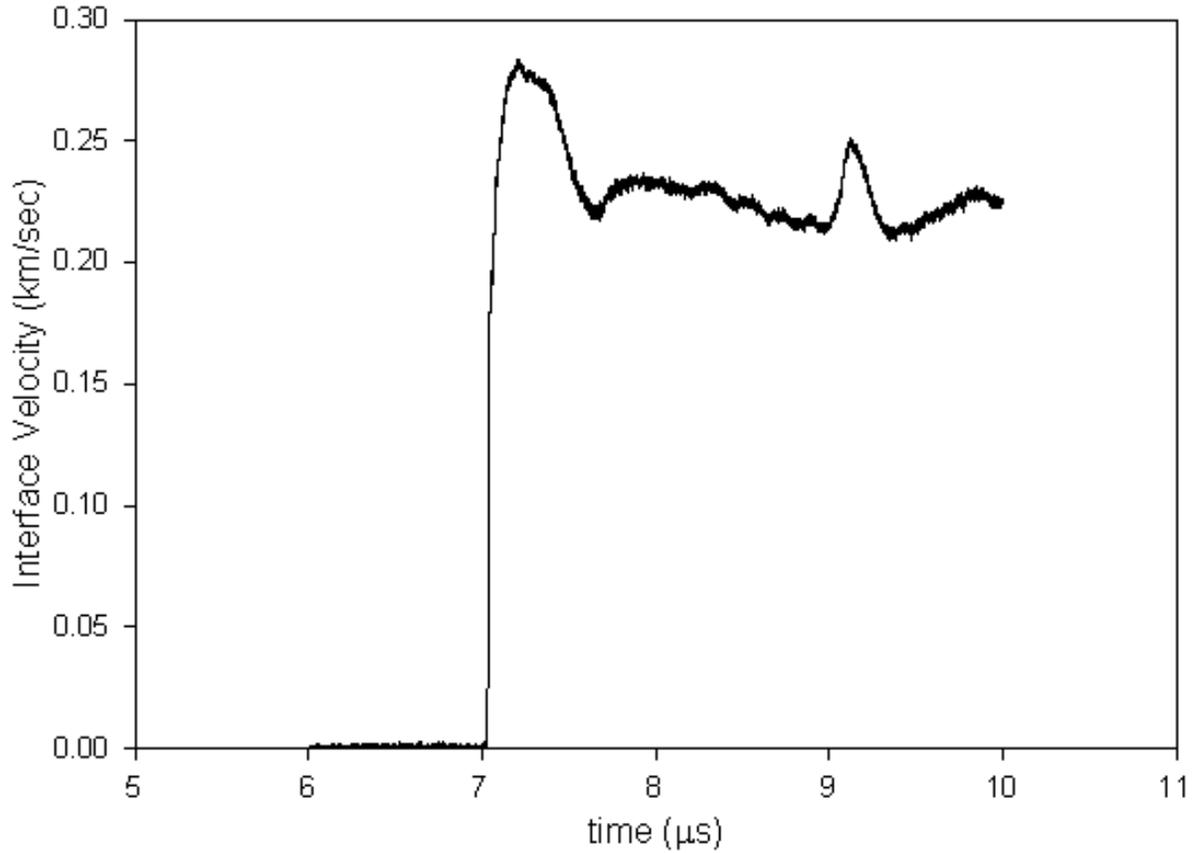
Figure 48.   NPS Shot #10_11 VISAR results showing pseudo flattop

Using the techniques outlined in Chapter II of this research the relevant shock properties were calculated. Specifically, the technique of impedance matching using the known properties of the impactor and the measured shock velocity of the target.

After accounting for all known corrections, the final shot parameters calculated for this shot are summarized in Table 9.

Table 9.   Calculated Hugoniot parameters for Dyneema shot #10_11

Shot Number	Target Material	Measured Projectile Velocity (km/s)	Tilt (mrad)	Shock Speed (km/s)	Particle Speed (km/s)	Stress (GPa)
10_11	Dyneema	0.404 ± 0.003	1.86	2.181	0.354	0.733

(b) Shot # 10_15. Figure 49 shows the final construction of the Target and projectile used for Shot #10_15.

Figure 49.   NPS Shot #10_15 target and projectile final assembly

Shot 10_15 used a set of four PZT flush pins to obtain an impact reference time fiducial, all of which triggered as expected and good signal was received by the digitizer. All velocity pins triggered yielding available high quality data for calculating projectile velocity and tilt. Good signal was obtained by the VISAR system but as in shot #10_11, the velocity trace was somewhat complex and is shown in Figure 50.
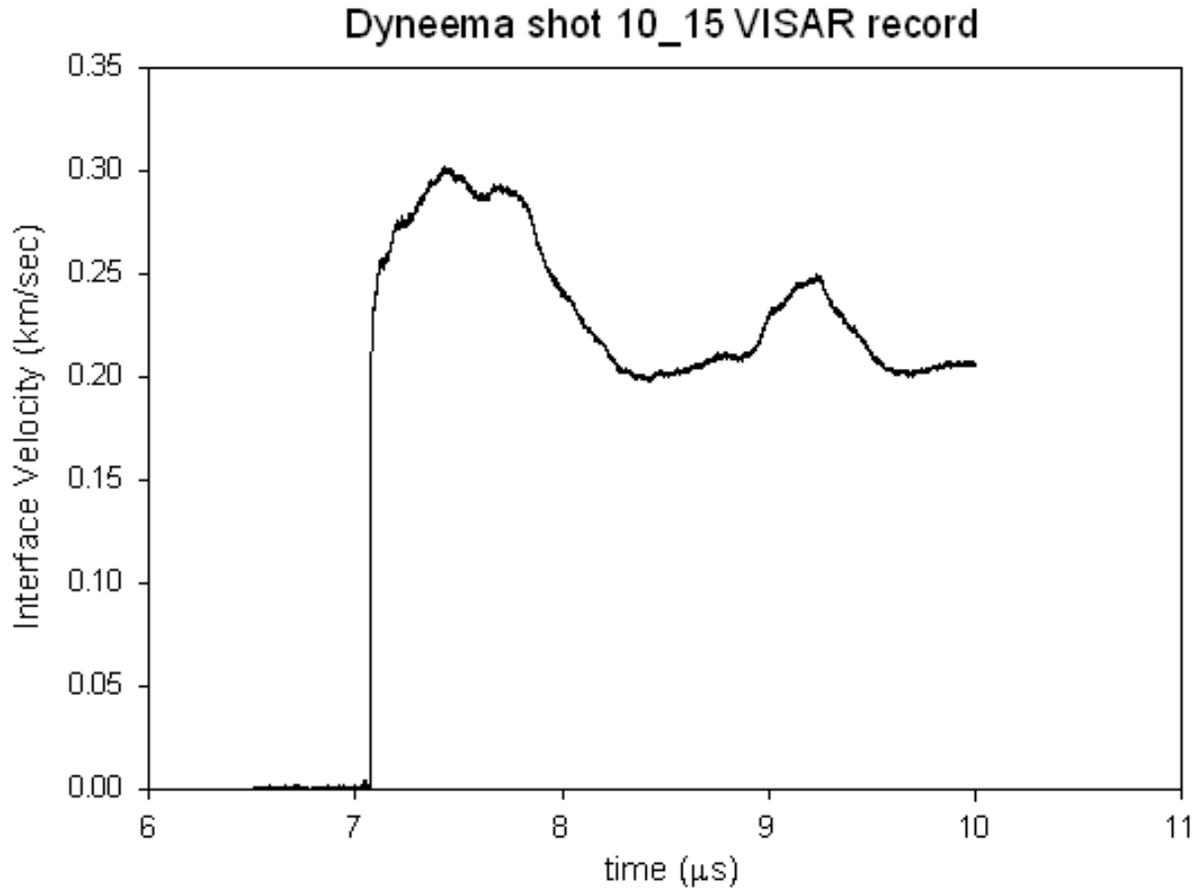
Figure 50.   NPS shot#10_15 VISAR results showing multiple wave structure in Dyneema

Once again, the VISAR system suffered a lost fringe during taking the shock rise which complicates data analysis. Also a slightly different wave profile was observed than that of the first Dyneema shot with what appears to be multiple shock arrivals at the rear of the sample. This shows that we are not obtaining exactly reproducible results for this material with this experimental design. Again, impedance matching was performed in order to deduce the particle velocity from the known properties of the impactor and the measured shock speed in the Dyneema. Final calculated values relevant to shot #10_15 are summarized in Table 10.

Table 10.   Summary of measured Hugoniot parameters for NPS shot #10_15

Shot Number	Target Material	Measured Projectile Velocity (km/s)	Tilt (mrad)	Shock Speed (km/s)	Particle Speed (km/s)	Stress (GPa)
10_15	Dyneema	0.408 ± 0.008	4.07	2.430	0.353	0.814

b.   NPS Shot # 10_17

(1) Shot Design. Shot 10_17 was the third in a series of Dyneema Hugoniot shots. For this experiment it was decided that a very low pressure shock Hugoniot anchor point would be attempted to be measured. The same basic assumptions pertaining to sound speeds in the through and along fiber directions still held true for this experiment that were assumed for the previous two experiments in this research; therefore, again it was expected that edge releases would not pinch off the shock before it arrived at the target/window interface. And again, it was decided that this would be a sufficient viewing time to measure the Hugoniot state. Initial experimental parameters are summarized in Table 11.

Table 11.   Summary of initial experimental parameters for NPS shot #10_17

Shot Number	Target Material	Expected Projectile Velocity (km/s)	Target Density (g/cc)	Target Thickness (mm)	Impactor Material	Impactor Density (g/cc)	Impactor Thickness (mm)
10_17	Dyneema	0.250	0.95	4.32	OFHC Cu	8.93	2.052

(2)   Shot Summary and Data Analysis
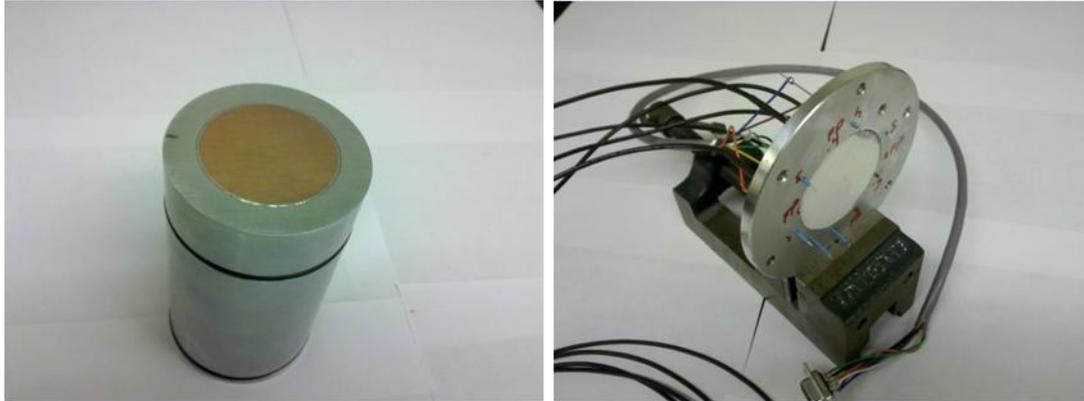
Figure 51.   View of NPS shot 10_17 target and projectile after final assembly

Figure 51 shows the target and projectile after final assembly for shot # 10_17. Diagnostics used for this experiment included single point VISAR, four PZT pins for calculating an impact reference time, and velocity pins for calculating projectile speed and tilt. All four PZT pins triggered as expected giving an average reference time of impact after corrections for pin protrusion and recession relative to target plate were considered. The velocity pin data was not recorded; therefore a calculated projectile speed was not available. But the performance curve of the NPS gas gun has been well characterized and knowing the initial mass of the projectile and the breech pressure at time of fire gives an accurate value of projectile velocity, and adjustments to error bars in calculations using this value were made. Tilt was required to be calculated by hand as well, and using the PZT flush pins, the calculated tilt was found to be a maximum of 1.2mrad.

Again, the VISAR trace at the window interface was less clear. This lead to once again using the known properties of the impactor and the calculated shock speed of the Dyneema to find the particle velocity in the Dyneema as outlined in Chapter II. The complex wave structure observed in the VISAR data are almost certainly due to wave interactions and reflections between epoxy and filament layers.
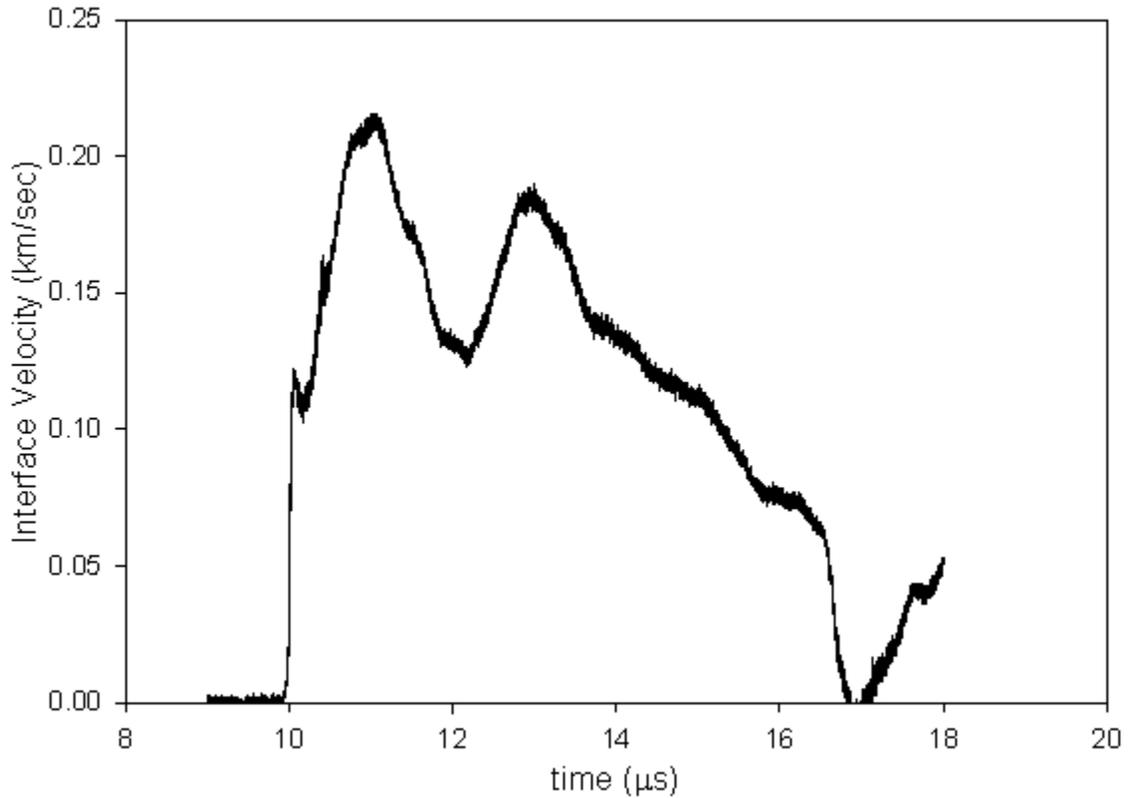
Figure 52.   Results of NPS shot #10_17 VISAR, depicting multiple wave arrivals at the interface

Following the same analysis as used for the previous Dyneema experiments, the particle speed and shock speed was calculated for shot #10_22. Table 12 summarizes the final values calculated pertaining to shot 10_17.

Table 12.   Calculated parameters from Dyneema shot# 10_17

Shot Number	Target Material	Measured Projectile Velocity (km/s)	Tilt (mrad)	Shock Speed (km/s)	Particle Speed (km/s)	Stress (GPa)
10_17	Dyneema	0.250 ± 0.15	1.198	2.046	0.237	0.460

74

c.   *NPS Shot # 10_22*

(1) Shot Design. Following the completion of the first three series of Dyneema shots it was decided that the transmission experimental geometry may not be the optimum approach for research on a complex material like Dyneema. The wave interactions and reflections within the Dyneema epoxy/polyurethane matrix led to multiple wave arrivals at the rear surface of the target sample and therefore led to a complex wave structure as recorded by the VISAR system. After consultation with personnel at ISP, a redesign of the Dyneema target was performed.

The second-generation Dyneema target was designed to correct two separate deficiencies of the first design. First, the edges of Dyneema sample were not flush with the face of the Dyneema sample due to the fabrication process, and due to the nature of the material made it un-practical to attempt to smooth the edges flat. This led to an inability to adjust the Dyneema sample face flush with the target plate and the flush pins, inducing another level of uncertainty and corrections that need to be accounted for in calculating an impact reference time. In order to correct this first deficiency a thin buffer plate was designed slightly larger than the Dyneema target sample with a recess machined into the buffer that matched the diameter of the Dyneema sample and allowed the protruding edges to be matched with the recess and mated the surface of the Dyneema to another flat surface. This is shown in Figure 53.

Figure 53.   Front Copper buffer plate used for second generation Dyneema target Assembly showing recess for accepting frayed edges of Dyneema

Diagnostics were then set to record the arrival of an impact at the rear of the surface of the front buffer plate, and thus provide an accurate reference time of arrival of the shock wave at the front surface of the Dyneema sample.

Second, complex wave interactions in the orthotropic material that was being studied leads to multiple wave arrivals at the rear of the sample. In order to achieve a representative "average" value of the Hugoniot state within the Dyneema, the multiple waves that were arriving at the rear of the surface needed to be integrated together into a single usable sample point. This was accomplished by adding a low strength buffer material to the rear of the Dyneema sample that would act as smoothing mechanism to the multiple waves that arrived. It was chosen to use OFHC Copper that had been annealed at 350C for 4 hrs to remove any residual internal stress as the rear buffer material. The final design is shown schematically in Figure 54.
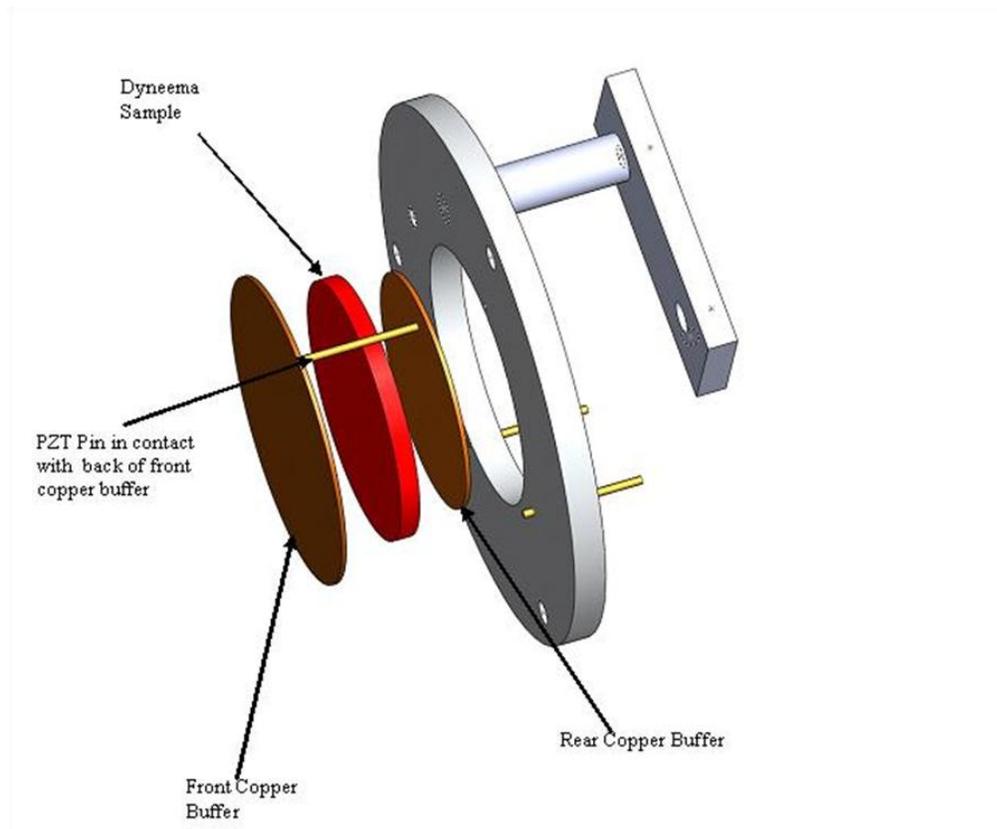
Figure 54.   Schematic view of second-generation Dyneema target assembly

Using this redesign in target assembly also caused an adjustment in the methods of analyzing the data that is recorded. This experiment is no longer a traditional shock Hugoniot measurement experiment, but more closely analogous to a metal 'plate-push' experiment. There will be multiple wave interactions throughout the time frame of the experiment through four different layers of material. But the only waves that will be of true interest to the results of the experiment are the first waves that travel through the Dyneema sample and the rear buffer plate. This is due to the fact that the reference time for the shock entering the front face of the Dyneema is directly measured by the two PZT pins in contact with the front buffer that is directly in contact with the Dyneema. The waves in the rear buffer material will be of further importance to ensure that the experimentalist understands the results that are obtained from the VISAR record trace of the free surface. Since there is not a window material on the rear buffer, when the shock wave that is traveling through the rear buffer reaches the free surface, the shock will be reflected back into the buffer as a release wave traveling back to the Dyneema-buffer interface. Once the release wave reaches the interface, it will be reflected once again back as a re-shock in the buffer material until it reaches the free surface again. This cycle of release and re-shock will continue to occur, continually stepping up the free surface particle velocity seen on the VISAR record up to a max value. The arrivals of the shocks at the rear of the buffer material should also correspond to times of a round trip shock wave in the buffer material. These interactions are represented graphically in a generic x-t diagram and VISAR record in Figure 55.
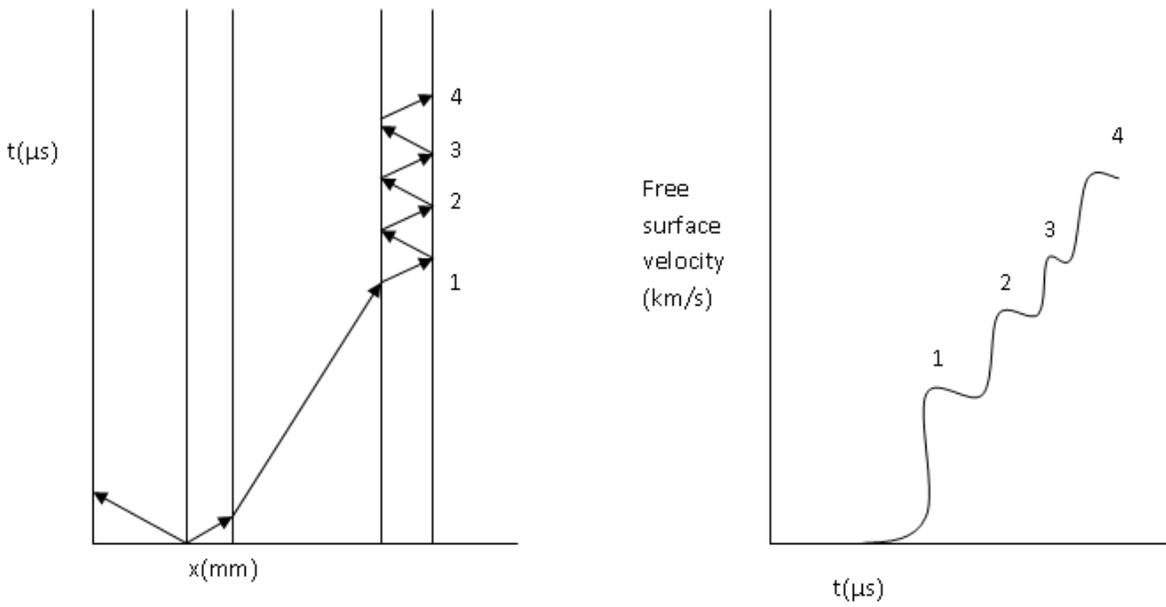
Figure 55.   Graphical representation of theoretical x-t diagram and anticipated VISAR trace for second generation Dyneema target design

Changes made to the Dyneema target design will greatly enhance our ability to obtain shock Hugoniot data points in the through-thickness direction for this material. The final setup parameters used during and after construction of the target for shot#10_22 are listed in Table 13.

Table 13. NPS shot #10_22 initial target parameters

Shot Number	Target Material	Expected Projectile Velocity (km/s)	Target Density (g/cc)	Target Thickness (mm)	Front and Rear Buffer Material	Buffer Density (g/cc)	Front/Rear Buffer Thickness (mm)
10_22	Dyneema	0.300	0.95	4.18	Annealed OFHC Cu	8.93	0.950/0.900

(2) Shot summary and Data Analysis

Figure 56. Final construction of projectile and target for NPS shot# 10_22

Figure 56 shows the final bullet and target assembly for shot # 10_22. Both flush pins triggered as expected giving a good signal for calculation of a reference time fiducial for the shock reaching the interface of the front buffer plate and the Dyneema sample. All six velocity pins triggered but when projectile velocity and tilt were calculated, values did not match with known values of gun performance curve and VISAR record for projectile velocity, and hand calculation of maximum tilt using flush pin arrivals. This was likely due to the velocity pins being located at near the extreme

limit of the available radius relative to the gun bore, and causing erroneous triggering or that the face of the projectile was not verified perpendicular to the long axis of the projectile body.

A good VISAR trace was obtained from the rear free surface of the second buffer plate. The VISAR trace showed an initial rise to a plateau correlating to the Hugoniot state in the Dyneema. A subsequent wave ring-up was observed as expected followed by a more defined ring up in the copper buffer as was predicted would occur. The VISAR trace is shown in Figure 57 with the Hugoniot state annotated.
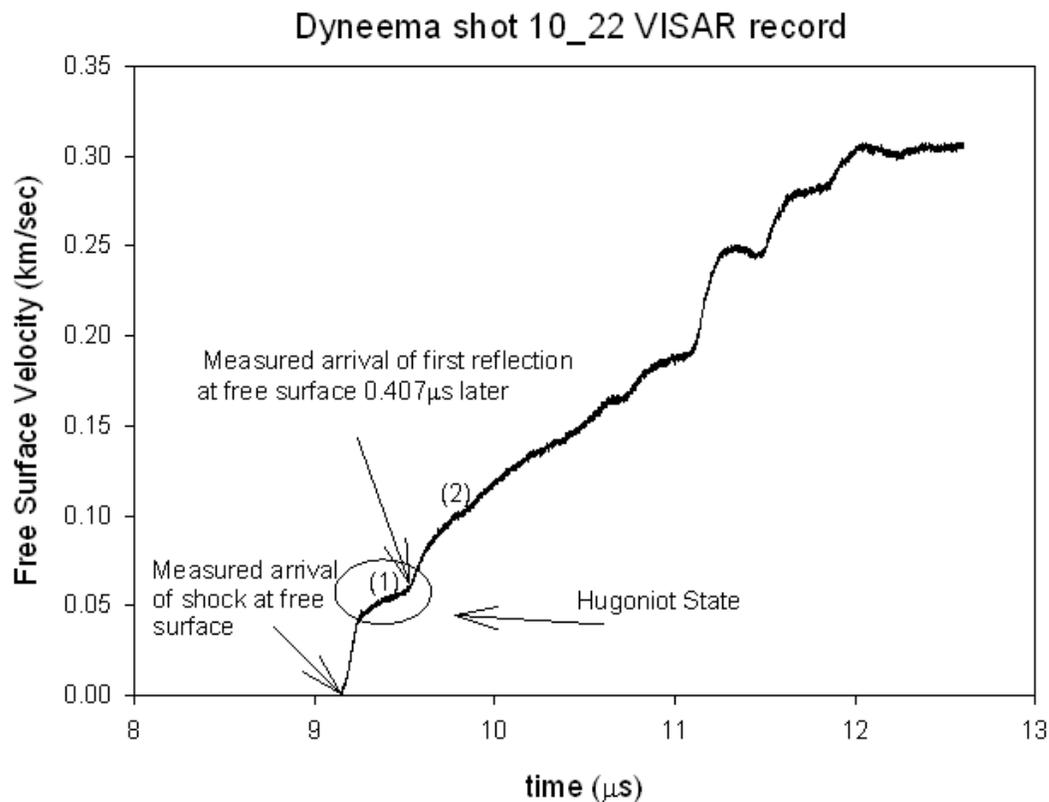
Figure 57.   NPS shot #10_22 VISAR results using second generation target design showing chosen Hugoniot point and the first two 'ring-up' states in rear buffer

In order to calculate the shock speed within the Dyneema sample, first the shock speed with in the rear copper buffer needed to be calculated. Taking the free surface velocity indicated in the VISAR trace and dividing by two gives the particle

velocity behind the shock in the rear copper buffer. Using known copper Hugoniot data from Marsh [11], the shock speed in the copper was calculated. Using this shock speed, the time required for the shock to transit through the copper buffer was determined. This time was subtracted from the time indicated in Figure 57 above as the shock arrival at the free surface and taken to be the raw time that the shock wave arrived at the Dyneema-Copper interface. Using the reference arrival indicated by the PZT flush pins, and this new calculated time, the shock speed in the Dyneema was calculated using a simple velocity relationship.

The particle velocity behind the shock in the Dyneema was calculated from the method of impedance matching as discussed in Chapter II. The Particle velocity and pressure state achieved during the experiment were also graphically represented in $P - u_p$ space in Figure 58. From the figure it can be seen that if given enough time, the rear surface of the copper should ring up to a particle velocity state of ~0.500 km/s, which would be indicated by a free surface velocity of ~1.000km/s
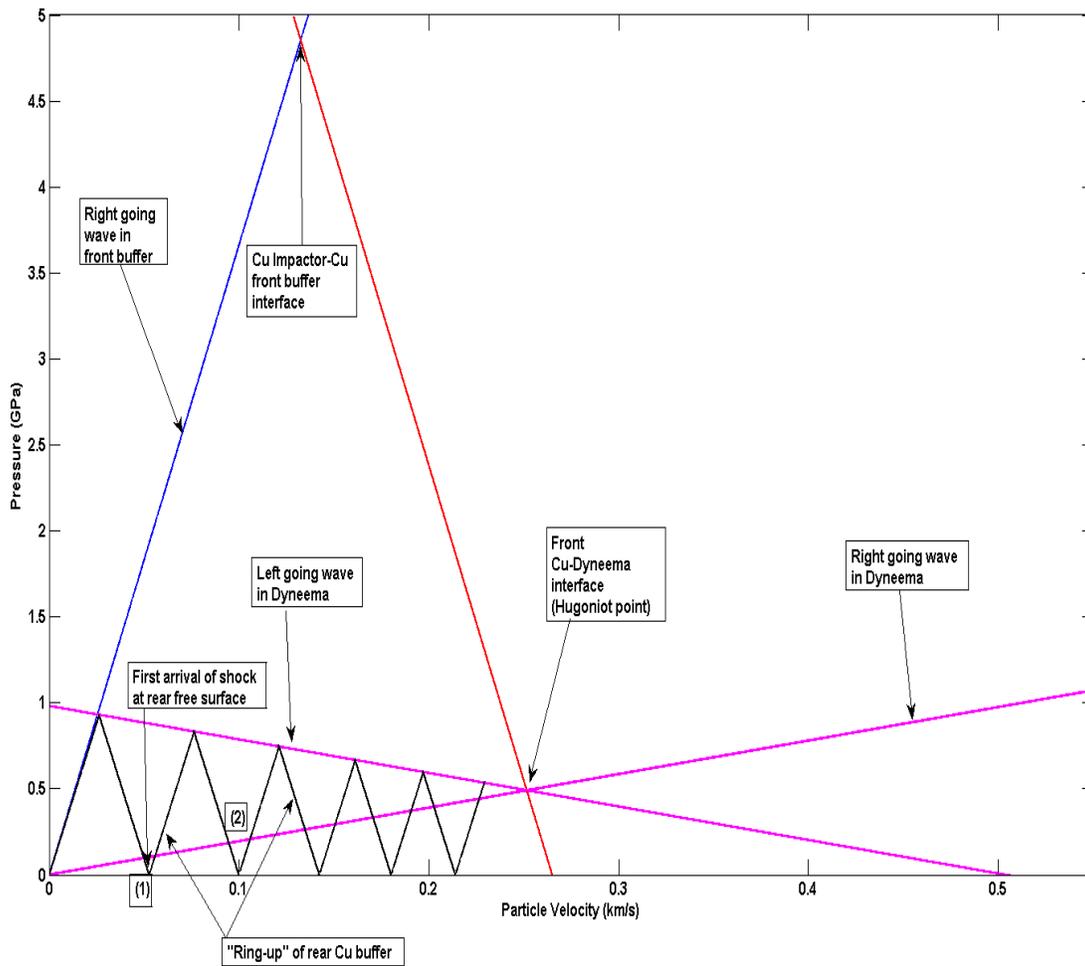
Figure 58.   Calculated $P - u_p$ diagram of NPS shot #10_22

In order to quantify the results received from the VISAR trace as an accurate representation of what actually occurred, the $P - u_p$ analysis also correlated not just the first arrival of the shock at the rear surface but subsequent ring ups indicated in the VISAR profile using both time and predicted particle velocity states in the rear surface of the copper. An x-t diagram of the actual events that occurred for the first set of wave interactions was constructed. This is shown below in Figure 59.
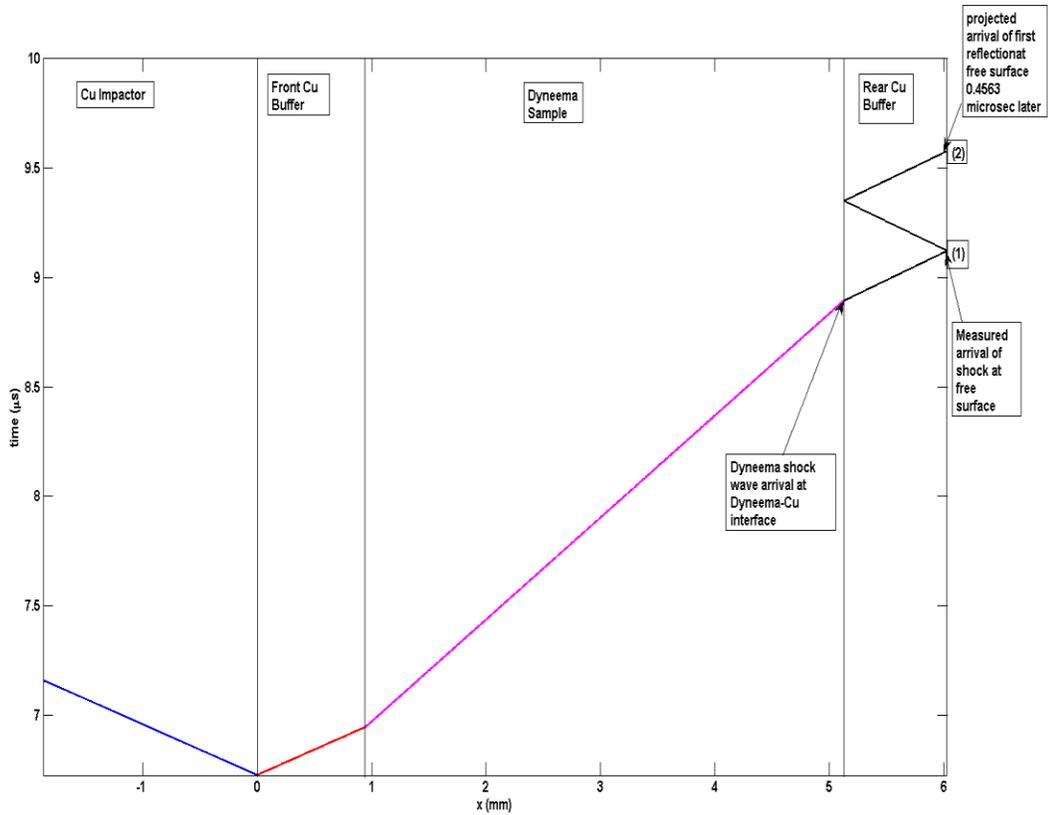
Figure 59.   Calculated x-t diagram of NPS shot #10_22

These times and particle velocities were compared to the actual
VISAR trace measured at the numbered states indicated in Figures 57, 58 and 59. It was
found that the projected round trip time of a copper ring up for the first ring agreed with
the VISAR trace within 50 ns. The final calculated values for the Hugoniot state for NPS
shot #10_22 are tabulated in Table 14.

Table 14.   Calculated shock parameters for NPS shot #10_22

Shot Number	Target Material	Measured Projectile Velocity (km/s)	Tilt (mrad)	Shock Speed (km/s)	Particle Speed (km/s)	Stress (GPa)
10_22	Dyneema	0.256 ± 0.027	3.99	2.144	0.245	0.499

2.   Washington State University Experiments

a.   Shot Design

A second experiment was conducted to determine a Hugoniot state in Dyneema using the second generation Dyneema target design. This shot was conducted at the ISP at WSU using the 40mm bore gas gun. Overall design was similar to the design used for NPS Shot #10_22, including the use of a copper flyer. Two differences existed, first the front Cu buffer was slightly thicker than that used on the previous shot and second, two channels of VISAR were used for measuring shock arrival at the front Cu buffer-Dyneema interface rather than PZT pins. This shot was intended to achieve a much higher pressure state in the Dyneema than could be achieved at the NPS gas gun thereby providing a higher pressure Hugoniot point for development of shock parameters of Dyneema. Initial shot design parameters are listed in Table 15.

Table 15.   Initial target parameters for WSU Dyneema shot

Shot Number	Target Material	Expected Projectile Velocity (km/s)	Target Density (g/cc)	Target Thickness (mm)	Front and Rear Buffer Material	Buffer Density (g/cc)	Front/Rear Buffer Thickness (mm)
WSU Dyneema	Dyneema	0.900	0.95	4.100	Annealed OFHC Cu	8.93	1.872/0.767

b. ***Shot Summary***

Figure 60 shows the final construction of the Dyneema target used for this shot.
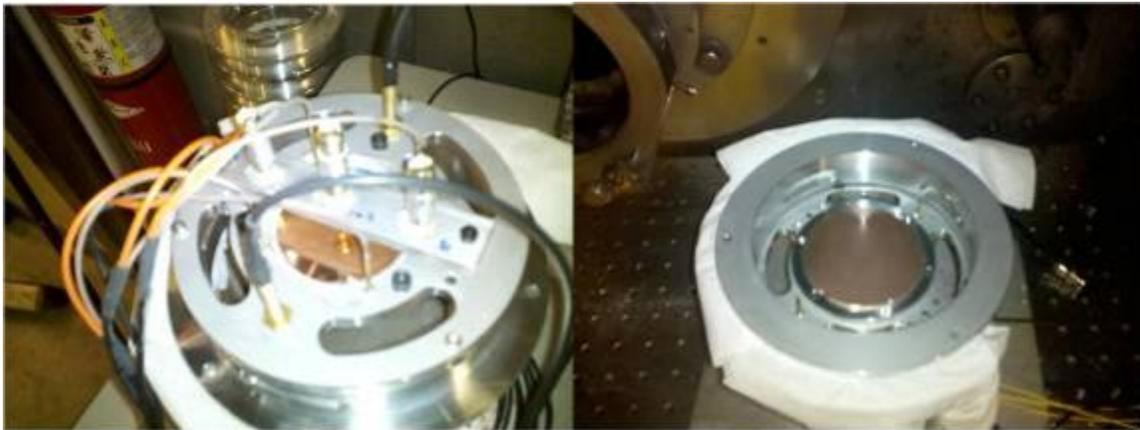
Figure 60.   Final construction of WSU Dyneema target

Both side VISAR channels triggered giving a good reference time of shock arrival at the front Cu-Dyneema interface and indicating a very low range of tilt in the shock wave that was transmitted to the Dyneema sample. The free surface VISAR channel triggered and a clear signal was received indicating a stepped rise in free surface velocity as expected. The Free surface VISAR record is shown in Figure 61.
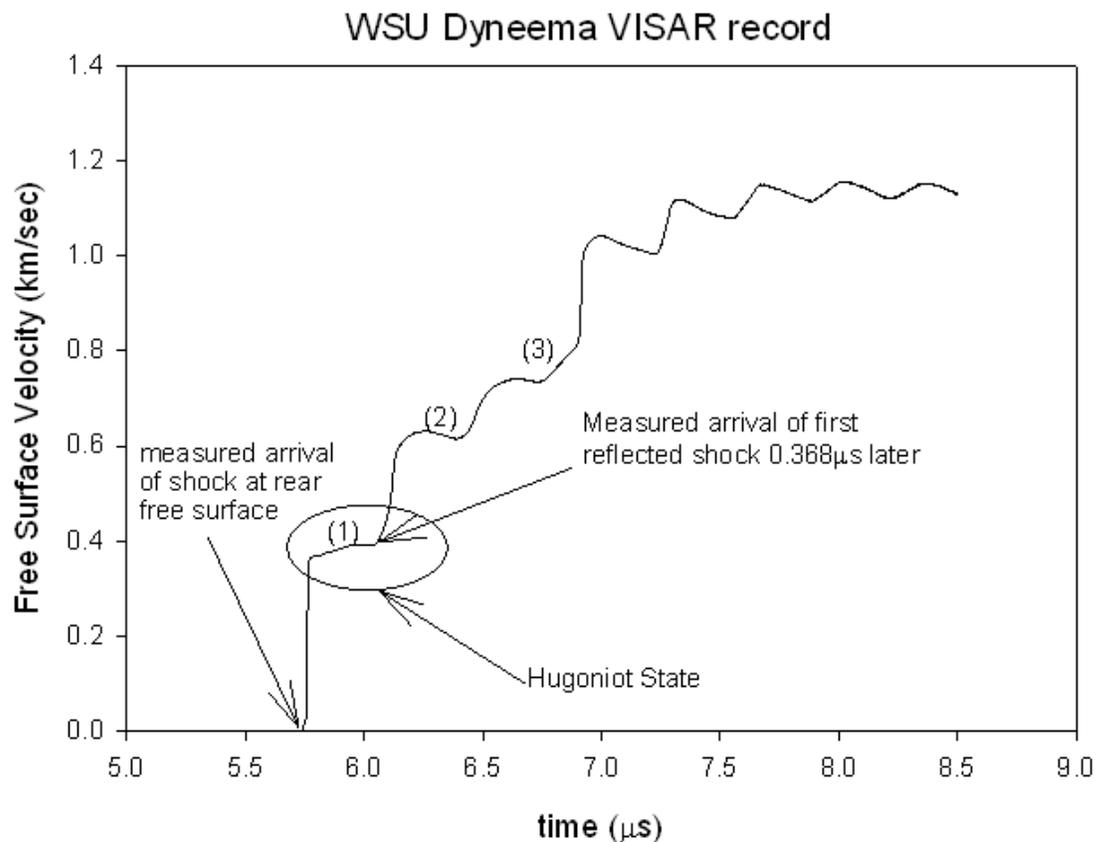
Figure 61.   WSU Dyneema impact experiment VISAR results with annotated Hugoniot state and "ring-ups" recorded

The same systematic analysis that was used to determine the shock speed and particle speed in the Dyneema sample in NPS shot #10_22 was used for this shot as well. Using the momentum jump condition:

$$P = \rho_o U_s u_p$$,

the stress state can be calculated.

A graph of the wave interaction history that occurred in the target is shown below in $P - u_p$ space in Figure 62. This figure includes a prediction of the ring up in the rear Cu buffer and a theoretical maximum particle velocity in the copper of more than 1.6 km/sec. States are annotated to correlate with those in Figure 61.
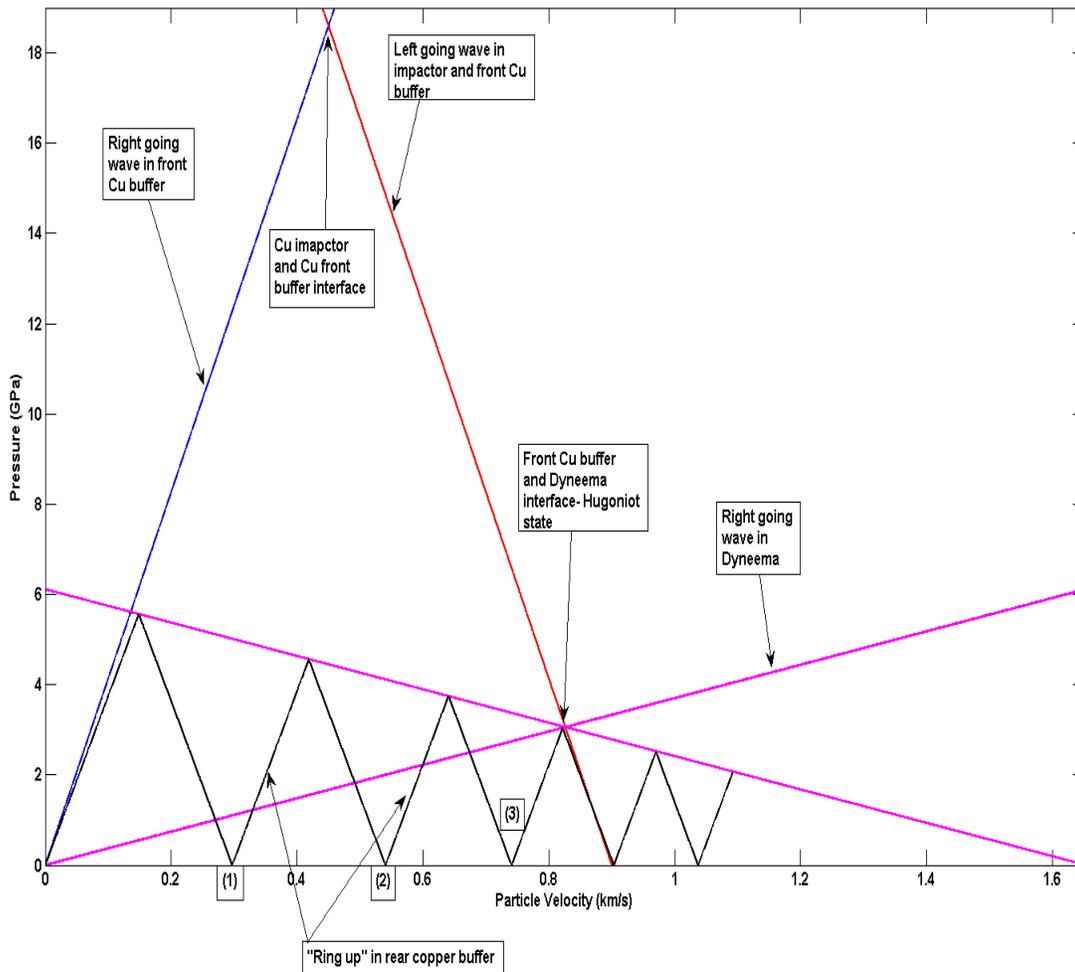
Figure 62.   Calculated $P - u_p$ diagram showing wave interactions for WSU Dyneema shot

As before, an x-t diagram of the waves traveling through the target was constructed and is shown in Figure 63. The correlating states to those in Figures 61 and 62 are annotated.
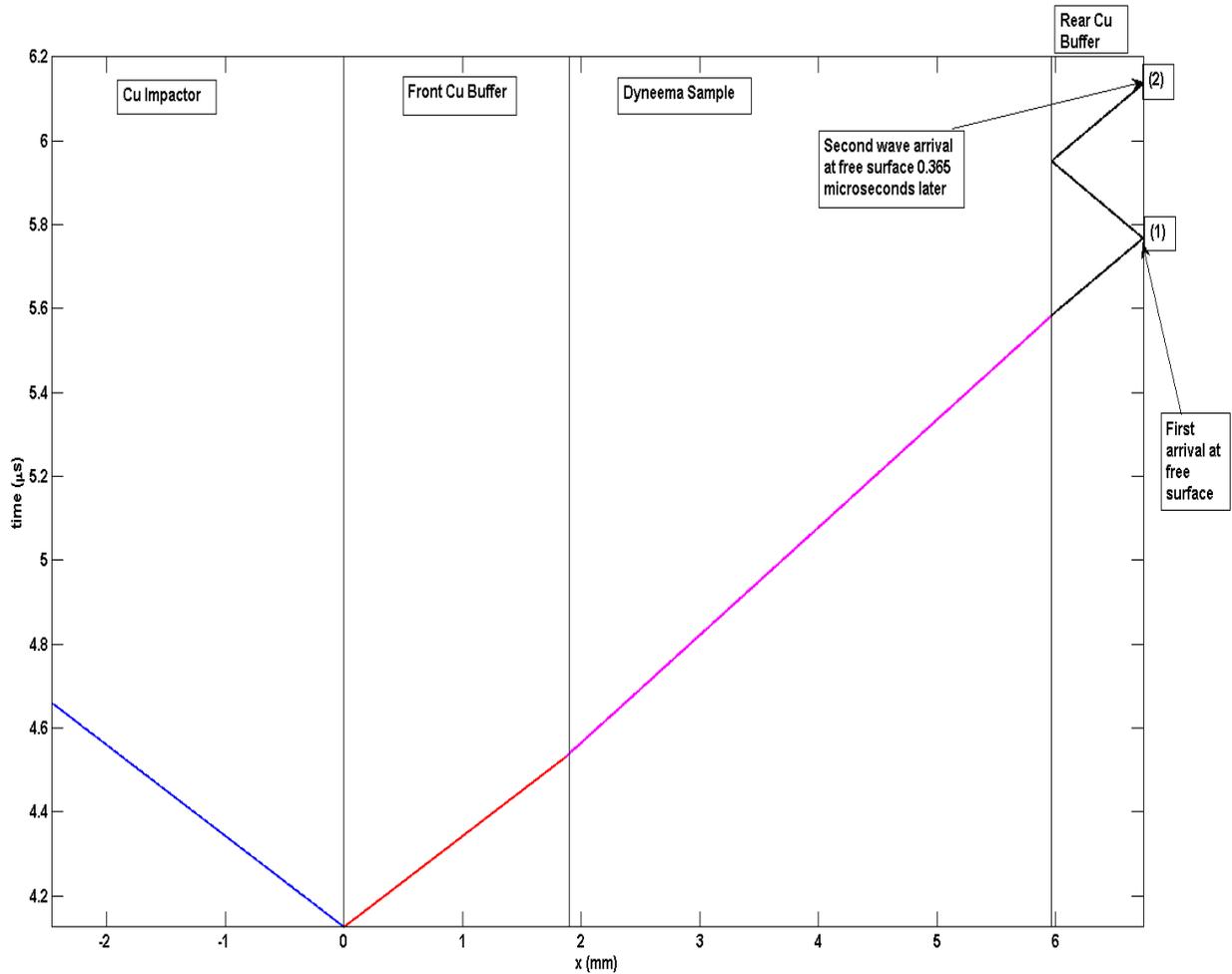
Figure 63.   Calculated x-t diagram for WSU shot with first two free surface arrivals indicated

The predicted round trip time of the first ring up wave in the copper was calculated and compared to the measured ring up time as observed in the VISAR trace. The difference between the measured time and the predicted time was less than 10ns indicating that the analysis methods are accurately calculating the correct state of the materials in the sample material within a certain degree of certainty. The Final calculated values of the of the Shock Hugoniot state within the Dyneema sample are listed in Table 16.

Table 16.   Calculated shock parameters for WSU Dyneema shot

Shot Number	Target Material	Measured Projectile Velocity (km/s)	Tilt (mrad)	Shock Speed (km/s)	Particle Speed (km/s)	Stress (GPa)
WSU Dyneema	Dyneema	0.900 ± 0.001	0.460	3.894	0.884	3.270

3.   Shock Hugoniot Measurement of Dyneema Uncertainty Analysis

Significant errors were noted during the measurement of Hugoniot parameters of Dyneema. Specifically the uncertainty in measuring the particle velocity at the target-window interface in the window experiments contributed to large errors that were calculated in final parameters. Another large contributing factor in the error of the final calculated values was due to the construction of the Dyneema samples themselves. Due to the nature of the material that the samples are made from, they cannot be machined or lapped to a flatness or thickness within an acceptable range. A third factor that contributes to errors encountered was due also to the manufacturing process of the Dyneema samples. Specifically, due to the water jetting process that cut the samples, edges were formed on the disk samples that prevented the target sample from being mounted flush with the target plate and thus requiring corrections to calculate time of impact at the target face. This error was largely negated by the development of the second generation target setup in later shots. The final cause of significant error was due to the errors encountered from the use of PZT flush pins as a measurement of impact in early shots. These pins were not mounted exactly flush with the surface of the target plate and sample and therefore required calculated corrections to determine time of impact. This error also was largely negated by the use of the second generation target design.

Following the analysis set forth in Chapter II of this research, the percent error in measured particle speed, shock speed, and stress level were calculated and summarized in Table 17.

Table 17.   Summary of percent error for Dyneema Hugoniot parameters

Shot Number	Percent Error in Shock Speed	Percent Error in Particle Speed	Percent Error in Stress
10_11	2.8%	1.8%	1.9%
10_15	6.0%	4.7%	4.8%
10_17	2.6%	9.5%	9.5%
10_22	0.8%	7.6%	7.5%
WSU	1.5%	3.5%	3.0%

The use of the second generation target design did tend to lower errors in measurements in shock velocity, but errors in particle velocity trended to remain consistent with previous experiments. This is due to the measured free surface velocity being an average of multiple wave arrivals at the rear plate and not just a single wave within the Dyneema sample and not a true point state as in traditional isotropic materials.

IV. CONCLUSIONS

A.   MOLYBDENUM

One of the goals of this research was focused on obtaining sound speed at pressure data for polycrystalline Molybdenum. Summarized results for are tabulated in Table 18.

Table 18.   Summary results of sound speed at pressure of Molybdenum experiments

Shot	Sound Speed @ Pressure (km/sec)	Shock Density (g/cm^3)
10_8	6.902 ± 0.14	10.507 ± 0.31
WSU	7.657 ± 0.21	11.037 ± 0.02
11_4	6.895 ± 0.18	10.547 ± 0.35

The goal of this portion of this research was to provide new low pressure data to either reinforce the proposed solid-solid phase transition that was originally proposed by Hixson [4], or contradict the original findings. Hixson proposed a solid-solid phase transition in polycrystalline Molybdenum under shock loading at ~200GPa. A summary of the results of this original work is shown graphically in Figure 64.
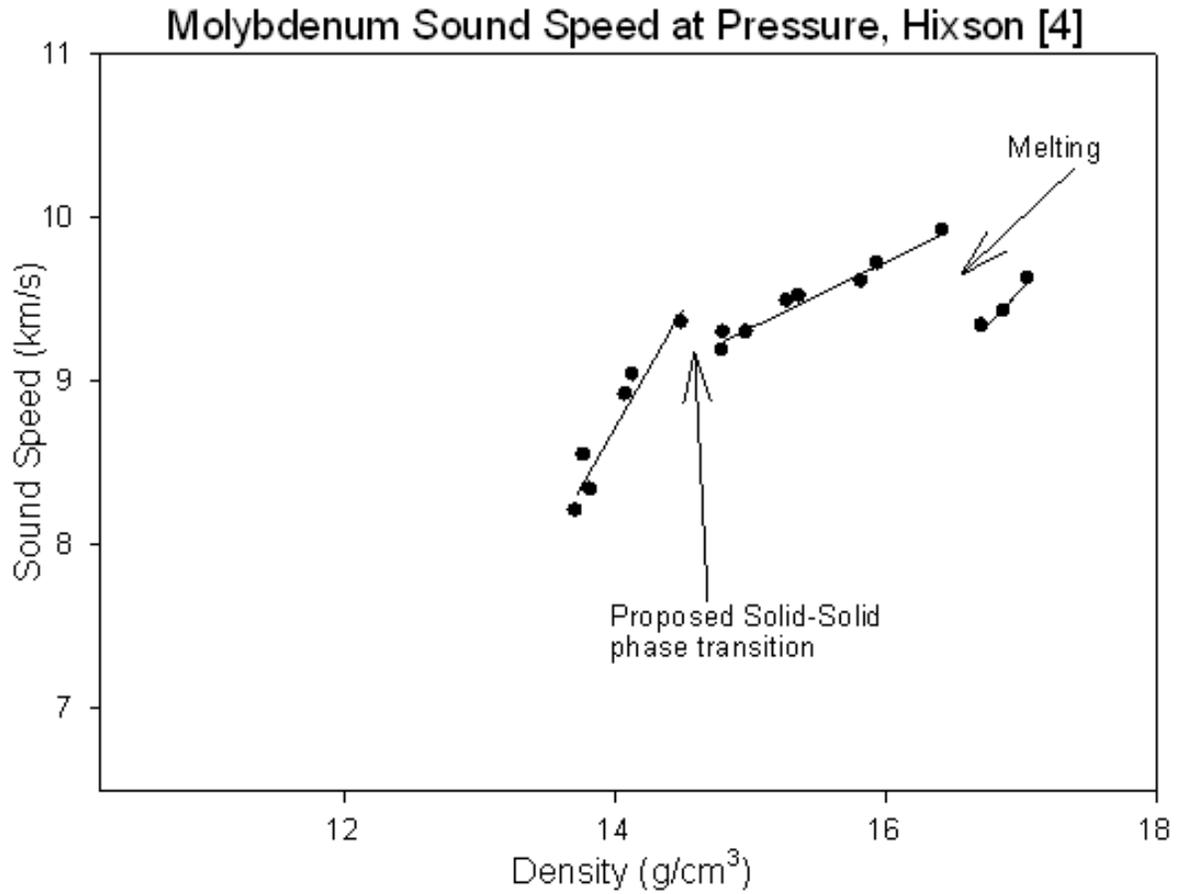
Figure 64.   Sound speed at shock density state originally found by Hixson et al. [4]

But these results are lacking a data in the low pressure region as anchor points to the curve. Consequently, the data points obtained for this research were added to the original data. The results of adding the new data sets are shown in Figure 65.
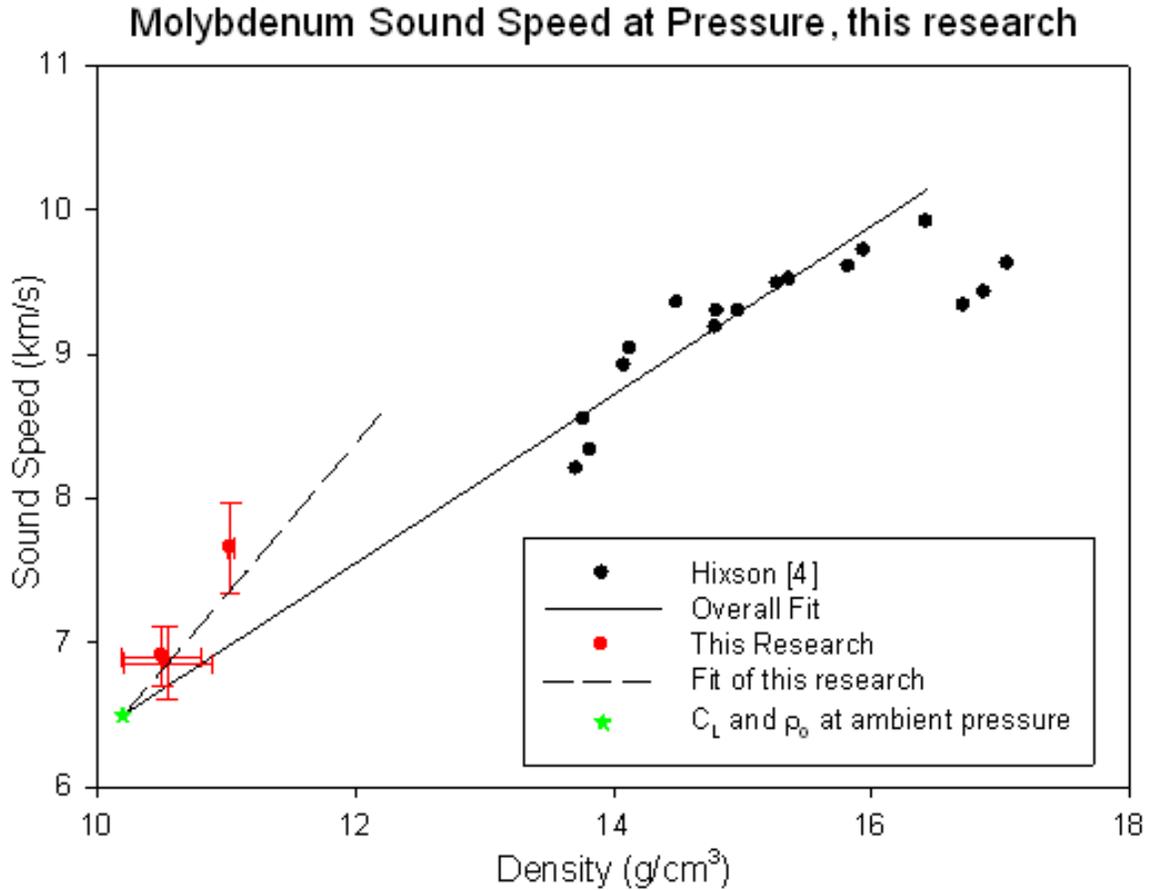
Figure 65.   Sound speed at shock density state for this research

By inputting the data points obtained from this research and using the ambient density and sound speed as an anchor point, one can not conclusively prove or disprove the solid-solid phase transition originally proposed by Hixson [4].   In fact, the trend established by the new data points in many ways raises more questions than it answers. Two possibilities exist when the current data is merged with existing data. First, is that there is not a solid-solid phase transition in the 200 GPa region and one of the data points from this research is erroneous. A second possibility exists as well. The data set forth in this research suggests that there may be an earlier solid-solid phase transition in the 25-150 GPa range that was previously unknown. More research in the very low level pressure regime needs to be completed to further anchor the sound speed data, and further

data needs to be obtained in the 25-150 GPa range to further understand exactly what is occurring in that regime. This work will be left to future research.

B.   DYNEEMA

The second goal of this research was to perform conventional shock Hugoniot experiments on Dyneema HB-25 and collect the data to be able to establish the Hugoniot relationships for the material in the through fiber direction. Three experiments using a traditional Hugoniot experimental setup were attempted and were successful at measuring the shock speed in the through direction of Dyneema and calculating the particle velocity behind the shock wave. Two additional experiments were performed using a modified target setup to provide more accurate data sets. The research performed here provides a sound starting point for further measurement of the dynamic response of Dyneema HB-25 to shock loading. Results for the Dyneema Hugoniot measurements are summarized in Table 19.

Table 19.   Summary of results for Dyneema Hugoniot experiments

Shot	U_s km/sec	P GPa	u_p km/sec
10_11	2.181 ± 0.062	0.733 ± 0.014	0.354 ± 0.006
10_15	2.432 ± 0.145	0.814 ± 0.039	0.353 ± 0.0165
10_17	2.046 ± 0.054	0.460 ± 0.044	0.237 ± 0.0220
10_22	2.144 ± 0.028	0.944 ± 0.038	0.245 ± 0.028
WSU	3.894 ± 0.060	3.270 ± 0.114	0.884 ± 0.027

Using these data points a best fit Hugoniot was found in both $U_s - u_p$ space and $P - u_p$ space. The $U_s - u_p$ shock Hugoniot is shown graphically below in Figure 66. For comparison the Hugoniot data measured by Chapman [12], and the best fit Hugoniot for HDPE of initial density of 0.916 g/cm^3 and 0.954 g/cm^3 found by Marsh [4] is also shown. In this research it was found that the best fit for the Dyneema Hugoniot points in

$U_s - u_p$ space was initially a quadratic function in the stress regime of this research and is shown below.

$$U_s = -1.673u_p^2 + 4.847u_p + 0.902$$

This fit assumes that the anchor point for the Hugoniot will be near the bulk sound speed of Dyneema and the shear and longitudinal sound speeds presented by Chapman [12] were used to calculate the bulk sound speed. It also appears from the data of this research that the $U_s - u_p$ Hugoniot for Dyneema will likely trend to a more traditional linear response at or near the edge of the range of this research. It is also worth noting that the material we studied is not identical to that studied by Chapman, and so some differences are to be expected.
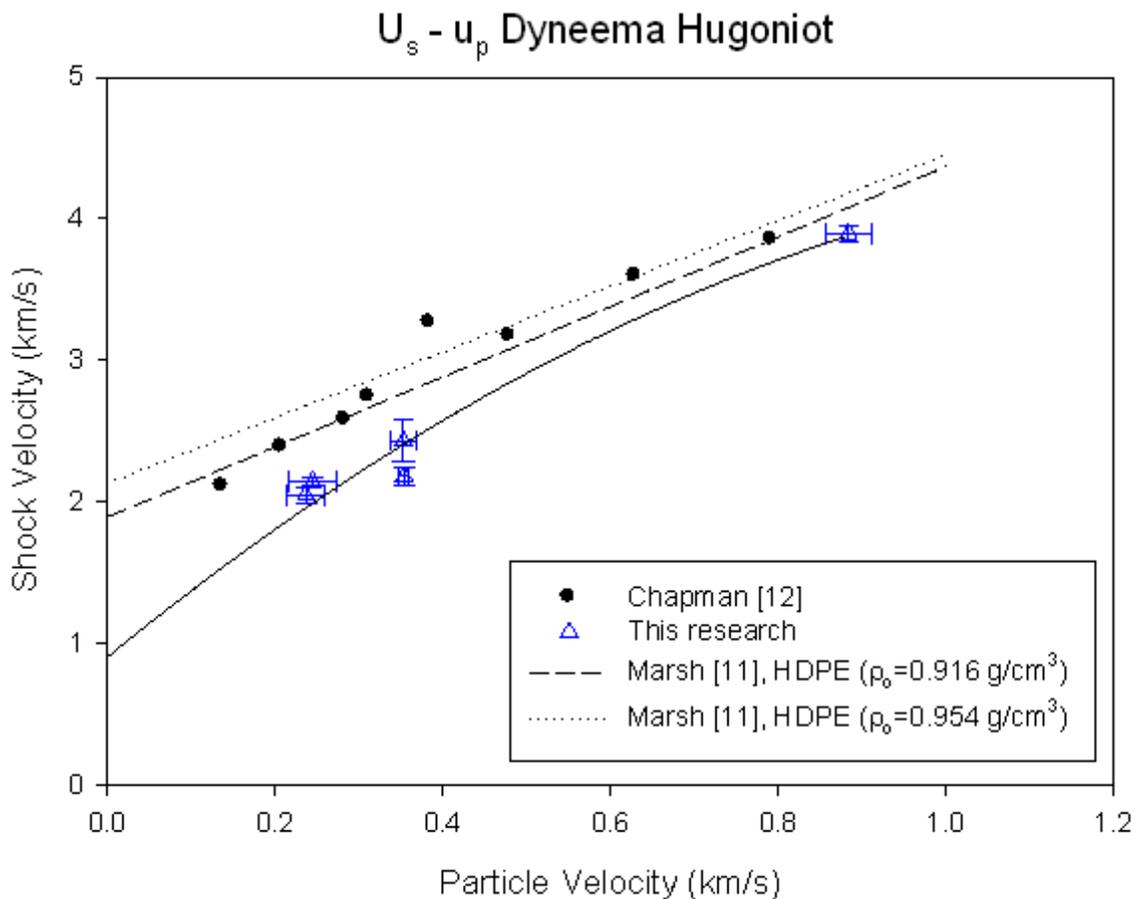
Figure 66.   Principal Dyneema Hugoniot data in $U_s - u_p$ space

The principal Hugoniot points can also be represented in $P-u_p$ space and that is shown below in Figure 67. For comparison, the data presented by Chapman is also included. It was found that the Dyneema data in this research fit the following relationship in $P-u_p$ space.

$$P = 3.365u_p^2 + 0.729u_p$$
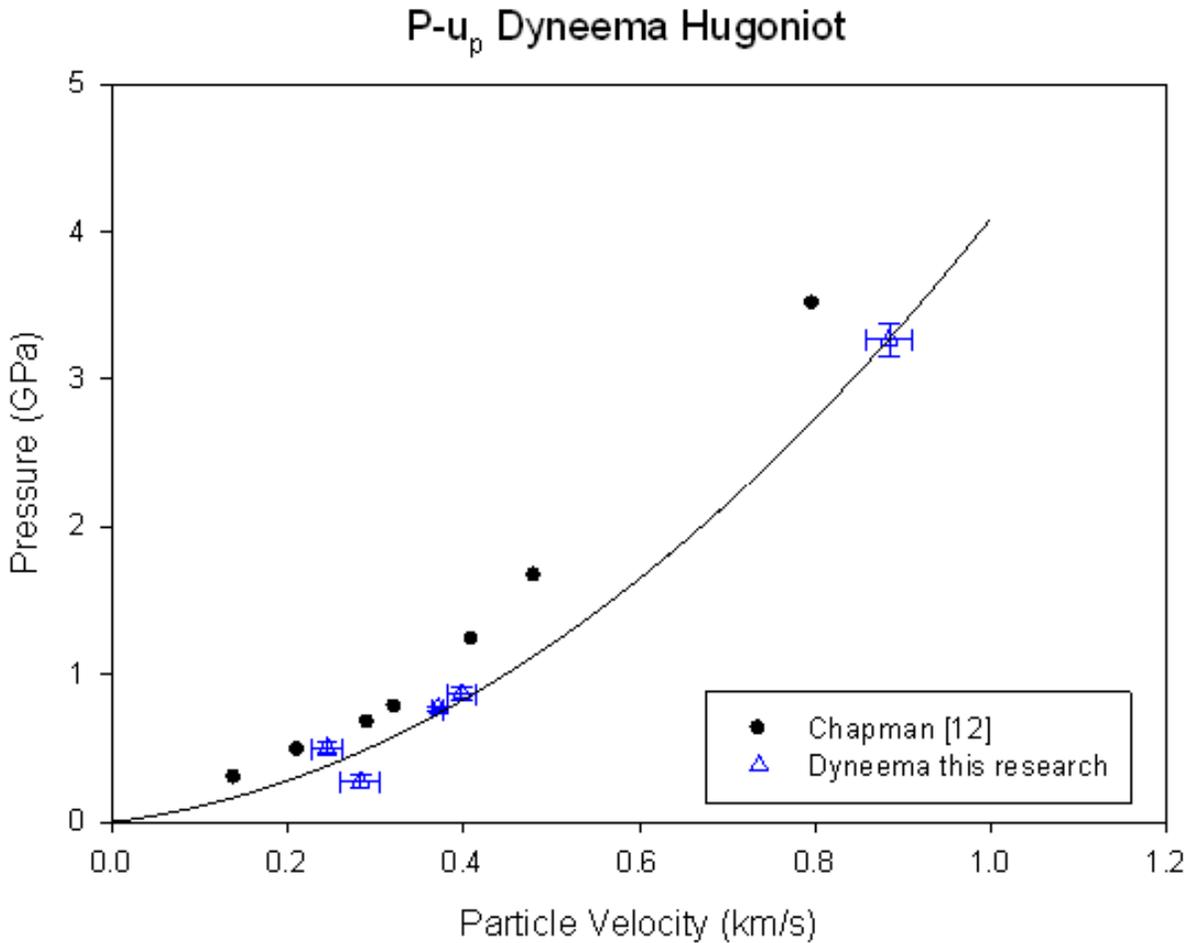
Figure 67.   Principal Dyneema Hugoniot data in $P-u_p$ space

This research has successfully obtained principal Hugoniot data for Dyneema HB-25 in both $P-u_p$ and U_s-u_p space in the through fiber direction. As well as measuring the Hugoniot states of Dyneema, the wave profiles were also obtained. Yet the wave profiles present many more questions than answers, and show evidence of multiple wave

structure interactions within the material, which can lead to larger than desirable errors and inconsistent measurements. These waves drove us to the use of buffer materials to average the wave arrivals at the rear of the target. This provides a measurement of the average response of the material.

In order to be useful as a material for the second layer of our layered armor concept, a material must be able to efficiently spread energy laterally and transfer a minimum amount of energy in the through-thickness direction. Initial first order approximations and penetration simulations and experiments performed by Ong [1] show that Dyneema should be able to perform this function, and using the properties found in this research, the material model used in the hydrocode simulation can be adjusted to better model the actual physical response of Dyneema under dynamic loading.

In order to conclusively prove that Dyneema HB-25 will be a superior material over others for this function, much more research on the dynamic properties must be performed. Specifically, more experiments in the low pressure region must be performed to effectively anchor the shock Hugoniot in the through fiber direction. And in order to completely model the orthotropic behavior of Dyneema there needs to be an effort to determine the shock Hugoniot in the along the fiber direction. These further experiments and simulations will be left for future research.

THIS PAGE INTENTIONALLY LEFT BLANK

APPENDIX A. SHOT PREPARATION CHECKLIST

PRE-SHOT MEASUREMENTS

TARGET Material	
Target Density (g/cm^3)	
Target Diameter (mm)	
Target Thickness (mm)	
Window Thickness (mm)	
Foil Thickness (mm)	

Pin Heights

Velocity Pin Radius (mm)						
VP1	VP2	VP3	VP4	VP5	VP6	GND

Flush Pin Radius (mm)						
FP1	FP2	FP3	FP4	TP		

Target offset from target plate after gluing:
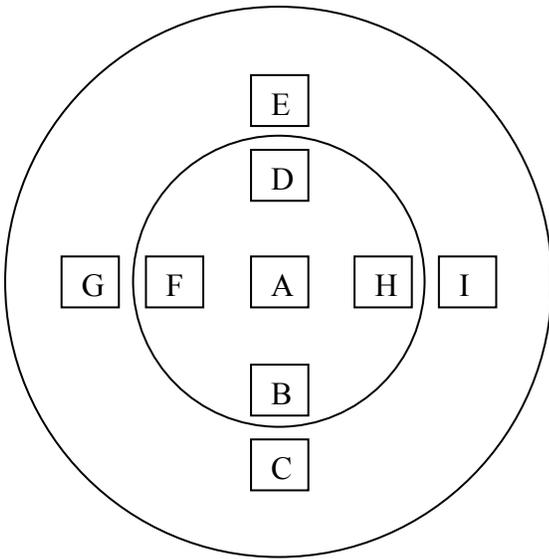
Sample Points	Measurements (mm)
A	
B	
C	
D	
E	
F	
G	
H	
I	

Impactor offset from bullet face:

Impactor Material	
Impactor Density (g/cm^3)	
Impactor Diameter (mm)	
Impactor Thickness (mm)	
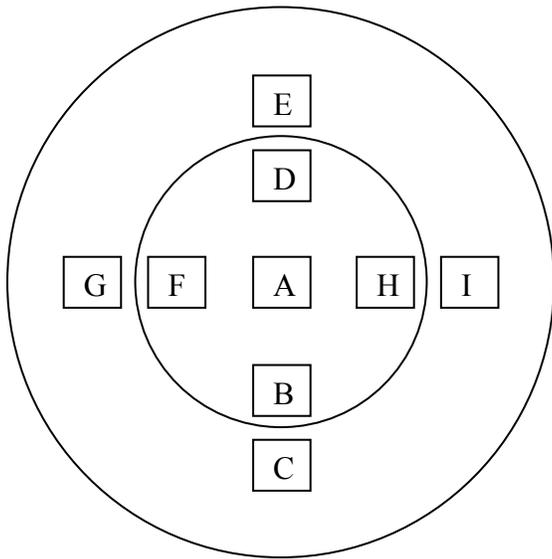
Sample Points	Measurements (mm)
A	
B	
C	
D	
E	
F	
G	
H	
I	

Mass of Bullet with O-rings (g)	
Desired Shooting Velocity (km/s)	
Required Pressure (PSI)	

POST-SHOT MEASUREMENTS AND CALCULATIONS

RAW PIN TIMES

VP1	VP2	VP3	VP4	VP5	VP6

	FP1	FP2	FP3	FP4	

Calculated Tilt:_____
Calculated Projectile Velocity:_____
Shock Arrival Time:_____
Shock Release Time:_____
Calculated sound speed:_____
Calculated Shock speed:_____
Calculated Pressure:_____

RAW Time Line:

_____

CORRECTED Time Line:

_____

NOTES:

THIS PAGE INTENTIONALLY LEFT BLANK

APPENDIX B. SHOT PROCEDURE

GUN EVACUATION PROCEDURE

1. Verify gun barrel and catch tank clear of debris
2. Verify target installed and diagnostics connected per target preparation and installation procedure
3. Install honeycomb and momentum absorbers in catch tank
4. Clean catch tank o-ring mating surfaces and apply fresh vacuum grease
5. Close catch tank to furthest point possible by hand
6. Apply vacuum grease to projectile o-rings
7. Install o-rings on projectile and wipe excess grease from projectile surfaces
8. Insert projectile into projectile cavity until projectile is fully inserted into breech
9. Install breech plug
10. Install breech screw cap
11. Connect vacuum hose between SV-1 and breech plug
12. Shut SE-1, SE-5
13. Check shut SE-3, SP-1, SP-2, SV-1, SV-2
14. Shut catch tank vent plugs, being careful not to pinch o rings
15. Verify VISAR probe bolt plug installed and filled with hardened epoxy on top of catch tank
16. Shut vacuum pump suction valve
17. Energize vacuum pump
18. Open SV-1 wait 30 seconds
19. Open SV-2
20. Slowly adjust vacuum pump suction valve to throttle position that corresponds to optimum operation
21. Move catch tank shock absorber forward when catch tank is fully seated and insert stop bolts and stop pins
22. When breech and catch tank press ≈500mtorr check for system leaks as follows:
    a. Open He bottle isolation valve
    b. Open SP-4 and SP-5 regulator isolation valves
    c. Adjust SP-5 to 1200psig
    d. Adjust SP-4 to 200psig
    e. Stand clear of pressure indication panel
    f. Open SP-1
    g. Verify system vacuum holding steady
    h. Shut SP-1

 i. If indication of failed projectile o-rings, depressurize and remove projectile as follows
   i. Shut SV-2
   ii. Shut SV-1
   iii. De-energize vacuum pump
   iv. Open SE-5 and allow catch tank to equalize with atmosphere
   v. Open SE-3 to vent breech to atmosphere
   vi. When local breech pressure indication reads 0 psig, remove breech screw cap
   vii. ***CAUTION: DO NOT STAND DIRECTLY BEHIND BREACH DO TO THE POSSIBILITY OF A REAR FIRING OF THE PROJECTILE IF PLUG IS SEPARATED FROM BULLET WHILE REMOVING FROM BREECH.***

    Carefully remove breech plug with vacuum hose attached. Projectile should be vacuum sealed to breech plug
   viii. Carefully remove projectile from breech plug and inspect o-rings for damage
   ix. Replace projectile o-rings and vacuum grease if necessary
   x. Repair any other known leaks in system
   xi. Open catch tank and inspect target integrity if necessary
   xii. Return to step 8.

23. Continue evacuating Projectile Cavity and Catch tank until vacuum indicates ≤100mtorr on both breech and catch tank vacuum gauges(≤50mtorr preferred)
24. If gun is not to be shot immediately
 a. Shut SV-2
 b. Shut SV-1
 c. De-energize vacuum pump
25. Continue to Gun Firing Procedure if gun is to be fired immediately

GUN FIRING PROCEDURE

1. Clear lab space of all unauthorized personnel
2. Verify completion of Gun Evacuation procedure
3. Setup system diagnostics per Diagnostic setup procedure
4. Verify catch tank shock absorber in the full forward position with stop pins and stop bolts installed
5. Check shut SP-1, SP-2, SE-3, SE-1, SE-5,
6. Check open SE-4, SV-1, SV-2
7. Verify vacuum pump energized
8. Verify SP-5 set to 1200psig
9. Adjust SP-4 to calculated firing pressure
10. Verify SP-6 set to ≈100psig
11. Verify all personnel clear of gun space and shut gun room doors
12. Shut and lock IPL door
13. Verify diagnostics armed and ready to receive data
14. Open SP-1 to charge breech
15. Shut SP-1 when calculated firing pressure is reached on remote breech pressure indication
16. Shut SV-2, SV-1
17. Turn off function generator
18. *CAUTION: THIS WILL CAUSE THE PROJECTILE TO FIRE*
   To fire Gun: Cycle SP-2 open then shut to fire gun and record breech pressure at time of fire
19. Verify proper operation of diagnostics
20. Press enter to save and back up data from diagnostic equipment
21. De-energize vacuum pump
22. Shut He bottle isolation valve
23. Open SE-1 and SE-5 to equalize pressure in gun with atmospheric pressure
24. Open SP-1 to relief line pressure
25. Adjust SP-5, and SP-4 to fully counter clockwise position
26. Close SP-5 & SP-4 isolation valve after pressure relieved.
27. De-energize laser power
28. Open catch tank vent plugs
29. Remove Catch tank shock absorber stop bolts and stop pins
30. Open catch tank
31. Clear debris from catch tank
32. Remove vacuum hose from breech plug
33. Remove breech screw cap
34. Remove breech plug

35. Clean barrel
36. Verify data saved from diagnostics
37. De-energize diagnostics
38. Return barrel to fully inserted position

NOTES:

DIAGNOSTIC SETUP

1. Power up diagnostics laptop
2. Energize oscilloscope #1 and #2
3. Energize laser power
4. Energize velocity pin circuit
5. Adjust velocity pin circuit voltage to 120 to 150V
6. Setup VISAR system as follows
    a. Energize BNC pulse generator
    b. Energize frequency generator
    c. Energize high voltage power supply as follows:
        i. Depress power button
        ii. Wait 10 seconds
        iii. Depress high volts switch
7. Test diagnostics triggering properly as follows:
    a. Connect test piezoelectric pin cable to EXT/GATE connection on pulse generator
    b. On Function generator:
        i. Depress stop button
        ii. Depress FUNCTION button until setup appears on screen
        iii. Depress NEXT until RECALL appears on screen
        iv. Depress up or down arrow button until #4 appears on screen
        v. Depress FUNCTION until setup once again appears
        vi. Depress RUN button
    c. On diagnostics laptop:
        i. Open test1.py program
        ii. Enter current setup file name both9.txt
        iii. Type "arm" in command window
    d. Tap test piezoelectric pin
    e. Type "no" when prompted to save data on diagnostics laptop
    f. Press STOP on function generator
    g. Remove test cable from function generator and replace with Trigger Pin connector
8. When ready to shoot:
    a. Type "arm" on diagnostics laptop
    b. Depress RUN on function generator

THIS PAGE INTENTIONALLY LEFT BLANK

LIST OF REFERENCES

[1]   R. Ong, "Investigation of new materials and methods of construction of personnel armor," M.S. thesis, Naval Postgraduate School, Monterey, CA, Dec 2009.

[2]   C. W. Poh, "Investigation of new materials and methods of construction of personnel armor," M.S. thesis, Naval Postgraduate School, Monterey, CA, Dec 2008.

[3]   J. R. Denzel, "Determination of shock properties of ceramic Corbit 98: 98% Alumina," M. S. thesis, Naval Postgraduate School, Monterey, CA, Jun 2010.

[4]   R. S. Hixson, D. A. Boness, and J. W. Shaner, "Acoustic velocities and phase transitions in Molybdenum under strong shock compression," *Physical Review Letters*, vol. 62, no. 6, pp. 637–640, February 1989.

[5]   R. S. Hixson and J. N. Fritz, "Shock compression of Tungsten and Molybdenum," *Journal of Applied Physics*, vol. 71, no. 4, pp. 1721–1728, February 1992.

[6]   J. R. Robbins, J. L. Ding, and Y. M. Gupta, "Load spreading and penetration resistance of layered structures—a numerical study," *Int. J Impact Eng.*, vol. 30(6), pp. 593–615, 2004.

[7]   Y. M. Gupta and J. L. Ding, "Impact load spreading in layered materials and structures: concept and quantitative measure," *Int. J Impact Eng.*, vol. 27, no. 3, pp. 277–91, 2002.

[8]   M. L. Wilkins, "Mechanics of penetration and perforation," *Int. J. Engng. Sci.*, vol. 16, pp. 793–807, 1978.

[9]   W. Herrman, "Constitutive equation for the dynamic compaction of ductile porous materials," Sandia Laboratories, Albuquerque, New Mexico, December 12, 1968. Reprinted from *Journal of Applied Physics*, vol. 40, no. 6, pp. 2490–2499, May 1969.

[10]   Molybdenum. Web Elements. http://www.webelements.com/molybdenum/.

[11]   S. P. Marsh, *LASL Shock Hugoniot Data*, University of California Press, 1980.

[12]   D. J. Chapman, C. H. Braithwaite, and W. G. Proud, "The response of Dyneema to shock-loading," *Shock Compression of Condensed Matter-2009*, American Institute of Physics, 2009

[13]   W. F. Hemsing, "Velocity sensing interferometer (VISAR) modification," *Review of Scientific Instruments*, vol. 50, no. 1, pp. 73–78, January 1979.

[14]   C. C. Ho, "Assembly and commissioning of Naval Postgraduate School gas gun for impact studies," M.S. thesis, Naval Postgraduate School, Monterey, CA, December 2009.

[15]   L. M. Barker, an R. E. Hollenbach, "Shock-wave studies of PMMA, Fused Silica, and Sapphire," *Journal of Applied Physics*, vol. 41, no. 10, pp. 4208–4226, September 1970.

[16]   M. D. Furnish and L. C. Chahabildis, "Dynamic material properties of refractory materials: Molybdenum," *High Strain Rate Behavior of Refractory Metals And Alloys,* The Minerals, Metals & Materials Society, 1992.

[17]   R. S. Hixson, "NPS Physics 4857 class lecture notes." Self Published, 2010.

INITIAL DISTRIBUTION LIST

1. Defense Technical Information Center
   Ft. Belvoir, VA

2. Dudley Knox Library
   Naval Postgraduate School
   Monterey, CA

3. Robert Hixson
   Los Alamos National Lab
   Los Alamos, NM

4. Jose Sinibaldi
   Lawrence Livermore National Lab
   Livermore, CA

5. William Short
   Office of Naval Research
   Washington, D.C.

6. Yogendra Gupta
   Institute for Shock Physics
   Pullman, WA

7. Yoshiama Toyoda
   Institute for Shock Physics
   Pullman, WA

8. Mark Garner
   Garner-Hill Farms
   Harrison, AR

9. Debi Garner
   UPS Store
   Pueblo, CO